Energy harvesting systems for low energy mobile robots

Technical Committee: Energy, Environment, and Safety Issues in Robotics and Automation

Aníbal T. de Almeida, Ricardo Faria, Pedro Santos
Institute of Systems and Robotics, University of Coimbra, Portugal

Toshio Fukuda
Meijo University, Japan

Tzyh Jong Tarn
Washington University, St. Louis, USA

MiniExplorer

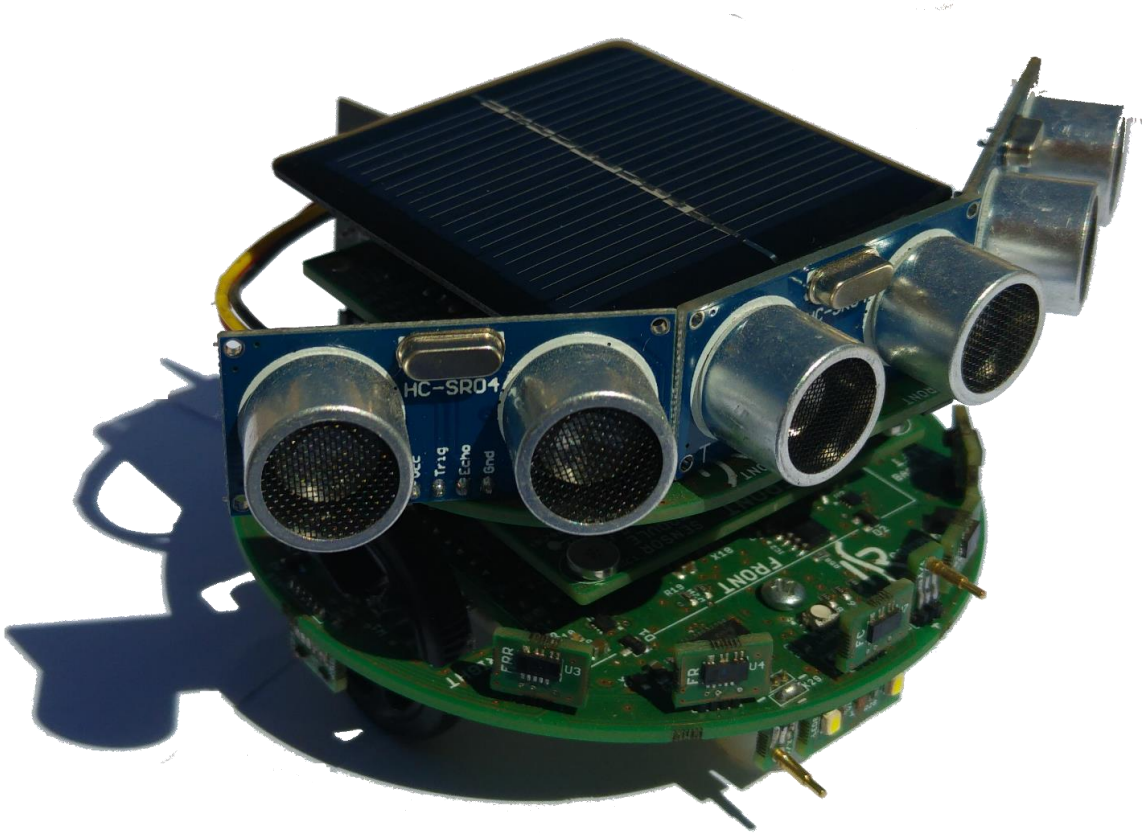

Institute of Systems and Robotics
University of Coimbra
Portugal

PR TronicSys
MECHATRONIC DEVELOPMENT SOLUTIONS

September 2016

Abstract

The use of energy harvesting technologies in mobile robotics is a prominent and growing research area. It enables partial or total energy autonomy when performing tasks. The mobile robots that can benefit from such solutions are typically small, low-consumption and with power management systems.

The developed mobile robot includes an integrated system for energy monitoring and management, allowing the tracking of the supplied and consumed power. This information is then used to manage energy consumption by acting on peripheral components. The robot consists of a modular architecture, with the three modules named base, sensor, and harvester. This arrangement facilitates changes in the hardware or addition of extra modules. It integrates various types of sensors, such as proximity infra red and ultrasonic, temperature, humidity, barometer, accelerometer, gyroscope, magnetometer, among others, thereby making it versatile for a number of applications such as environmental monitoring and swarm robotics. The energy storage unit may use lithium batteries or supercapacitors allowing autonomy tests in both cases.

This document has the objective of explaining in detail the mobile robot developed. All features and possible applications are presented.

Keywords: energy harvesting, storage, robot, sensors, autonomy.

Contents

List of Figures

List of Tables

List of Acronyms

MPPT	*Maximum Power Point Transfer*
PWM	*Pulse Width Modulation*
MOSFET	*Metal Oxide Semiconductor Field Effect Transistor*
PCB	*Printed Circuit Board*
I2C	*Inter-Integrated Circuit*
SPI	*Serial Peripheral Interface*
ADC	*Analog to Digital Converter*
DAC	*Digital to Analog Converter*
DC	*Direct Current*
USB	*Universal Serial Bus*
RGB	*Red Green Blue*

Chapter 1

Energy Harvesting Systems for Autonomous Mobile Robots

This chapter discusses concepts related to the work developed in the dissertation and an overview of the state of the ar. It is divided into two sections: The first section presents the concept of energy harvesting and the main types of energy collection technologies from the environment, targeted for their work; The second presents a review on the development of chemical batteries and the main forms of energy storage in today's mobile robotics;

1.1 Energy harvesting

Energy harvesting also known as Power Harvesting or Energy Scavenging is a process of capturing small amounts of energy from the environment, transforming it into usable electricity. The energy available for build up is mainly provided by ambient light (artificial or natural light), radio frequency, thermal sources or mechanical sources. The use of such technologies in mobile robotics provides greater autonomy to robots, allowing them able to operate longer without need to charge or the use of power cables. To understand better what incorporates an energy harvesting system is shown in figure: 1.1 that contains a transducer responsible for the conversion of energy from the environment into electrical energy, is then carried controlled energy storage and later a conversion DC- DC is made to ensure the desired amplitude voltage for feeding low consumption loads.

It is possible to classify the main types of Energy Harvesting technologies, as shown in figure 1.2;

It is important to know what is the typical power provided by this type of

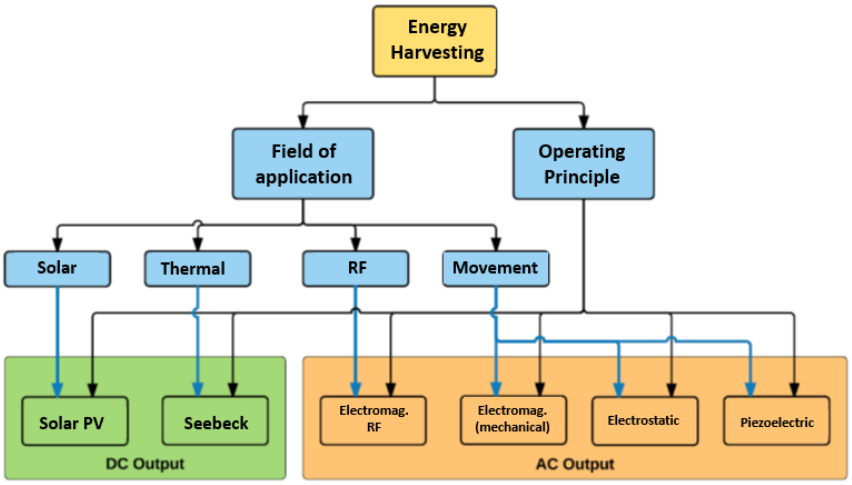

Figure 1.1: Exemplary diagram of an Energy Harvesting system, adapted from the source [1];

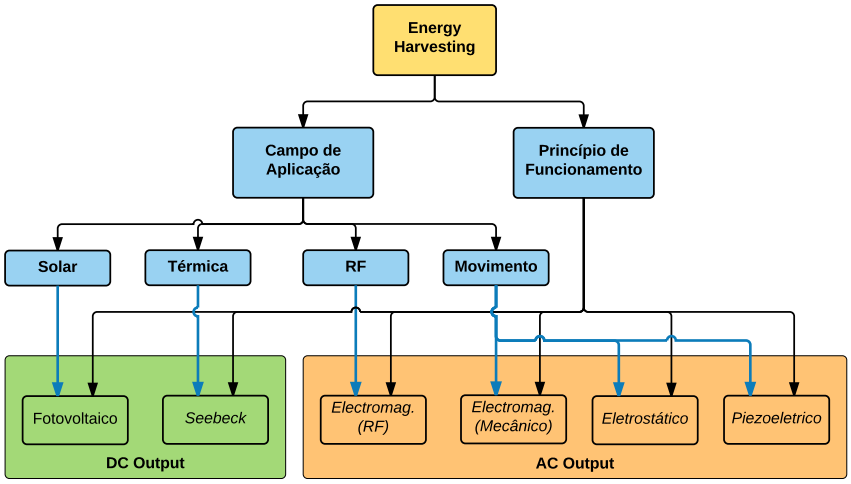

Figure 1.2: Main hierarchy of energy harvesting technologies, adapted source [2];

solution, per unit area or volume. For that is presented the table 1.1 that relates the type of technology used, the environment in which it is applied and the power supplied.

1.1.1 Photovoltaic Solar Energy

Solar Energy

Solar energy is the most important renewable energy sources has gained attention in recent years, their high abundance in relation to other energy sources makes it very used. The amount of energy supplied to the earth by the sun for a day is sufficient to establish the total requirement of land for one year [12]. Solar radiation emitted by the sun is received by the terrestrial surface with alternating

Table 1.1: Typically provided powers from technologies *energy harvesting*, source adapted from [10];

Energy Harvestintg Surce	Local Environment	Harvester Power	Harvester Considerations	Circuit Considerations
Solar/Light	Indoor	10uW/cm^2	Light intensity and wavelength	MPPT Required
	Outdoor	10mW/cm^2		
Piezoelectric Mechanical Vibration	Humans	4uW/cm^2	Vibration amplitude and resonance frequency	Required AC/DC converter
	Machines	250uW/cm^2		
Mechanical Vibration Electromagnetic	Humans	50uW/cm^3		
	Machines	50uW/cm^3		
Thermal	Humans	25uW/cm^2	Thermal gradients and heat flows	Low starting voltage
	Machines	10mW/cm^2		
Radio Waves	Indirect	0,1uW/cm^2	Distance from the source and resonant antenna	Good efficiency, low voltage rectification
	Direct	1mW/cm^2		

distribution due to the existence of clouds, gas, water vapor, dust and vegetation. After crossing the atmosphere reaches the earth's surface in three distinct ways:

- **Direct radiation** – Directly affects the surface;
- **Diffuse radiation** – It is deflected in different directions by atmospheric components;
- **Reflected radiation** – It is reflected by the soil and surrounding objects.

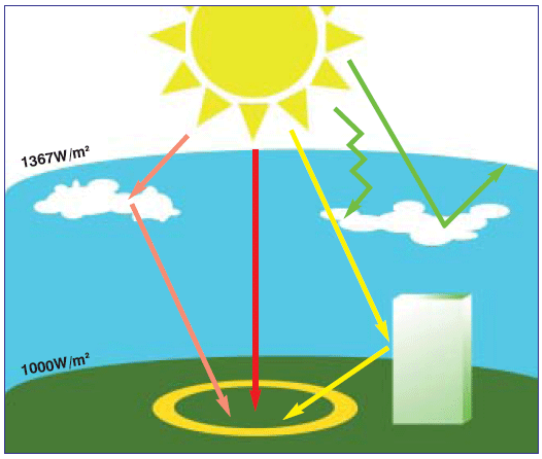

Figure 1.3: Distribution of solar radiation, source portal of renewable energy [3];

The instrument measures the total solar radiation is called pyranometer, is used to measure all the radiation that reaches the Earth's surface [3]. One day sun with a clear sky, at about the noon radiation is approximately 1000 W/m^2.

Photovoltaic cells

Solar or photovoltaic cells are responsible for the transformation of energy from a light source into electrical energy, this phenomenon is possible due to the photovoltaic effect. There are three most common types of photovoltaic cells, with monocrystalline silicon crystals, polycrystalline crystals and amorphous silicon.

- **Monocrystalline silicon** - The monocrystalline silicon cell is the most commercially used in the composition of photovoltaic panels, although the cost is high in relation to its thickness is around 300 microns [**?**]. The laboratory efficiency can reach 24% and the trade level to 16% [11] [4];
- **Polycrystalline silicon** - The polycrystalline silicon cell is obtained from intermediate purity silicon blocks, the cost of manufacture is reduced, but the efficiency is lower. The laboratory efficiency can reach 18% and the trade level to 14% [11] [4];
- **Amorphous silicon** - Amorphous silicon is used particularly in consumer products such as watches and calculators, so it is possible to place a thin film of amorphous silicon on a substrate (metal, glass, plastic). The laboratory efficiency can reach 13% and the commercial level to 7% [11] [4].

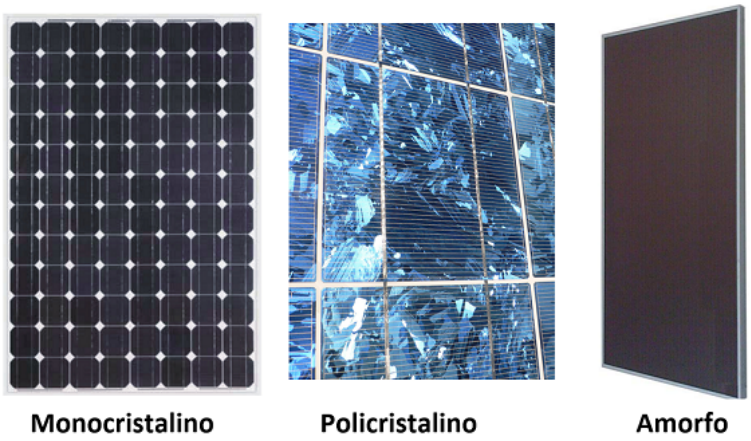

Figure 1.4: Types of photovoltaic panels, adapted source [4];

Each panel consists of several photovoltaic modules, wherein each module comprises a number of cells, the power of the panel is related to the number of cells used and voltage/current characteristic is related to the type of connections between cells, and these series/parallel respectively.

The table 1.2 shows the maximum efficiency of each panel commercially and in the laboratory.

Table 1.2: Performance of different photovoltaic cells, adapted source [4] e [11];

Type of cell	**Efficiency**		
	Typical	Maximum	
		Commercial	Laboratory
Monocrystalline	14-16%	22%	24%
Polycrystalline	11-13%	15%	18%
Amorphous silicon	6-7%	10%	12%

Theoretical model of photovoltaic cell

The equivalent circuit of a photovoltaic cell (figure 1.5) includes a current source, a diode (D), the equivalent series resistance (Rs) and Resistance equivalent leak (Rsh). The output of the current source is directly proportional to the light falling on the cell [5].

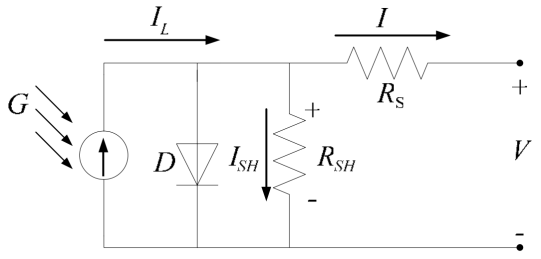

Figure 1.5: Equivalent diagram of a solar cell, adapted source [5];

The increased model sophistication as precision and complexity can be introduced by adding more dependencies [5]:

- Temperature dependence on saturation current I_0 diode and thermal voltage Vt;
- Temperature dependence on photo current I_L;
- Series resistance Rs which gives a more accurate way to model between the maximum power point and the open circuit voltage, represents losses due to current flow;
- Leaks resistance Rsh representing the leakage current to the earth is important that this value is high;
- Quality factor n of diode, thus becoming one variable parameter in the model.

The equation: 1.1 represents the schematic model of a photovoltaic cell of figure 1.5 [13]:

$$I = I_L - I_0 \left[exp\left(\frac{V + IR_s}{V_t}\right) - 1 \right] - \frac{V + IR_s}{R_{sh}} \tag{1.1}$$

The generated current I_L is dependent on the irradiance that reaches the solar cell (E) and the cell temperature (Tc), current can be approximated by the equation 1.2, where $I_{ph,ref}$ represents the photo current generated measured with $T_{c,ref}$ e E_{ref}.

$$I_L = \frac{E}{E_{ref}} \left[I_{ph,ref} + \alpha_{Isc}(T_c - T_{c,ref}) \right] \tag{1.2}$$

The thermal voltage (Vt) and the diode saturation current (I_0) are temperature dependent parameters, these are described in the equations 1.3 and 1.4,

where n is the quality factor of the diode; q- electron charge; k- Boltzmann constant; α- empirical thermal coefficient; Eg - band gap [13].

$$V_t = \frac{nkT_c}{q} \tag{1.3}$$

$$I_0 = I_{0,ref}\left(\frac{T_c}{T_{c,ref}}\right)^3 exp\left[\frac{1}{k}\left(\frac{E_g}{T_c} - \frac{E_{g,ref}}{T_{c,ref}}\right)\right] \tag{1.4}$$

The value of resistors Rs (series resistance) e Rsh (leakage resistance) can be estimated by analysis of the characteristic curve voltage-current of a PV panel, figura 1.6. For a better estimation of these values, various values of irradiance must be taken in consideration, doing a final average of all values [14] [15].

$$Rs = \frac{V_{oc} - V_{MAXpower}}{I_{MAXpower}} \tag{1.5}$$

$$Rsh = \frac{V_{MAXpower}}{I_{sc} - I_{MAXpower}} \tag{1.6}$$

For a detailed analysis of the performance of a PV module it is necessary to make a study of the characteristics curve I-V 1.6 that relates the voltage to the current generated by the panel. It is obtained by applying a constant source of light on the dashboard and varying the load to which it is connected, that is, we have a power generator circuit with a variable load. The temperature of the panel must be constant during the test to not influence the results.

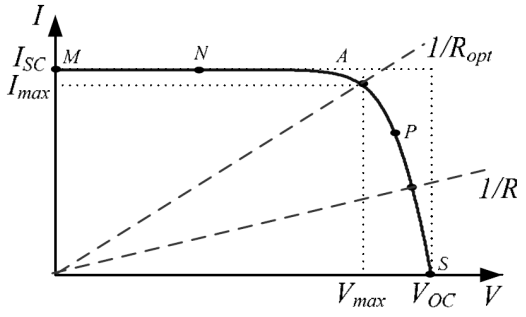

Figure 1.6: Characteristic curve I-V of a photovoltaic panel [5];

In resistive loads the panel load characteristic is a straight line with slope $I/V = 1/R$ and to obtain the maximum power transfer is necessary to connect the panel to a circuit *Maximum Power Point Transfer* (MPPT).

To understand which effects are caused by the variation of solar radiation and temperature in a photovoltaic panel the figure is displayed 1.7:

Lookink at the figure 1.7 (a) it follows that the current varies proportionally to variation of solar radiation. When it decreases, there is a decrease of the current supplied by the panel and the maximum power point ($P_{max} = V_{max}I_{max}$)

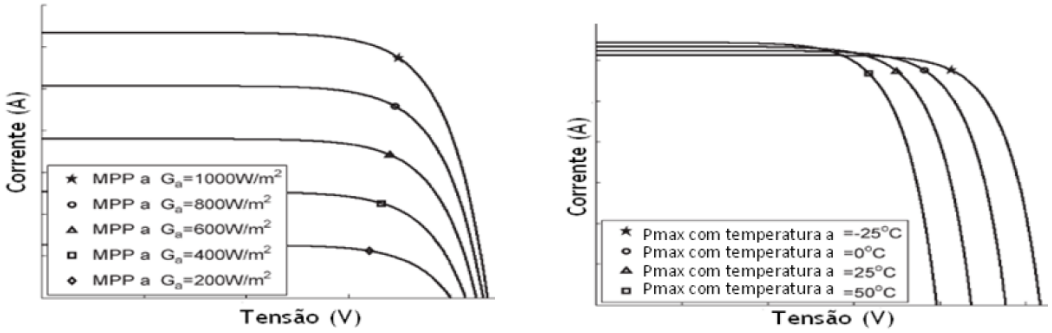

(a) Variation of the incident radiation; (b) Temperature variation;

Figure 1.7: Effects caused in the I-V characteristic curve with variation of the incident radiation and change in panel temperature [4];

is also directly affected by the decline in the current, the voltage remains practically constant. In figure 1.7 (b) is observed that when there are temperature variations, the PV voltage is proportionally affected, the higher will be at the lowest temperature. In short, the maximum power of the panel is reduced at increasing temperature of the photovoltaic cells.

The efficiency of a photovoltaic panel is given by the equation 1.7, with A - panel area and G_a - solar irradiance.

$$\eta = \frac{P_{max}}{P_{in}} = \frac{I_{max}V_{max}}{AG_a} \tag{1.7}$$

1.2 Energy storage

In portable electric/electronic devices it is very important to have an energy storage form, enabling its operation. Examples of these devices are mobile robots, smartphones, laptops and others. The figure 1.8 (a) shows the evolution of batteries over the years are displayed various kinds of chemical batteries, and their associated energy density. Figure 1.8 (b) shows the relationship power vs power, relative to conventional capacitors, super-capacitors, batteries and fuel cells (gasoline).

Currently, lithium-ion is the most widely used in portable devices, have good energy storage capacity in relation to their size and have no memory effect. Some models of electric vehicles already incorporate this storage technology [18]. However in mobile robotics in addition to the lithium batteries are still used often traditional lead batteries, they have a reduced cost which makes that is often used.

1.2.1 Lithium batteries

Energy storage using the lithium battery in portable devices require care for their safety. The possibility of overloading, overheating or short circuit can cause a

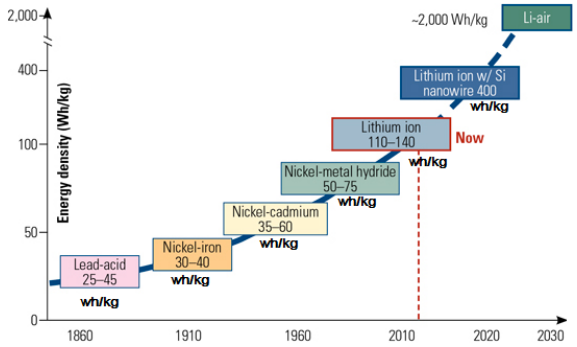

(a) Historical evolution of batteries, 2013 adapted source [16];

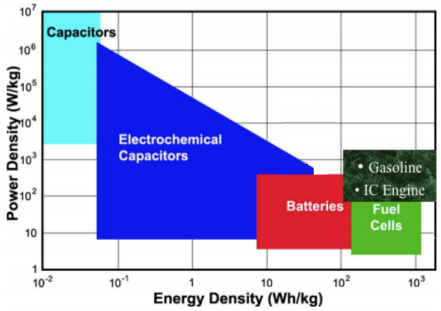

(b) Power ratio vs Energy, 2013 adapted source [17];

Figure 1.8: Historical evolution of batteries and compared the relationship power vs energy of different types of storage;

fire or explosion, so these parameters should be monitored during use. The term lithium ion refers to a diverse family of chemical batteries, most differs in the composition of the positive electrode, the materials vary in cost, safety and energy density. The table 1.3 lists the different types of materials the make up the positive electrode for batteries currently on the market. For the negative electrode the type of material used is graphite, although they are being studied and developed new materials [19].

Table 1.3: Propriedade dos materiais do elétrodo positivo;

Material	**Chemical formula**	**Description**
Lithium cobalt oxide (LCO)	$LiCoO_2$	Commercial type; Materials expensive materials
Nickel cobalt aluminum (NCA)	$LiNi_{0.8}Co_{0.1}5Al_{0.05}O_2$	High energy density per unit mass
Nickel manganese cobalt (NMC)	$LiNi_{1-x-y}Mn_xCo_yO_2$	More security and cheaper than (LCO)
Lithium manganese oxide (LMO)	$LiMn_2O_4$	Cheaper than (COM) Low temperature stability
Lithium iron phosphate (LFP)	$LiFePO_4$	Very safe, high power, but lower energy density;

The figure 1.9, shows the movement of the lithium ions during charging and discharge battery, during the charge flow from the positive electrode to the negative through the electrolyte and the discharge flow back from the negative electrode to positive.

The charge control is essential in a lithium battery. Some batteries already contain integrated circuits to ensure that control, when they do not have to,it must be designed load circuits with appropriate safeguards, such as temperature monitoring and overload. The load profile of a lithium battery is generally composed of two phases:

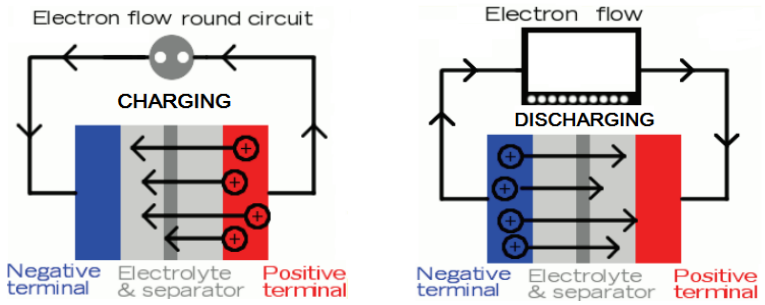

(a) Ions movement during charging;

(b) Ions movement during discharge;

Figure 1.9: Flow of lithium ions during charging and discharging of the lithium battery, adapted source [6];

- **1ª phase** - Charge with constant current until the battery reaches its peak voltage, typically 4.1-4.2 V/cell;
- **2ª phase** - Charge with constant voltage until the current absorbed by the battery to approximately zero amperes.

If the battery is severely depleted, it must have a slow charge so that the voltage reaches 2.5-3V/cell, may subsequently be applied to normal charge as described above. Discharge battery to the end is not advisable as it can be damaged and lose storage capacity. Fig 1.10 illustrates the load profile for a lithium ion and its ability to function of the voltage per cell.

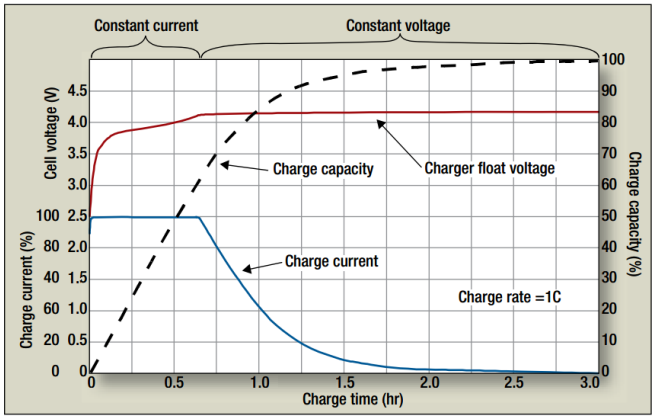

Figure 1.10: Charge profile and capacity of lithium-ion [7];

1.2.2 Supercapacitors

Supercapacitors, or Ultracapacitors also known as electrochemical double-layer capacitors are electrical storage devices with high energy storage density and

high power density. The cost is superior to the batteries, although it has advantages with respect to power density and lifetime. In applications requiring quick charging and discharging cycles, it is common to use this type of solution [8]. The construction of supercapacitors basically consists of two electrodes, a separator and an electrolyte, the main difference compared to the conventional constitution of electrodes is used, which are based on carbon technology (nanotube). This technology creates a high surface area with an extremely small separation distance. To better understand its constitution this is shown in figure 1.11 [9].

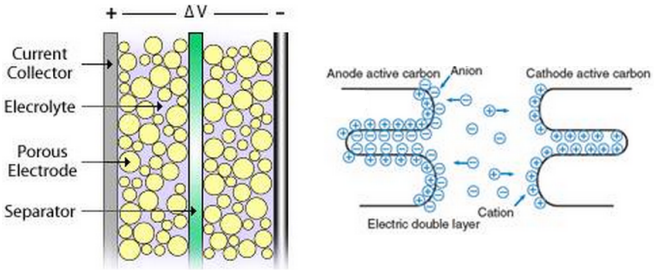

Figure 1.11: Internal constitution of a supercapacitor, adapted source [8];

The theoretical analogy of a supercapacitor can be seen as the conventional condenser, the figure 1.12 presents its equivalent circuit, with ESR - the equivalent series resistor, Rp - the insulation resistance, C - the capacitance and Xl - the inductance.

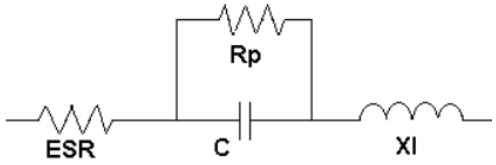

Figure 1.12: Equivalent circuit capacitor [9];

The capacity of a capacitor can be obtained from equation 1.8 , with C - the capacitance, Q - the positive charge e V - the applied voltage [20];

$$C = \frac{Q}{V}[F] \tag{1.8}$$

The energy stored in a capacitor is given by the equation 1.9;

$$E = \frac{1}{2}CV^2[J] \tag{1.9}$$

The maximum power density of the capacitor is given by the equation 1.10 [21];

$$P_{max} = \frac{V^2}{4ESR}[W/kg] \tag{1.10}$$

One of the disadvantages of supercapacitors is the maximum voltage that supports, the most conventional are 2.7V, when applying for a supercapacitor

bank with the largest resulting strain, you must connect them in series, however there must be a balance circuit to ensure that they are not in overvoltage to be damaged. At the junction of capacitors in parallel there are any balancing restrictions.

The load of a supercapacitor should be controlled to limit current, its low internal resistance causes the current tends to a high value when the initial charge time, in most cases the absorbed power tends to the maximum value that the source can provide. It should also usable in the discharge current limiter, since the existence of a short circuit will discharge the supercapacitor causing large current flow that could damage the conductors (wires or PCB).

Chapter 2

Mobile Robot Developed

This chapter presents the mobile robot developed. It is divided into five sections: The first section presents the physical structure and the high-level architecture; In the second the differential locomotion system and the necessary theoretical formulation; In the third the modular architecture; In the fourth the hardware used; In the fifth and last the platform used in programming the robot.

2.1 General description

2.1.1 Physical structure

The mobile robot developed is composed of three modules, that are denominated by base, sensor and harvester. The base has a circular shape about ten centimeters in diameter, the remind modules are square, having about six centimeters from the side and are placed on top of the base. For a better perception is shown in Figure 2.1.

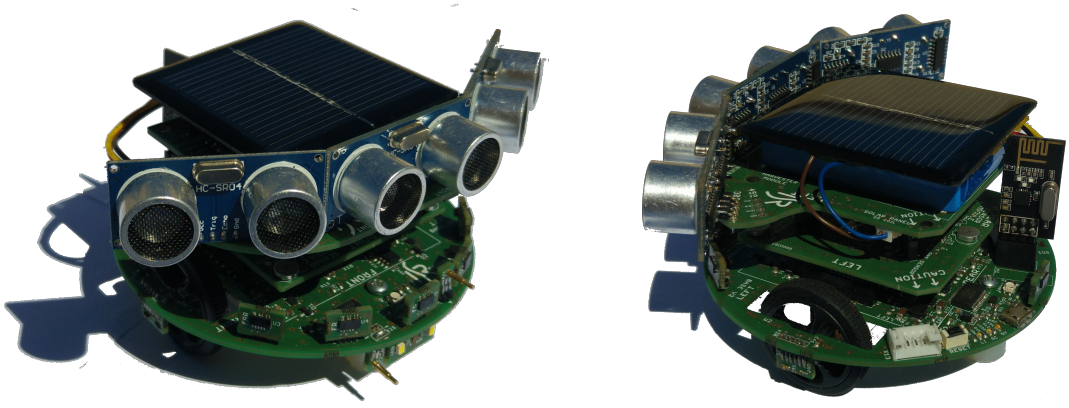

(a) Front view; (b) Rear view;

Figure 2.1: Physical aspect of the developed robot;

2.1.2 High level architecture

The high level architecture of mobile robot can be seen in figure 2.2, presents in general all the components that are integrate. It is visible in the upper part of the figure the components which comprise the energy harvesting module, on the left side the set of all sensors used, in the center the microcontroller, at the bottom of the drive motor system and the right side the various types of communication, data storage and light feedback. The robot also contains an energy management system, which can meet the electrical power supplied and consumed, later adopting energy saving measures by disconnecting peripherals power busses or opt for the placement of these in sleep.

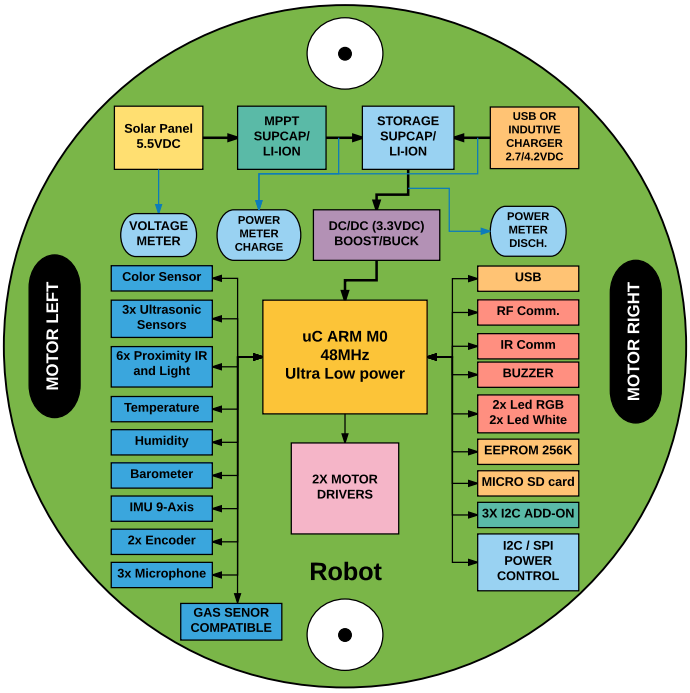

Figure 2.2: High level architecture of developed robot;

2.1.3 Robot applications

A mobile robot with these characteristics has enormous potential for various applications. The differential steering system allows an easy shaping for movement control, the ability to integrate expansion modules allows for new features, the integration of a wide range of existing sensors is a real asset to the increasing number of applications. The robot can operate indoor or outdoor with suitable road conditions.

Here are some types of applications for robot:

- Differential mobility tests with point source and destination;

- Lines follower adding module with sensors on base;
- Environmental monitoring, for example, temperature, humidity and atmospheric pressure;
- Structural analysis using the inertial unit of the robot;
- Energy harvesting studies and energy management;
- Location test between robots using triangulation (microphones);
- Area recognition, using the proximity sensors, odometry and inertial unit;
- Swarm robotics algorithms;
- Among others.

Due to the characteristics of robot developed that can be used by a wide academic range, from basic education with simple tests of differential movement and use of some sensors in high school already with some complexity, eg search and rescue competition and a university degree with advanced algorithms testing behaviors of swarm and energy management. To reduce the cost of the robot is possible to place sensors depending on the needs of the intended application.

2.2 Differential robot model

The robot locomotion system was developed based on the differential model, due to its characteristics, it is one of the most widely used types of locomotion in mobile robotics applications, shown in Figure 2.3. It comprises two wheels aligned with one another and control of its movement is performed by varying the speed of each of the wheels.

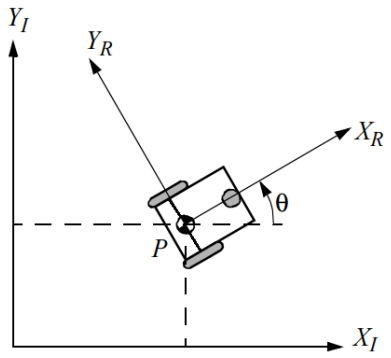

Figure 2.3: Differential robot model;

The structure of the differential robot shown in Fig 2.3, prevents translational movement made along the axis passing through the shafts of the wheels. Whereas there is no lateral slip, namely, the wheel speeds at the contact point with the ground is always perpendicular to the axes of the wheels, the state vector can be

represented by the equation, with $x(t)$, $y(t)$ e $\theta(t)$ represents the position of the point P the figure 2.3 on the plain, $v(t)$ represent the linear velocity and $w(t)$ the angular velocity.

$$X(t)^T = (\ x(t)\ \ y(t)\ \ \theta(t)\ \ v(t)\ \ w(t)\ ) \tag{2.1}$$

The linear speed of each wheel is determined by the relationship between the angular velocity (w) and ideal radius of the wheels (r), described by the equation 2.2;

$$V_E(t) = w_E(t)r_E\ ,\ V_D(t) = w_D(t)r_D \tag{2.2}$$

The linear velocity and the angular velocity is represented by equation 2.3, with (b) the distance between wheels;

$$v = \frac{v_D + v_E}{2} = \frac{R(w_D + w_E)}{2}\ \ ;\ \ w = \frac{v_D - V_E}{b} = \frac{R(w_D - w_E)}{b} \tag{2.3}$$

Knowing the linear velocity (v) and the angular velocity (w) the angular velocities to be applied in each wheel are given by the equation 2.4

$$w_E = \frac{v - (b/2)w}{r}\ \ ;\ \ w_D = \frac{v + (b/2)w}{r} \tag{2.4}$$

The evolution of model variables (degrees of freedom $\rightarrow$ configuration space $\Re^3$) can express themselves through the relationships of equations 2.5, 2.6 and 2.7;

$$\dot{x} = \frac{r \cdot cos(\theta(t))}{2} w_E + \frac{r \cdot cos(\theta(t))}{2} w_D \tag{2.5}$$

$$\dot{y} = \frac{r \cdot sin(\theta(t))}{2} w_E + \frac{r \cdot sin(\theta(t))}{2} w_D \tag{2.6}$$

$$w \equiv \dot{\theta}\frac{R}{b} w_D - \frac{R}{b} w_E \tag{2.7}$$

By integrating the above equations is possible to obtain the temporal evolution of vector robot pose position, with the possible extraction of pet pose over time.

2.3 Modular architecture

The project was developed based on a modular architecture, allows changes in a simple and less expensive way comparatively to the integration of all components in a single module. As stated, the robot incorporates three modules, each one of these is responsible for specific functions. The existence of an extra I2C connector on each module allows to add other components. In this section is given to know in detail each robot module.

2.3.1 Base module

The base module is the support of the robot, the printed circuit board in addition to containing electronic components, serves as a physical structure for fixing the motors and nylon supports. The figure 2.4 displays in more detail which components are in this module.

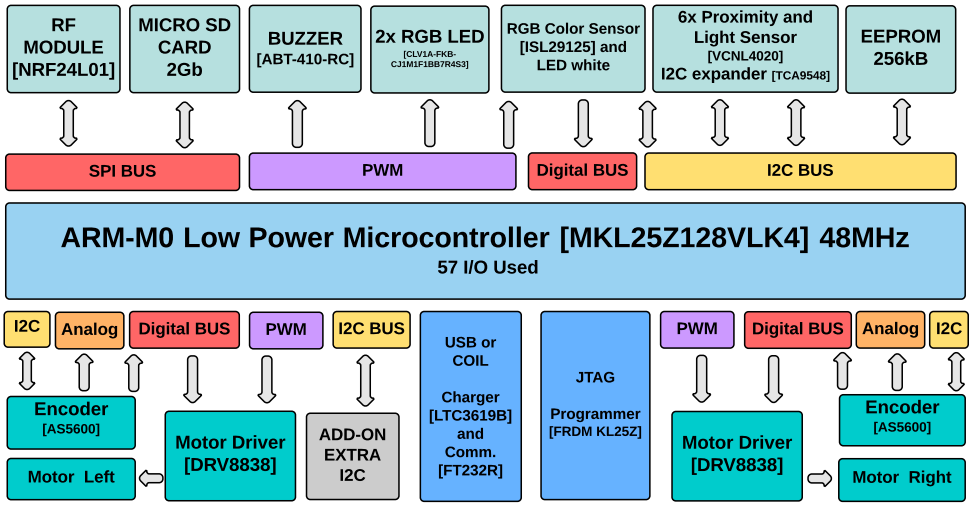

Figure 2.4: Components of the base module and types of communication;

2.3.2 Sensor module

The sensor module is placed on top of the module base, includes various sensors, infrared communication and serves as an intermediary for signs connecting the base module to the harvester. The figure 2.5 displays in more detail which components are in this module.

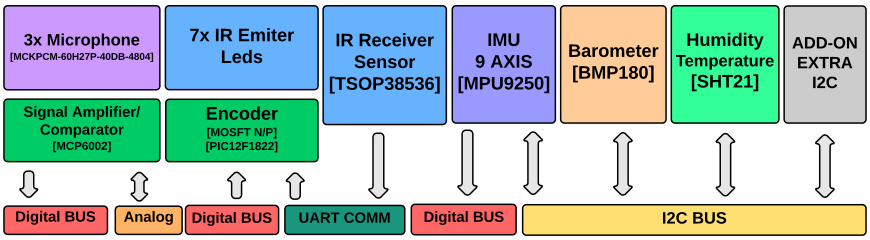

Figure 2.5: Components of the sensor module and types of communication;

2.3.3 Harvester module

The harvester module is responsible for harvesting, storage and energy monitoring, the use of two different types of storage, supercapacitors or lithium battery, requires to be used different topologies in MPPT and DC/DC conversion.To

minimize production costs, the PCB is designed so as to serve for both types of storage. It requires two units of the same PCB, although they are only welded components for the respective type of storage used. The figure 2.6 shows the diagram of connections and components used in case of using supercapacitors in the energy storage.

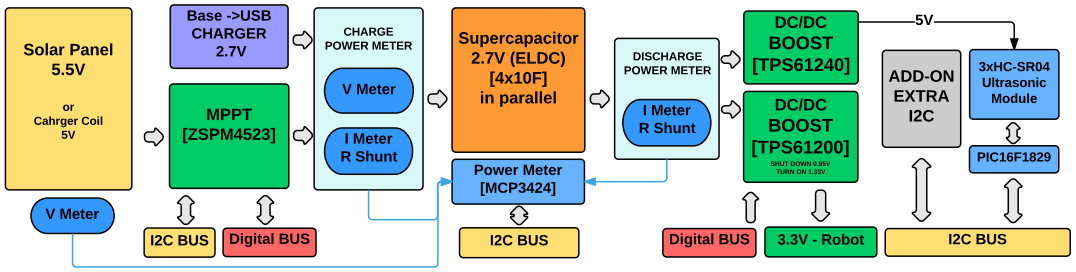

Figure 2.6: Components of the harvester module and types of communication - Supercapacitors;

The figure 2.7 shows the diagram of connections and components in case of using lithium battery.

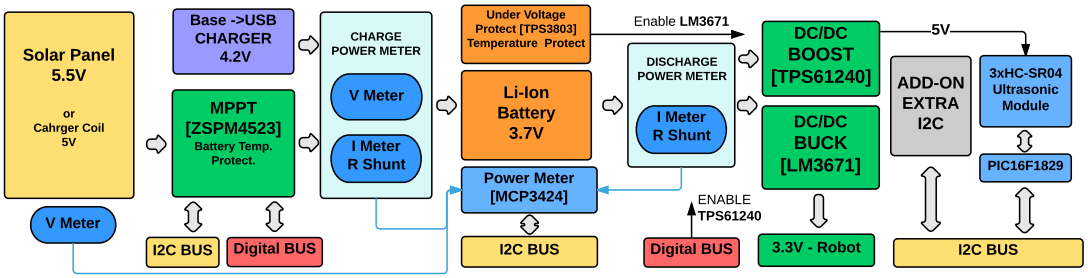

Figure 2.7: Components of the harvester module and types of communication - Lithium battery;

2.4 *Hardware*

2.4.1 Microcontroller ARM®-M0

The microcontroller used in the project is manufactured by Freescale® Semiconductor, we opted for the choice due to its characteristics and the existence of a low-cost development board that incorporates. The main features are:

- **Model** - ARM® CORTEX®-M0 - MKL25Z128VLK4;
- **Performance** - 48MHz, 16KB RAM, 128KB FLASH;
- **Peripherals** - 2xSPI, 2xI2C, 3xUART, 24xPWM, 6xADC (16Bits), 1xDAC (16Bits), 80 Pins, 66 I/O;
- **consumption** - *Run mode* $47uA/MHz$, *static power* $2uA$.

2.4.2 Sensors

In this section are reviewed all sensors which are integrated in the robot and its main features as well as some sample applications for each. Which were selected by comparing the cost, power consumption and the desired effect, all have low power technologies to minimize energy consumption.

Color sensor

The RGB color sensor used is produced by INTERSIL® manufacturer, model ISL29125 (Figure 2.8 (a)), communicates via I2C, integrates ultra low power technology and has high sensitivity in color detection. The resolution can be adjusted by software, can operate with 12 or 16 bit of resolution. It is positioned at the front of the base module along with two white high brightness LEDs. It allows color detection of specific objects or targets in performing tasks.

Proximity and light sensor

The proximity and light sensor used is produced by the Vishay® manufacturer, model VCNL4020 (figure 2.8 (b)), communicates via I2C and incorporates both functions in a single integrated circuit, the proximity sensor has a maximum range of 20cm and the current of LED emitter can be controlled by software. The light sensor operates in range of 0.25lx (Lux) to 16klx and has the noise flicker rejection capability at frequencies of 100Hz and 120Hz. Five sensors are exposed on the front of the base module with directions of twenty five degrees relative to each other, at the rear a sensor is placed at the center. They can be used to detect obstacles, walls, other robots, or follow light sources for the use of the solar panel.

Humidity and temperature sensor

The humidity and temperature sensor used is produced by the SENSIRION® semiconductor manufacturer, model SHT21 (figure 2.8 (c)), communicates via I2C and incorporates both functions in a single integrated circuit, the relative humidity sensor should be operated in the range of 5 to 90%RH and the maximum resolution is 12 bits. The temperature sensor should be operated in the range of -20ºC to 100ºC with a maximum resolution of 14 bits. It is placed on the sensor module and can be used to measure temperature and humidity.

Barometer

The barometer sensor used is produced by the BOSCH® semiconductor manufacturer, model BMP180 (figure 2.9 (a)), communicates via I2C and operates in a pressure range 300hPa (hectopascal) to 1100hPa, and is possible to know the temperature. The resolution can be set by software with options of 16 bits or 19 bits. The sensor is inserted into sensor module and through the values given we know the relative altitude at which the robot to sea level, this is used for the

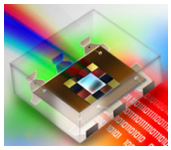

(a) ISL29125;

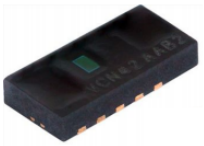

(b) VCNLl4020;

(c) SHT21;

Figure 2.8: RGB color sensor ISL29125, proximity and light sensor VCNL4020, Humidity and temperature sensor SHT21;

equation 2.8 with p is the pressure of the location of the robot and p_0 (example: 1013.25hPa) is the pressure at sea level.

$$Altitude = 44330 \left(1 - \left(\frac{p}{p_0}\right)^{\frac{1}{5.255}}\right) \tag{2.8}$$

Inertial sensor

The inertial sensor used is produced by the IvenSense® manufacturer, model MPU9250 (figure 2.9 (B)), communicates via I2C and contains an integrated gyroscope, a accelerometer and a magnetometer, each of these are three-dimensional. The use of the gyroscope can measure angular velocities around the three axes of the robot, with the accelerometer we can measure inclinations and linear accelerations and the magnetometer allows to measure magnetic fields, making it possible to know the orientation of the robot relative to the Earth's magnetic field. This sensor is placed on sensor module aligned exactly with the center of the robot.

Magnetic encoders

The magnetic encoders used are produced by the Ams® manufacturer, model AS5600 (figure 2.9 (C)), has a 12 bit resolution and communicates via I2C, analog signal or *Pulse Width Modulation* (PWM). This system is without mechanical contact and measures the absolute position of a magnet placed on the shaft of each motor. It can estimate the position of the robot by odometry.

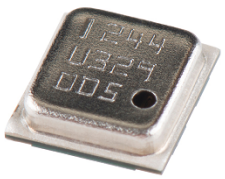

(a) BMP180;

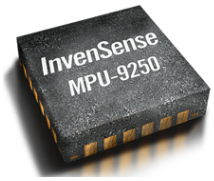

(b) MPU9250;

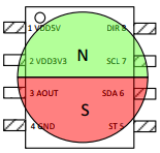

(c) AS5600;

Figure 2.9: Barometer BMP180, inertial sensor MPU9250, magnetic encoders AS5600;

Microphones

The robot includes three microphones integrated in the sensor module, it can analyze the waveform and amplitude of sounds in the environment. In the figure 2.10 we can see how they are positioned and the circuit is used.

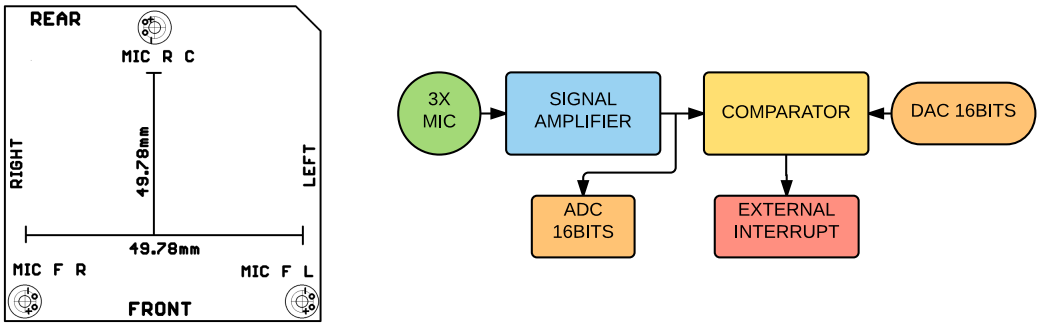

(a) Disposition of microphones in the module sensor;

(b) Diagram used for signal acquisition of the microphones;

Figure 2.10: Layout and signal acquisition diagram of microphones built into the robot;

Through the arrangement of microphones and signal acquisition circuit used, as well to know the waveform, you can know the orientation of the sound source using the triangulation method. The recognition of waveform is limited by the ADC sampling rate, to be able to reconstruct a signal with minimal losses it is necessary that the sampling frequency is at least double of the signal frequency. To work around the problem limiting the ADC sampling rate, a comparator module was added in the circuit, it can be set in the microcontroller software which the *Digital to Analog Converter* (DAC) value for comparison. With the use of comparator it is possible to know how much time there was between shots and estimate of the sound wave frequency. In a situation where a robot intends to know the position of the other robot relative to his position.It must send the information through infrared or radio emission. Using a sound emission buzzer. As soon the information is sent. It should start a lap timer.When the first external interruption trigger occurs, the time is measured between events, until all three microphones are reached.After the recognition of all the time relative to all three microphones are known, it is possible to know the distance and position of the other robot.

Ultrasonic Modules - SR04

The robot includes three ultrasonic modules integrated in the harvester module with 30 degrees offset, they can measure distances between $1cm$ and $4m$ with a resolution of about $4mm$. In the figure 2.11 we can see the module and performance test.

(a) Ultrasonic module HC-SR04;

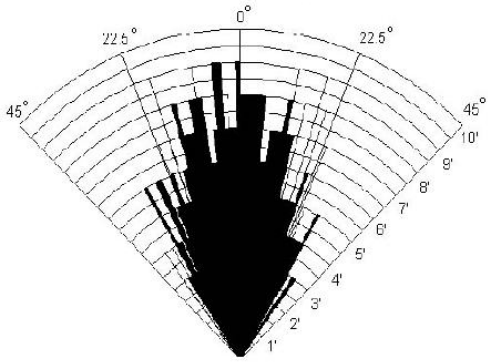

(b) Diagram used for signal acquisition of the microphones;

Figure 2.11: Ultrasonic module and performance test ;

This module on robot contain the PIC16f1829 that allow a interface between ultrasonics module and ARM® of robot. The protocol used is I2C, can be high-level function calls to find the distance of each sensor.

2.4.3 Actuators

In this section are reviewed all the actuators which are integrated in the robot and its main features and functionalities.

Motors

The robot traction system equipped with two brushed DC motors. They were chosen taking into account the small size and low power consumption. Added to the DC motor is a metal gearbox, thus providing additional mechanical strength. For the same engine there are several gearboxes, in this robot are used 100 RPM motors with maximum allowable voltage of 6 VDC. The driver used for the control is produced by the Texas Instruments® manufacturer, model DRV8838, incorporates an H-bridge that supports currents up to 1.8 A. The engine consumption is around 15 mA with no load application and about 100 mA with the shaft locked in tests carried out with a voltage of 3.3 V. For a better perception of the components described is shown in figure 2.12. Table 2.1 shows the type of DC motor behavior depending on the logic signals of the microcontroller.

Table 2.1: Logic signals from the microcontroller and effect produced in DC motor;

Signals uC			**Output Driver**		**Motor DC**
Nsleep	**PHASE**	**ENABLE**	**OUT1**	**OUT2**	**Function**
0	X	X	Z	Z	Coast
1	X	0	L	L	Brake
1	1	1	L	H	Reverse
1	0	1	H	L	Forward

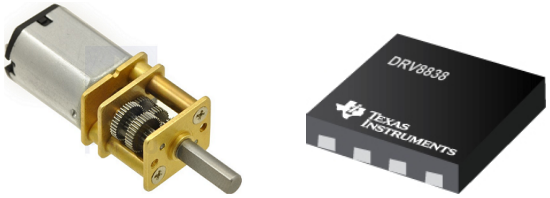

(a) Brushed DC motor; [22]

(b) Driver DRV8838;

Figure 2.12: Motor and driver used on the robot;

Buzzer

The buzzer used is produced by the PRO-SIGNAL® manufacturer, model ABT-410-RC (figure 2.13 (a)) and is placed on the base module. Its resonance frequency is 2.048 kHz, being the most intense emission. The control is effected by a PWM signal and the used driver is a *Metal Oxide Semiconductor Field Effect Transistor* (MOSFET). The buzzer may be used for example to generate audible alarms or spatial location.

RGB leds

The RGB LEDs used are produced by the CREE® manufacturer, model CLV1A-FKB (figure 2.13 (b)) and are strategically placed on the base module. An RGB LED is located in front of the robot and the other at the rear. The control of the digital signals are totally independent. The LEDs can be used for example to identify the position and orientation of the robot with a camera in tracking systems.

White leds

The white leds used are produced by the CREE® manufacturer, model CLM3C-WKW (figure 2.13 (c)), control is effected by a PWM signal and the used driver is a MOSFET. Is placed close to the color sensor and the main function is the projection of white light to the objects being subsequently reflected to the RGB color sensor.

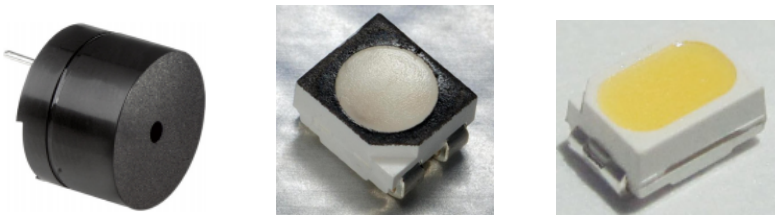

(a) Buzzer;

(b) RGB led;

(c) White led;

Figure 2.13: *Buzzer* ABT-410-RC, RGB led CLV1A-FKB, White led CLM3C-WKW;

2.4.4 Communication

The robot has integrated two forms of wireless communication, radio and infrared communication. They can be used to communicate between different robots or devices incorporating compatible hardware. It is also possible to communicate with a computer using a micro USB cable type B.

RF communication

The module used for the radio communication is produced by Nordic® semiconductor manufacturer, was chosen considering the maximum range, the cost and energy consumption. The model is the nRF24L01 and has the following characteristics:

- 2.4GHz GFSK RF *transceiver*;
- Low cost, 2 a 3 €;
- Low power consumption, *26uA em stanby*;
- Transmission 1Mbps to 2Mbps, power controllable by software;
- SPI communication.

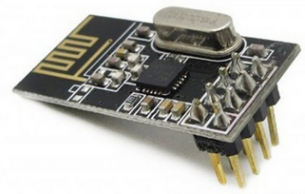

The maximum range varies with the signal power emitted, without attenuation it consumes 11.3 mA to transmit, and 12.3 mA at data receive. The maximum range is around twenty meters on open field.

Figure 2.14: Módulo *transceiver* nrf24l01;

Infrared communication

Infrared communication was developed to be simple to implement in software. The emission of the light beam is made with emitting LEDs controlled by two mosfet. In reception is used a modulated sensor produced by Vishay® semiconductor manufacturer, model TSOP38536. The figure 2.15 shows the operation of the communication.

The 36 kHz frequency PWM modulates the signal from the UART port, after being modulated the signal is sent and acknowledged by the receiver, which in turn makes the demodulation sending it directly to the RX pin of the UART port of microcontroller. In this type of application the baud rate must be low so that the modulation area can take the maximum pulse width. Tests were made with the baud rate to 2400 bps and the results were satisfactory, resulting in a range of 1.5 meters without data loss. While it is advisable to check data using appropriate techniques.

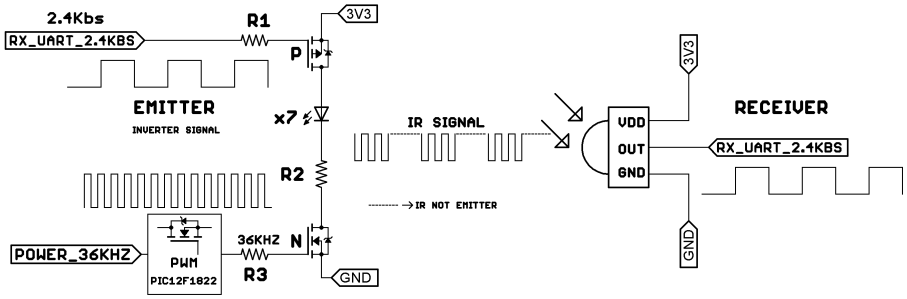

Figure 2.15: Communication diagram by infrared, emission - reception;

2.4.5 Data storage

In autonomous robots it is important have data storage solutions. The EEPROM placed in base module and communicate via $I2C$, it allow fast and easy access of data. A Micro SD CARD was incorporated into the base module, communicates via SPI and stores a large amounts of data that can be consulted using a microcontroller or a computer through a card reader. Robot ID, PID controller gains, sensor measurement results data and others can be stored.

2.4.6 Energy harvesting module

The energy harvesting module consists of several components and they are suitable for each specific function, in this section presents the components used and what are its main features.

Solar panel

The solar panel used on the robot must take into account its size and the voltage amplitude at peak power transfer (Vpmax). Due to the characteristics of the used MPPT, the voltage at the point of maximum power transfer (Vpmax) should be higher than 0.3 V with the voltage of storage used. The storage solution in lithium batteries and the value Vpmax of the panel should be at least $4.2 + 0.3 = 4.5V$. The use of supercapacitors the Vpmax value should be at least 3.2V, voltage to which the MPPT starts. The size of the solar panel should not exceed the size of the harvester module, that is six centimeters aside.

MPPT

The MPPT used is produced by the ZMDI® manufacturer and model varies depending on the type of energy storage used, in the case of use of supercapacitors the module is SZPM4523 and the use of lithium batteries is ZSPM4521. The MPPT obtain the point of maximum power transfer and incorporates a DC/DC converter that controls the charge storage. The communication of these integrated circuit with the microcontroller is through the I2C protocol and may

change some parameters such as maximum load current and maximum temperature of the lithium battery during charging. The enable can be controlled by software, using a digital signal connected to a switching MOSFET.

Supercapacitors / Lithium battery

The robot is designed so as to allow the use of two types of energy storage, supercapacitors or lithium batteries. The supercapacitors must have a maximum voltage of 2.7V and should be chosen having into consideration the available space on the PCB, four is a maximum number of units that can be welded. On the use of lithium batteries should be 3.7 V/cell and its size shall not exceed the harvester module. If integrate temperature sensor (thermistor) must be connected directly to MPPT, otherwise, should be welded on top of the module harvester one thermistor which is in permanent contact with the battery. As the PCB is the same for both storage solutions, are welded only the necessary components, verification of solder jumpers that select the indicated circuit is essential. To understand which solder jumpers must be welding, see table 2.2;

Table 2.2: Storage type used and associated solder jumpers - harvester module;

Storage Mode	**Solder Jumper Select**									
Supercapacitor	SJ2	SJ4	SJ5	SJ6	SJ7	SJ9	SJ10	SJ11	SJ12	SJ13
Battery Li-Ion	SJ3	SJ4	SJ5	SJ6	SJ7	SJ8	SJ10	SJ11	SJ12	SJ13

DC/DC converters

The DC/DC converters used are produced by Texas Instruments® manufacturer and model/topology varies depending on the type of energy storage used, the use of supercapacitors model is the TPS61201 (boost) and the use of lithium batteries model is the LM3671 (buck). The boost converter used allows a maximum current 1.35A input, it is possible trough via a digital signal to control the power save mode, it still contains a system to use a voltage divider to set the threshold that must shut down. The buck converter used allows a maximum current at 600mA output, for the lithium battery does not fully discharge was added an integrated circuit, model TPS3803-01, that from a voltage divider is possible to define the voltage threshold above which the battery supports without damage.

2.4.7 Power management

With the use of energy harvesting in robot is important that this integrates the power management systems, for this was designed a power meter to know the power supplied to the battery, the power consumed by the robot and also the voltage to the solar panel terminals. Once the values are known, it is possible to estimate whether a particular task may or may not be performed/completed. The consumption minimization can be done in several ways, some examples

are: the motor speed control; The periodic rate control communication between robots; Control of LEDs; Peripheral placement in sleep mode; Power control of the bus where peripherals are connected. To understand the last option is shown the figure 2.16, where all devices using I2C and SPI to communicate with the microcontroller and the system of microphones and infrared receiver.

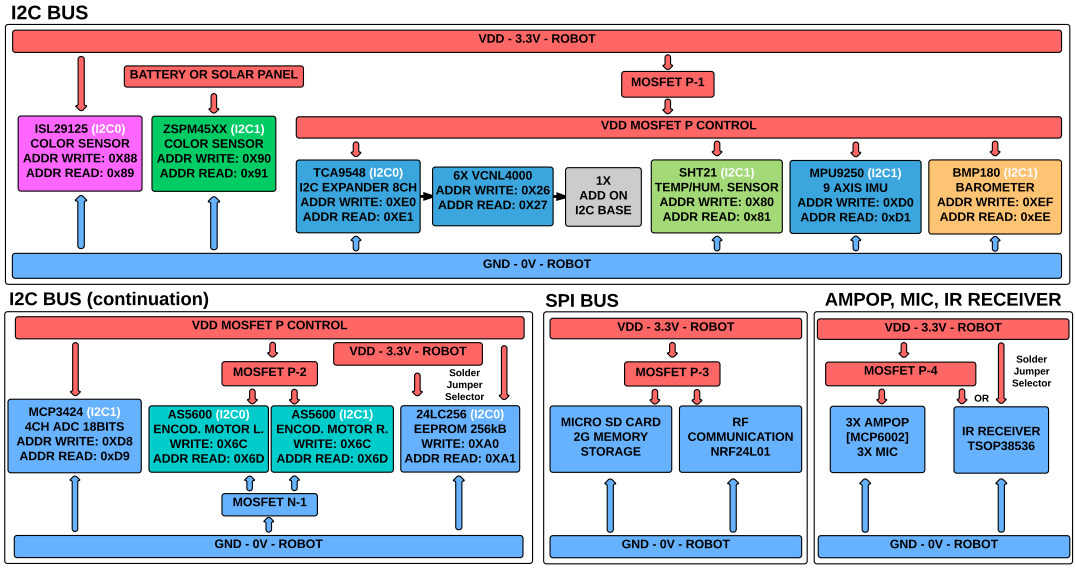

Figure 2.16: Bus power control diagram of I2C and SPI components, peripheral distribution to I2C0 and I2C1 channels, microphones and infrared receiver, system power control;

The MOSFETs of figure 2.16 can be controlled by software, the MOSFET P-1 controls the power of the I2C bus, the MOSFET P-3 controls the power of the SPI bus communication. The MOSFETs P-2 and N-1 control the power of the encoders, were placed because consumption was significant (about 5 mA each). The MOSFET P-4 controls power to the microphone circuit, and there is the possibility of supply the infrared circuit receiver through a solder jumper on PCB. MOSFET P-5 controls power to the oscillator circuit of 36kHz, carrier wave of infrared communication. The color sensor does not have any kind of power control, because during the test phase went into failure impairing the I2C0 communication bus.

Power meter

The power meter developed is composed of an ADC Microchip® manufacturer, model MCP3424, it contains four differential channels of 18-bit and an internal amplifier with gain up to eight. For the voltage reading were used voltage dividers and an external voltage reference (MCP1525). For current reading it was used traditional method which uses a precision power resistor in which the ADC does the voltage drop reading at its terminals. The figure 2.17 shows the circuit used.

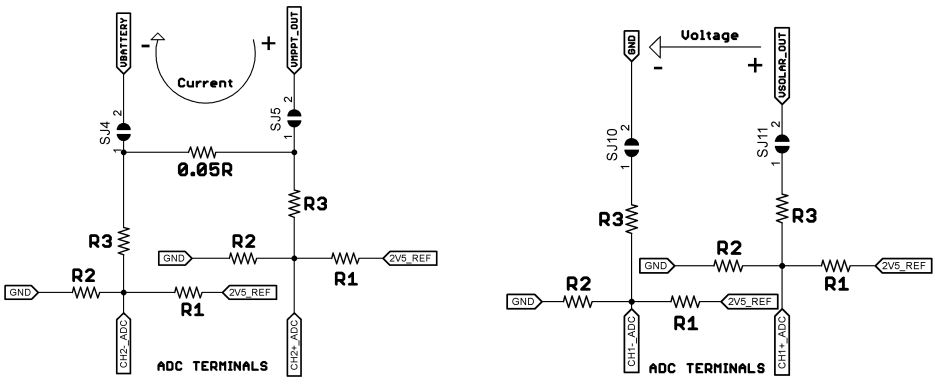

(a) Current reading circuit; (b) Voltage reading circuit;

Figure 2.17: Circuits used for reading voltage and current in the differential ADC;

Analyzing the circuit it is possible to write the equation 2.9 that relates the value measured by the ADC to the voltage to the circuit terminals.

$$Vin_{circuit} = -\frac{((-Vin_{adc}/Ganho)(R1R2 + R1R3 + R2R3))}{(R1R2)} \tag{2.9}$$

One should take into account the gain in reading, since it does not enter into the calculations will influence the result. To know what the current value of the application is necessary Ohm's Law, in which $I = Vin_{circuit}/R$, with $R = 0.05Ohm$.

Figure 2.17 are visible solder jumpers (SJx), were placed in order to make the simple calibration of the ADC, welds are removed and the circuit is isolated from the robot. Should be adjusted to offset voltage and placed a constant current loop in order to calibrate the value of rshunt (power resistance). Calibration must be done when you want to do readings with more precision. Data on performed calibration can be saved on the robot memory card.

2.4.8 Robot charging

In situations where there is insufficient solar radiation for the solar panel to charge the battery, it is necessary to charge the robot in another form. Three forms of charging were designed, through a micro USB type B cable, induction, or by using the spring pins placed in front of the robot. In this section are explained in detail the three forms of charging. The diagram 2.18 illustrates the robot charging architecture.

USB charging

The USB charging uses the 5V available at the door of communication. The input current is limited to 400mA and is possible to adjust through a resistance

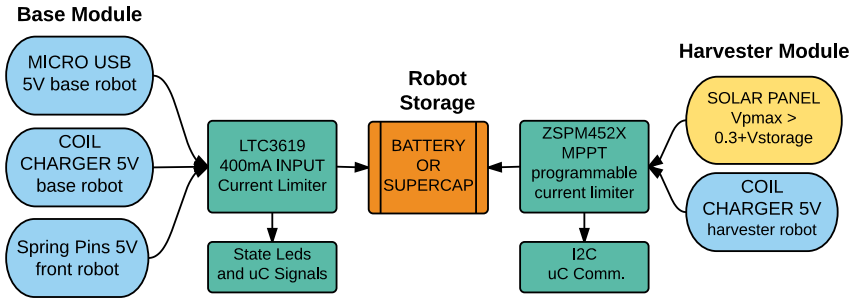

Figure 2.18: Robot charging methods;

placed between a pin of LTC3619 and ground of circuit. The integrated circuit is connected via digital signals to the microcontroller allowing to know the charge state. The table 2.3 relates the state of the digital signals and the state of charge.

Table 2.3: Digital signals from the LTC3619 and its state of charge;

Microcontroller Signals		**Storage**
USB Connect Signal	**Li-Ion or SuperCap State Chager**	**Final State**
High	High	Charging
High	Low	Charged
Low	X	Disconnected

Wirless charger

The wireless charging allows non existence of physical connections to the robot. The receiver coil may be placed on base module directly connected to LTC3619, or can be placed in the harvester module thus replacing the solar panel, in this case connected to the MPPT. The coil should contain integrated rectification and regulation circuits as the robot prepared to receive 5VDC.

Spring Pins charging

In front of the robot are two spring pins visible in Figure 2.1 may be used to charge the robot when there is contact with two conductive strips supplied with 5VDC. The polarity must be taken into account, because if changed can damage some integrated circuits.

2.5 Programming ARM®mbed^{TM} platform

All programming of the robot can be performed online using the programming ARM®mbed^{TM} [23] platform, incorporates a text editor and an online compiler, the used programming language is C/C++. By using mbed.h library is possible to access a set of high-level functions for many different functionalities of the microcontroller. In addition to storing the codes online in the user's account is

an open source platform that allows easy access and sharing of libraries. One of the advantages of using it is the speed the development of prototypes, it is not necessary to waste time installing IDE, compilers and others. The programming environment can be seen in figure 2.19;

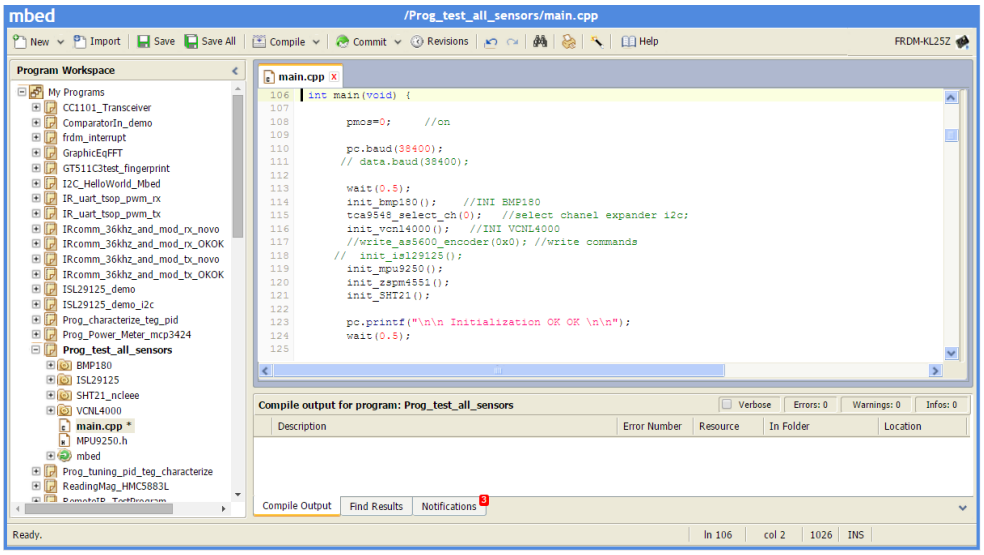

Figure 2.19: Graphical environment of online programming ARM®mbed^{TM} platform;

ARM®mbed^{TM} platform supports a wide range of development boards manufactured by ARM® microcontroller brands. In this case the chosen development board was the Freescale® manufacturer, model FRDM-KL25Z (figure 2.20). There is also the possibility to program offline using the IDE as Kinetis design studio, KEIL MDK uVision, CodeWarrior and others. To program the microcontroller of robot is used the development board , it is an easy and low cost solution. The pins of the SWD connector available are attached to the robot connector. For more detail appendix 3 should be consulted.

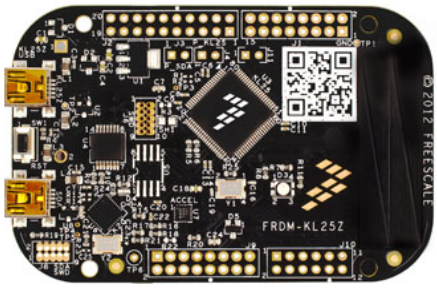

Figure 2.20: Development board, Freescale® - FRDM-KL25Z;

Chapter 3

SWD - Mode of programming

This chapter introduces the method used to program the developed robot. It is explained in detail the steps needed to program and connect between robot and development board (programmer).

3.1 Required hardware

To program the robot is needed hardware , that is, a programmer and the physical connection between the two devices. Figure 3.1 shows the diagram for programming.

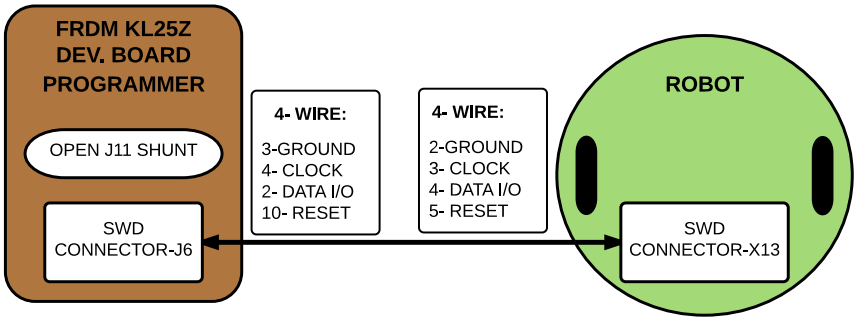

Figure 3.1: Robot programming diagram, programmer - connection - robot;

The programmer used is integrated into the development board used during the project design, FRDM-KL25 (Figure 2.20) manufactured by Freescale®. The SWD module is used to program the robot and has been adopted because of their cost to be significantly lower than a specific universal programmer. However to use the development board programming is necessary to change the hardware. The steps to be followed are the images 3.2, 3.3 e 3.4.

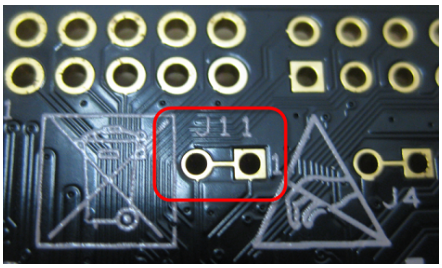

Figure 3.2: Step 1: Detection of solder jumper - SJ11;

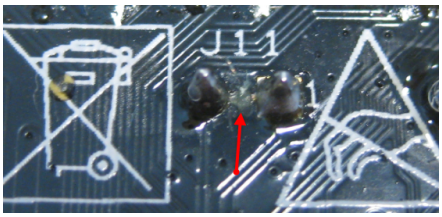

Figure 3.3: Step 2: Cut the solder jumper - SJ11;

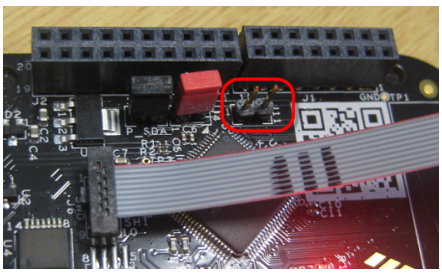

Figure 3.4: Step 3: Welding of header 2.54mm-pitch on the solder jumper SJ11;

To program the robot is necessary to make the physical connection and open the SJ11 jumper to isolate the microcontroller. The physical connection is between the J6 connector programmer and X13 robot.

3.2 Drivers ad Firmware

To be able use ARM®mbed^{TM} [23] platform is necessary putting firmware on FRDM kl25Z and install USB drivers on computer.

Drives USB: https://developer.mbed.org/handbook/Windows-serial-configuration

Firmware FRDM KL25Z: https://developer.mbed.org/platforms/KL25Z/

An important note is that the operating system Windows 8 sometimes does not recognize the board with the original firmware and it is advisable to put the firmware on the board using another operating system. After all the described steps, will appear on the computer an image 3.5 named MBED^{TM}.

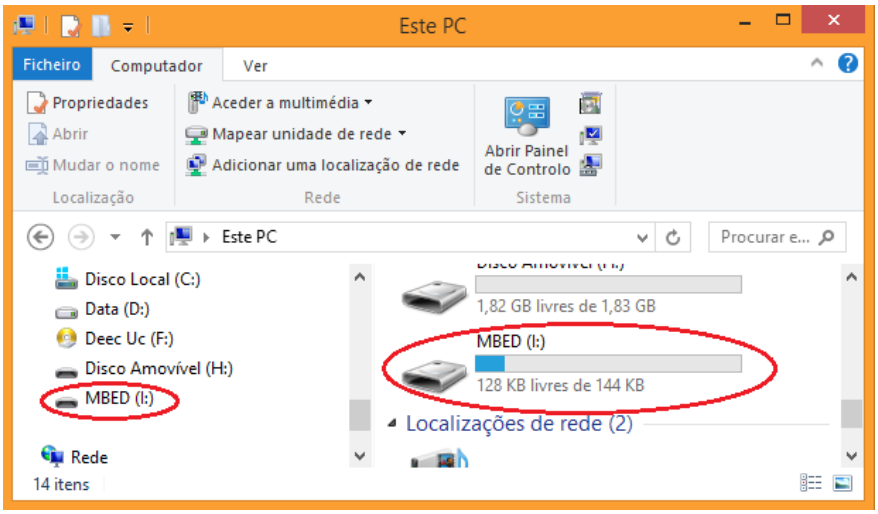

Figure 3.5: Disk created by the board FRDM KL25Z ;

After compiling the file on the online ARM®mbed^{TM} platform it automatically downloads to your computer, it is necessary to drag the file into the mbed^{TM} disk drive and then press the RESET button on the board or robot.

Chapter 4

Quick Start Guide

The quick start guide is designed to integrate the user with the developed robot, in the first phase the caption of the essential components, then a list of ordered instructions so that the user can start the robot successfully and finally a list of frequent questions and respective answers.

4.1 Caption of the essential points

The following figures show the caption of each module that compose the robot, finally shows the final assembly of all modules.

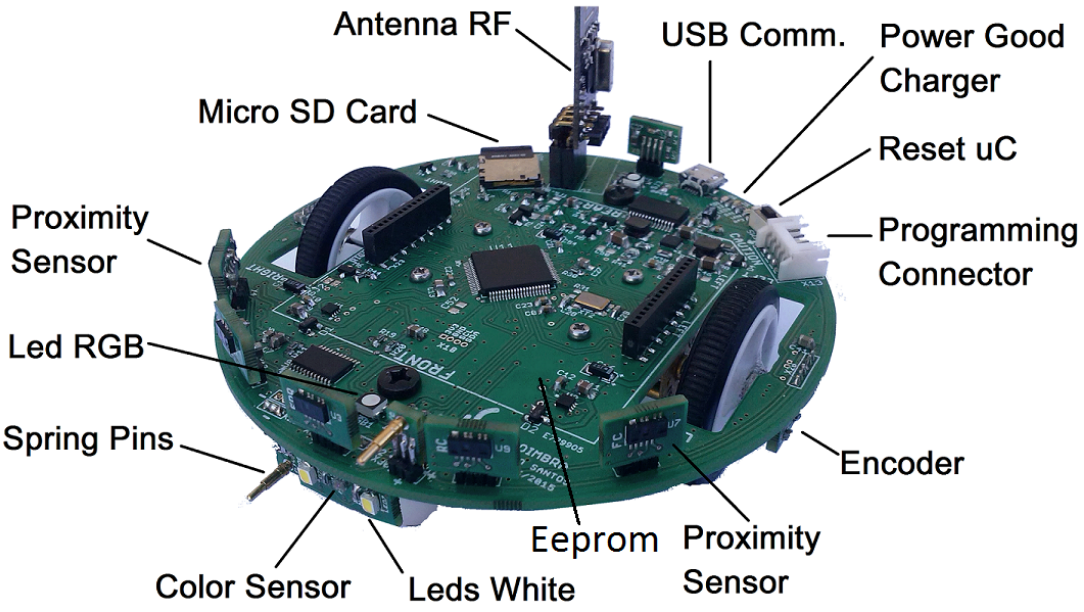

Figure 4.1: Layer top - base module;

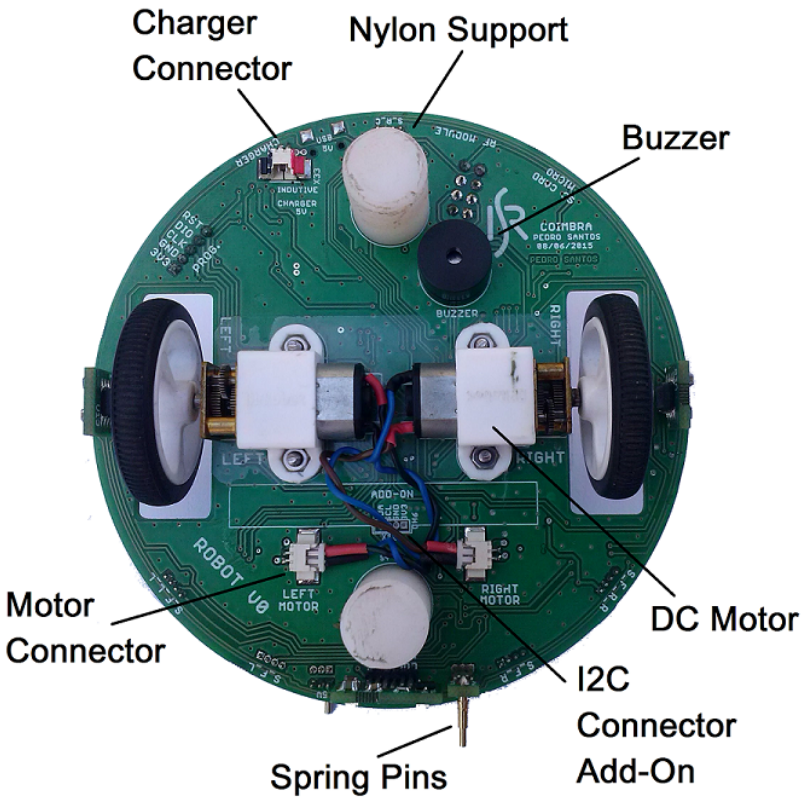

Figure 4.2: Layer bottom - base module;

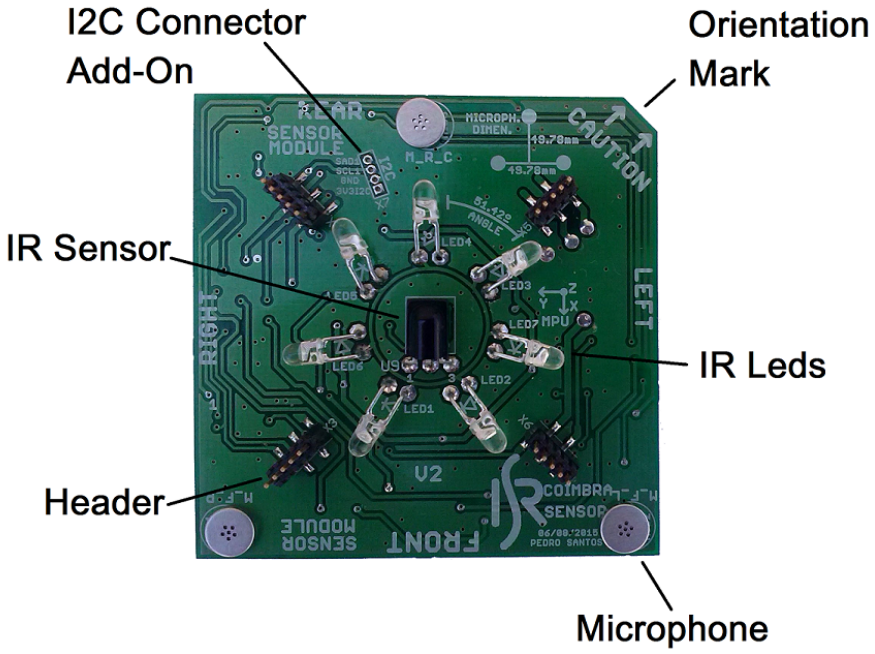

Figure 4.3: Layer top - sensor module;

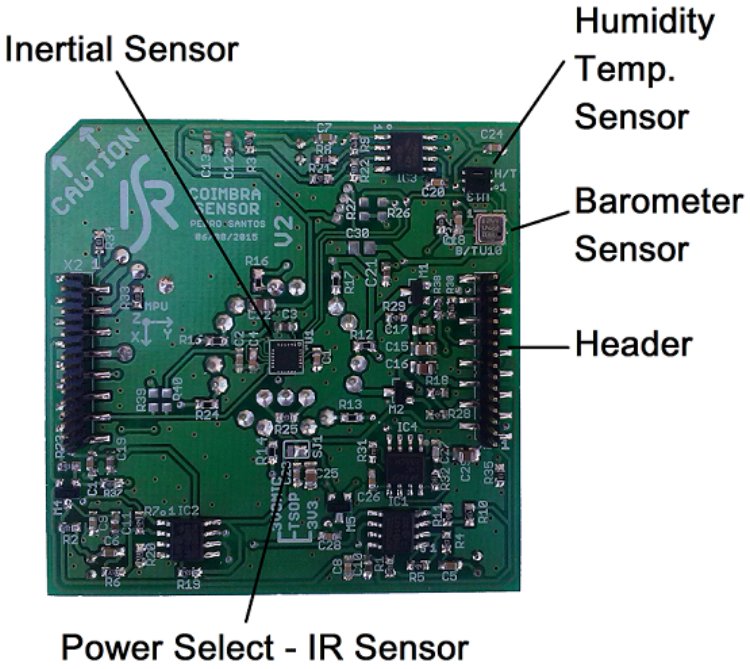

Figure 4.4: Layer bottom - sensor module;

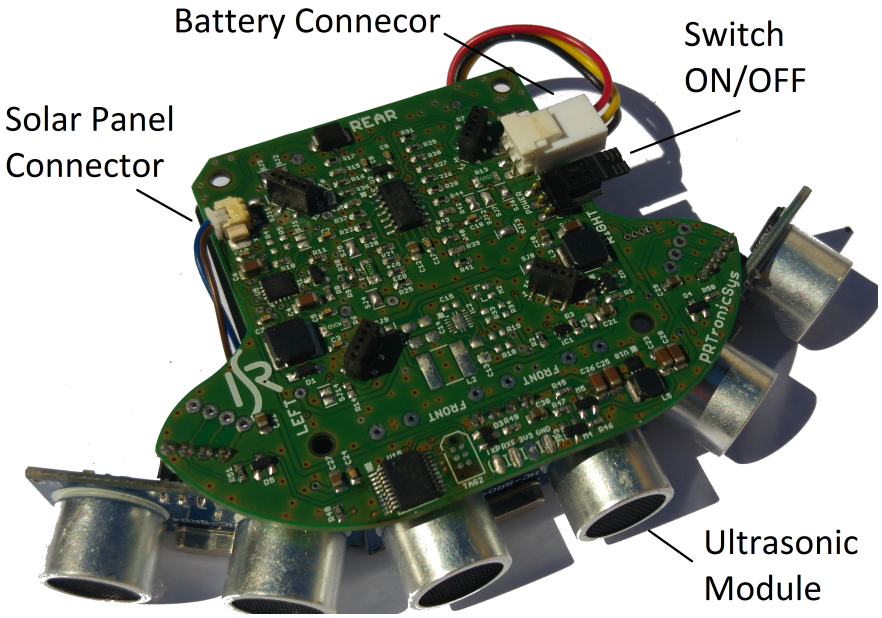

Figure 4.5: Layer bottom - harvester module;

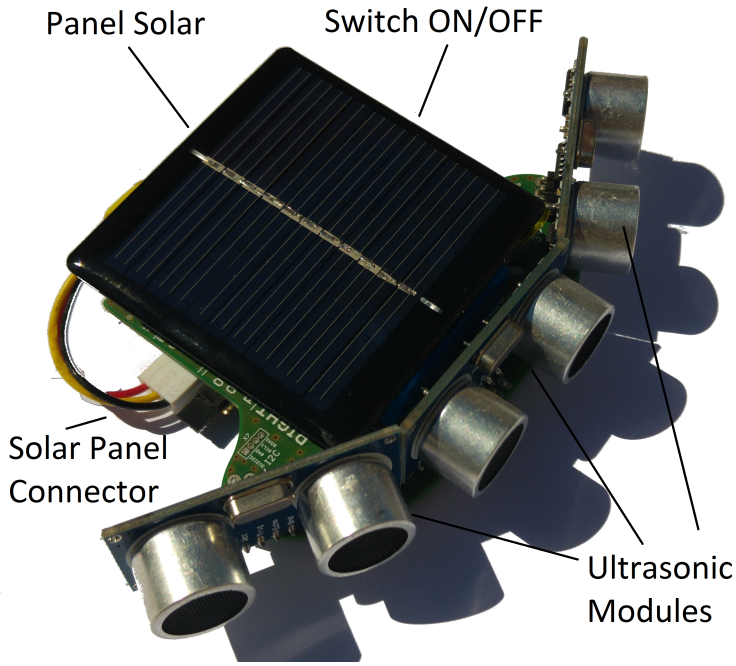

Figure 4.6: Layer top - harvester module with solar panel;

Figure 4.7 shows the final assembly with all modules, the components that integrates the robot can get damaged in case an exchange occurs.

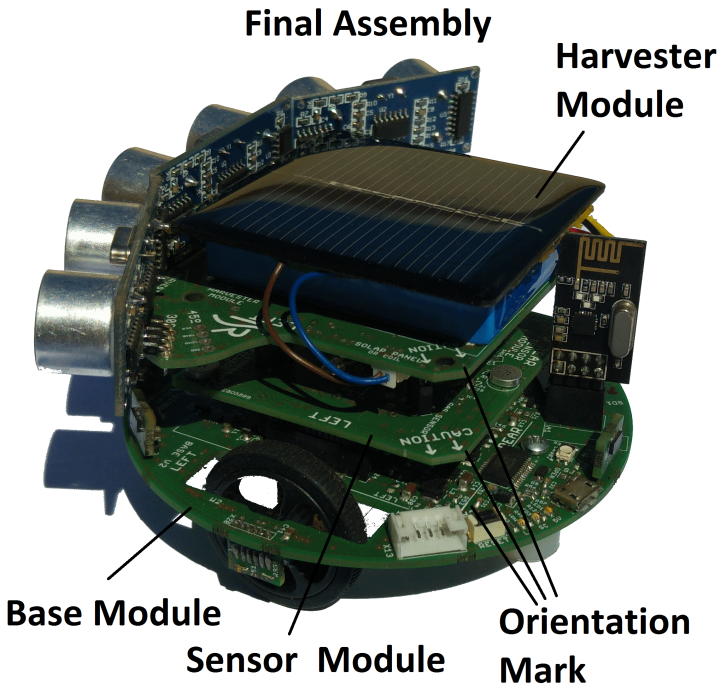

Figure 4.7: Final assembly with all modules;

4.2 Instructions and Procedures

After they acquired the modules that the robot composes, initiate the following instructions:

1. Assembly of modules as shown in figure 4.7, taking into account the orientation of each module;
2. Connect the solar panel to the connector (Solar Panel Connector) shown in figure 4.5, taking into account the correct polarity;
3. When using the lithium battery, it must be connected to the connector (Battery Connector) shown in figure 4.5, taking into account the correct polarity;
4. Check that the connectors of the motors (Motor Connector) are connected to the base module, figure 4.2;
5. After the robot is mounted, the charging must be made by one of the possible solutions, for example choose to use a cable Micro USB Type B connected to the computer.
6. To make the programming, the drivers must be installed on your computer, found on online page:

   - https://developer.mbed.org/handbook/Windows-serial-configuration

   Later on the firmware needs to be downloaded on the online page:

   - https://developer.mbed.org/platforms/KL25Z/

   Windows 8 sometimes does not recognize the card with the origin firmaware, a possible solution is to make the operation in another operating system;
7. Connect the programmer board FRDM-KL25 USB to the computer and the programming cable to robot connector (Programming Connector), shown in figure 4.1;
8. Open the program on the ARM®mbed^{TM} platform, compile and verify in download folder of the computer;
9. Drag the file from the download folder to drive disk of mbed^{TM} on my computer;
10. Press the reset button (*Reset uC*) shown in figure 4.1.

After steps are completed the program will run on the robot.

4.3 Frequently Asked questions

In this section we present the solutions of frequently asked questions that may exist when using the robot.

Below is the list of questions and answers to the problem:

1. **The robot does not run even when the switch ON/OFF is ON?**

   - Should again confirm that the switch ON / OFF is in the ON position, if so, then put the robot on charge by placing the switch in the OFF position and wait for the LED (Power Good Charger) to turn off. Then put switch in the ON position, the robot will work;

2. **The robot does not charge from the *Universal Serial Bus* (USB) computer?**

   - The cable connecting the robot to the computer should be replaced. If the problem continues you should test a USB of another computer;

3. **Communication between the robot and the computer does not work properly?**

   - The Baud Rate communication speed that is set in both the robot and the computer should be reviewed. If the problem persists, the USB cable must be changed;

4. **One motor or both motors are not working properly?**

   - You should check the motor connector on the bottom of the base module, figure 4.1, If the problem persists, probably the issue is in the developed firmware, a simple code should be tested to check motor;

5. **It is not possible to program the robot?**

   - Check on My Computer if the disk FRDM-KL25 board appears, if so, the problem may be the link between the programmer board and the robot, ie the physical link must be reviewed, noting the connector (Programming Connector) is seated and the strands appear to be cut. If there are defects, repair following the circuit;

6. **A sensor does not work correctly?**

   - There is probably an error in the code developed, it is advisable to download a simple code of the respective sensor and evaluate the results, if the problem is not solved the hardware is damaged. The MOSFET that supply the I2C bus and the sensor must be checked;

7. **The MPPT does not respond to I2C commands?**

    - The MPPT only responds to commands sent by I2C properly if there is enough light on the solar panel, ie it is necessary to expose the robot to solar radiation to write or read on the MPPT;

8. **The MICRO SD CARD does not work?**

    - The MICRO SD CARD should be formatted in **FAT** and its capacity should not exceed 2GB, the power to the BUS SPI has to be active.

9. **The RF antenna does not work?**

    - Check if the power of the SPI bus is connected, if the problem persists, a new simple code must be downloaded to the robot to evaluate the behavior;

10. **The direction of a module was changed and the robot does not work?**

    - Contact the responsible for the project in order to assess the damage caused, for possible repair.

Bibliography

[1] R. Allan, *Energy Harvesting Powers Wireless Sensor Networks In Industrial Apps*, Sep 2012. http://electronicdesign.com/4g/energy-harvesting-powers-wireless-sensor-networks-industrial-apps.

[2] R. C. U. B. R. D. C. M. M. C. S. G. de Petris Calogero Maria Oddo, *Piezoelectric Energy Harvesting Solutions*, 2014. http://www.mdpi.com/1424-8220/14/3/4755/pdf.

[3] J. C. Quadrado, *Medição da radiação solar*, Sep 2008. http://www.energiasrenovaveis.com/DetalheNoticias.asp?ID_conteudo=102&ID_area=15.

[4] M. Ângelo Silveiro Valente, *Caracterização Automática de um Painel Fotovoltaico*, 2011. http://run.unl.pt/bitstream/10362/6110/1/Valente_2011.pdf.

[5] F. M. González-Longatt, *Model of Photovoltaic Module in Matlab*, 2005. http://matlabproject.ir/forms/files/618671.pdf.

[6] M. O. J. Paul and R. Zhao, *A comparative study of Lithium-Ion Batteries*, May 2010. http://www-scf.usc.edu/~rzhao/LFP_study.pdf.

[7] F. Hoffart, *Proper Care Extends Li-Ion Battery Life*, Abr 2008. http://powerelectronics.com/site-files/powerelectronics.com/files/archive/powerelectronics.com/portable_power_management/battery_charger_ics/804PET22li-ion-battery-life.pdf.

[8] A. S. R. Gallay, *Properties and applications of supercapacitors From the state-of-the-art to future trends*, 2000. http://www.garmanage.com/atelier/root/public/Contacting/biblio.cache/PCIM2000.pdf.

[9] I. ICillinois Capacitor, *Supercapacitors*. http://www.illinoiscapacitor.com/pdf/Papers/supercapacitors.pdf.

[10] J. Carpenter and Y. R. T. Instruments, *Fundamentals of ambient energy transducers in energy harvesting systems*, Mar 2012. http://www.ecnmag.com/articles/2012/03/fundamentals-ambient-energy-transducers-energy-harvesting-systems.

[11] P. das Energias Renováveis, *Tecnologias: Paineis Fotovoltaicos (PV)*, Mai 2015. http://www.energiasrenovaveis.com/DetalheConceitos.asp?ID_conteudo=43&ID_area=8&ID_sub_area=26.

[12] A. Khaligh and O. Onar, *Energy Harvesting: Solar, Wind, and Ocean Energy Conversion Systems*. Energy, Power Electronics, and Machines, CRC Press, 2009.

[13] S. Spataru, *Experiment Based Teaching of Solar Cell Operation and Characterization Using the SolarLab Platform*, 2014. http://vbn.aau.dk/ws/files/198852776/IWTPV14_Solarlabv4.pdf.

[14] A. Technologies, *IV and CV Characterizations of Solar/Photovoltaic Cells Using the B1500A*, 2009. http://www.ccontrols.ch/cms/upload/applikationen/Solar-Cell/5990-4428EN.pdf.

[15] F. Spertino and J. Akilimali, "Are manufacturing 2013; v mismatch and reverse currents key factors in large photovoltaic arrays?," *Industrial Electronics, IEEE Transactions on*, vol. 56, pp. 4520–4531, Nov 2009.

[16] A. M. EPRI, *Emerging Technologies Enable "No Regrets" Energy Strategy*, Jan 2013. http://www.powermag.com/emerging-technologies-enable-no-regrets-energy-strategy/?pagenum=8.

[17] M. Whittingham, "History, evolution, and future status of energy storage," *Proceedings of the IEEE*, vol. 100, pp. 1518–1534, May 2012.

[18] S. Netherlands, "Electric vehicle integration into modern power networks," in *Electric Vehicle Integration into Modern Power Networks*, 2196-3185, p. 325, Springer Netherlands, 2013.

[19] L. Global, *Lithium-ion Battery Overview*, May 2012. https://www.lightingglobal.org/wp-content/uploads/bsk-pdf-manager/67_Issue10_Lithium-ionBattery_TechNote_final.pdf.

[20] L. B. R. 2007, *Capacitors and Capacitance*, 2007. http://www.physics.byu.edu/faculty/rees/220/book/lesson6.pdf.

[21] P. A. M. e Silva, *SUPERCONDENSADORES*, 2013. https://www.google.pt/url?sa=t&rct=j&q=&esrc=s&source=web&cd=1&cad=rja&uact=8&ved=0CB8QFjAAahUKEwj90ZKB6enHAhWHzxQKHSYLCn8&url=http%3A%2F%2Frecipp.ipp.pt%2Fbitstream%2F10400.22%2F6271%2F1%2FDM_PedroSilva_2013_MEEC.pdf&usg=AFQjCNFpYygLfhfOM14d5a0lzifAoz2mUw&sig2=5Y15vtvEhdae9R6Ck8X4nQ.

[22] Nicegear, *Pololu Micro Metal Gearmotor HP*. https://nicegear.co.nz/robotics/pololu-micro-metal-gearmotor-hp-10001/.

[23] A. mbed, *ARM mbed Developer Site*. https://developer.mbed.org/.

Appendix A

Powers Meter Calibration

This appendix presents the calibration method used for the robot power meter. The developed power meter is composed by one ADC and precision resistances (0.1% and 0.5%). The calibration is intended to compensate the error so that the measurement is more precise.

A.1 Hardware changes

To implement the adopted calibration method is necessary to isolate the ADC from the remaining circuitry of the PCB, the solder of jumpers is removed and welded external wires as shown in figure A.1.
Note: The harvester module shoes in figure A.1 not include three ultrasonic sensors, however, the procedure is similar of the actual harvester module.

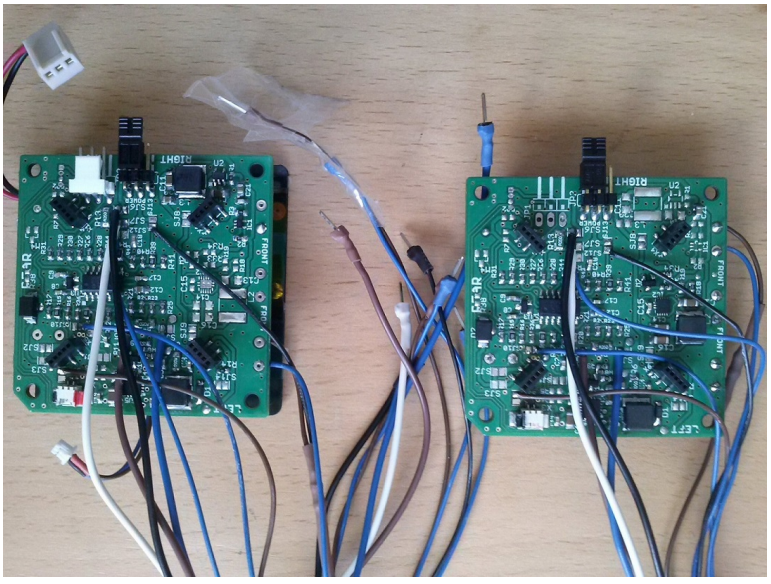

Figure A.1: Auxiliary wires for calibration of power meters;

The wires used for the voltmeter has a section of 0.25mm^2 and the wires used for the ammeter have a section of 0.5mm^2 to minimize the voltage drop. The

welding must be done carefully so there are no errors in the connections or short circuits that connect the ADC the rest of the circuit PCB.

A.2 Calibration method

To calibrate the power meter is used a simple method that consists in performing the following steps:

1. Placing the voltmeters wires in short-circuit and ammeters wires in open circuit;
2. Measuring the actual current and voltage values are called offset values;;
3. If the offset values are positive they should be subtracted from the value read or if they are negative must be added subsequently getting the current measures all zero.
4. Applying a constant voltage or current, measured by a high precision calibrated system;
5. Register of values acquired by the adc and the measured equipment, making the division between the value of the measured equipment and the value read by the adc, thus resulting of the multiplicative factor error.
6. Multiply the multiplicative factor of error by the value read. Resulting the following expression: $FinalValue = (ReadValue \pm offset) \times MultiplicativeFactor$.

Appendix B

Scheme, PCB, Bill of Material

This appendix shows a full scheme of the printed circuit board and the bill of material of the mobile developed robot.

B.1 Schematic

B.1.1 Base module scheme

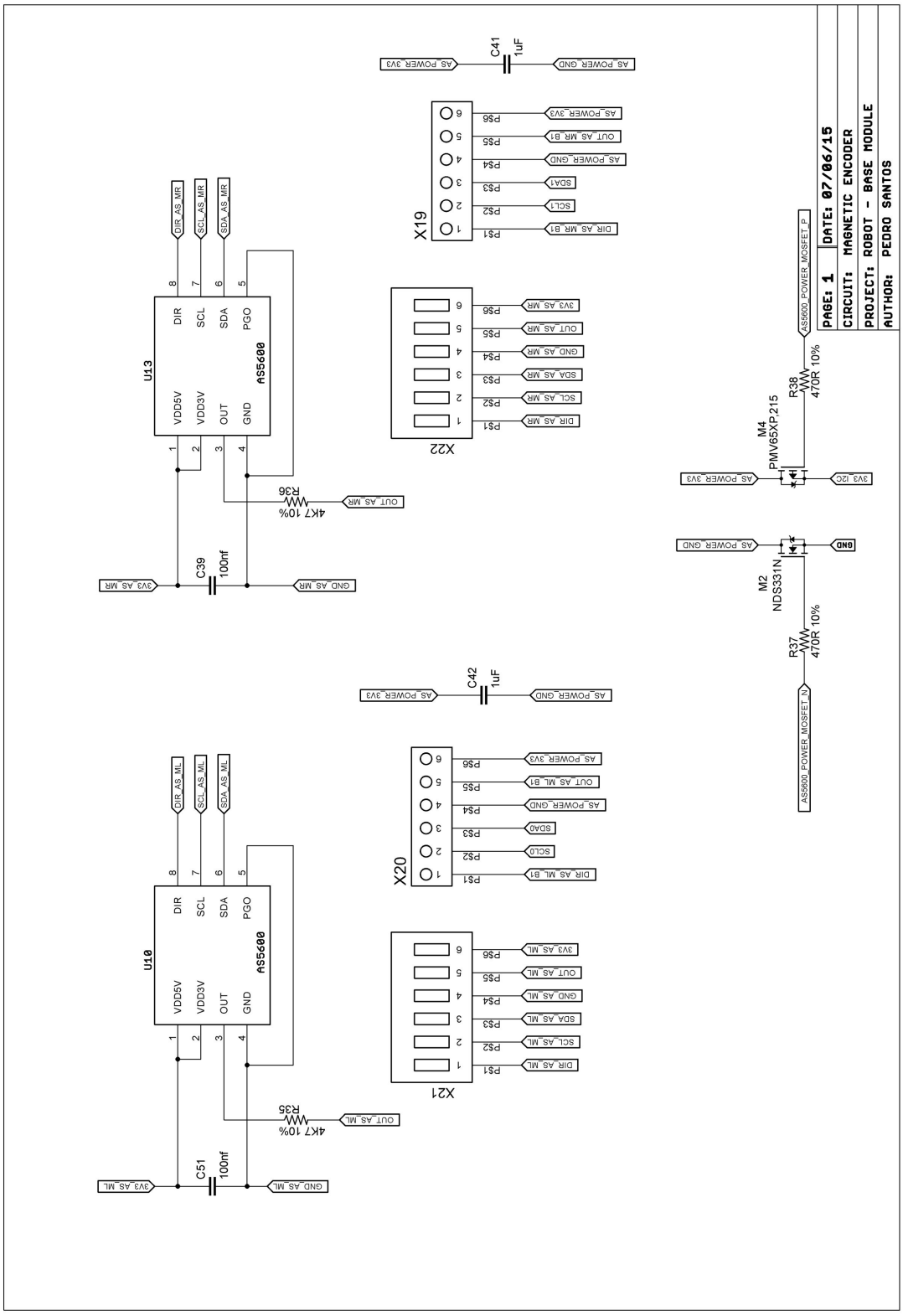
PAGE: 1
DATE: 07/06/15
CIRCUIT: MAGNETIC ENCODER
PROJECT: ROBOT - BASE MODULE
AUTHOR: PEDRO SANTOS
AS5600_POWER_MOSFET_P
AS5600_POWER_MOSFET_N
M4
PMV65XP,215
M2
NDS331N
R38
470R 10%
R37
470R 10%
AS_POWER_3V3
AS_POWER_GND
3V3_I2C
GND
C41
1uF
C42
1uF
X19
X20
X21
X22
DIR_AS_MR_B1
SCL1
SDA1
OUT_AS_MR_B1
3V3_AS_MR
OUT_AS_MR
GND_AS_MR
SDA_AS_MR
SCL_AS_MR
DIR_AS_MR
DIR_AS_ML_B1
SCL0
SDA0
OUT_AS_ML_B1
3V3_AS_ML
OUT_AS_ML
GND_AS_ML
SDA_AS_ML
SCL_AS_ML
DIR_AS_ML
U13
U10
AS5600
DIR
SCL
SDA
PGO
VDD5V
VDD3V
OUT
GND
R36
4K7 10%
R35
4K7 10%
C39
100nf
C51
100nf

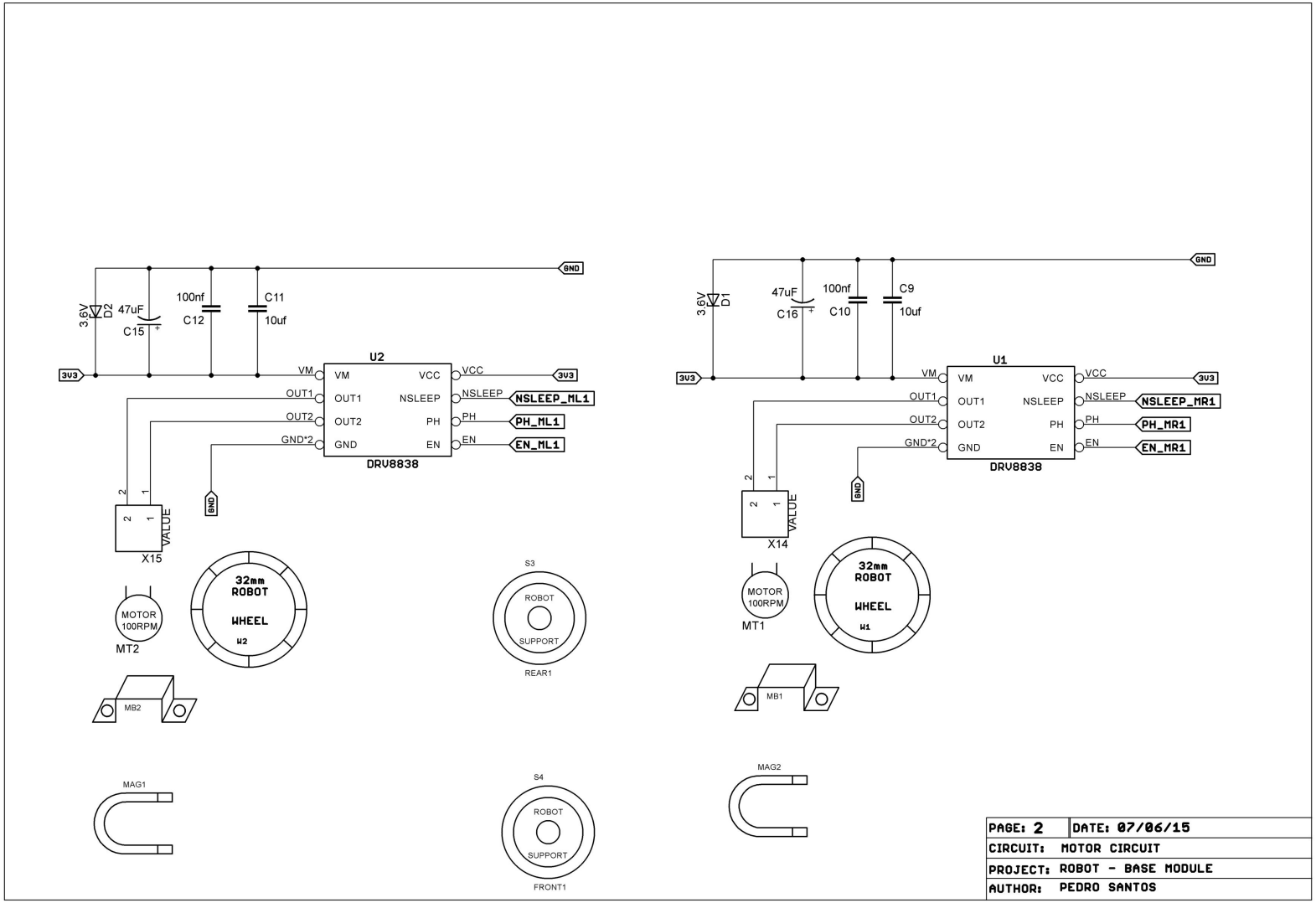
GND
3.6V
D2
47uF
C15
100nf
C12
C11
10uf
3V3
U2
VM
OUT1
OUT2
GND*2
VM
OUT1
OUT2
GND
VCC
NSLEEP
PH
EN
VCC
NSLEEP
PH
EN
NSLEEP_ML1
PH_ML1
EN_ML1
DRV8838
2
1
2
1
VALUE
X15
GND
32mm
ROBOT
WHEEL
W2
MOTOR
100RPM
MT2
S3
ROBOT
SUPPORT
REAR1
MB2
MAG1
S4
ROBOT
SUPPORT
FRONT1
GND
3.6V
D1
47uF
C16
100nf
C10
C9
10uf
3V3
U1
VM
OUT1
OUT2
GND*2
VM
OUT1
OUT2
GND
VCC
NSLEEP
PH
EN
VCC
NSLEEP
PH
EN
NSLEEP_MR1
PH_MR1
EN_MR1
DRV8838
2
1
2
1
VALUE
X14
GND
32mm
ROBOT
WHEEL
W1
MOTOR
100RPM
MT1
MB1
MAG2
PAGE: 2
DATE: 07/06/15
CIRCUIT: MOTOR CIRCUIT
PROJECT: ROBOT - BASE MODULE
AUTHOR: PEDRO SANTOS

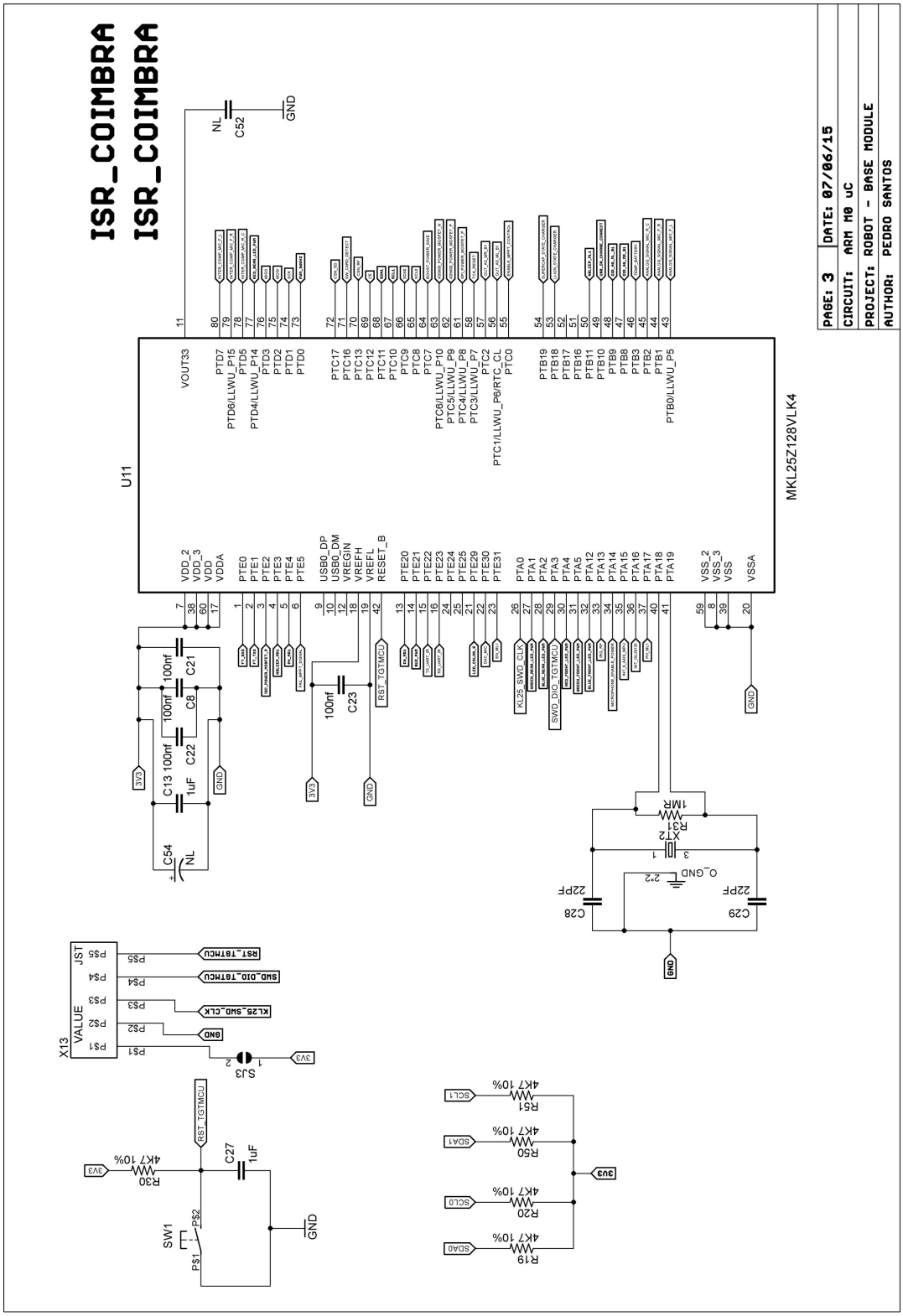
ISR_COIMBRA
ISR_COIMBRA
PAGE: 3
DATE: 07/06/15
CIRCUIT: ARM M0 uC
PROJECT: ROBOT - BASE MODULE
AUTHOR: PEDRO SANTOS
U11
MKL25Z128VLK4
VOUT33
VDD_2
VDD_3
VDD
VDDA
VSS_2
VSS_3
VSS
VSSA
USB0_DP
USB0_DM
VREGIN
VREFH
VREFL
RESET_B
PTA0
PTA1
PTA2
PTA3
PTA4
PTA5
PTA12
PTA13
PTA14
PTA15
PTA16
PTA17
PTA18
PTA19
PTB0/LLWU_P5
PTB1
PTB2
PTB3
PTB8
PTB9
PTB10
PTB11
PTB16
PTB17
PTB18
PTB19
PTC0
PTC1/LLWU_P6/RTC_CL
PTC2
PTC3/LLWU_P7
PTC4/LLWU_P8
PTC5/LLWU_P9
PTC6/LLWU_P10
PTC7
PTC8
PTC9
PTC10
PTC11
PTC12
PTC13
PTC16
PTC17
PTD0
PTD1
PTD2
PTD3
PTD4/LLWU_P14
PTD5
PTD6/LLWU_P15
PTD7
C52
NL
GND
C54
C13 100nf
C22 100nf
C8 100nf
C21 100nf
1uF
3V3
C23
100nf
RST_TGTMCU
SWD_DIO_TGTMCU
KL25_SWD_CLK
C28
C29
22PF
X12
1MR
R31
O_GND
X13
VALUE
JST
SJ3
SW1
R30
4K7 10%
C27
1uF
R19
R20
R50
R51
SDA0
SCL0
SDA1
SCL1

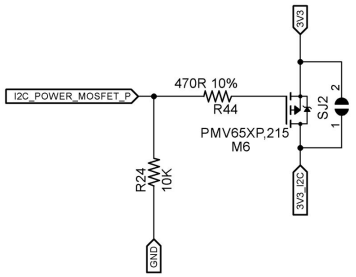

PAGE: 4	DATE: 07/06/15
CIRCUIT: I2C POWER BUS	
PROJECT: ROBOT - BASE MODULE	
AUTHOR: PEDRO SANTOS	

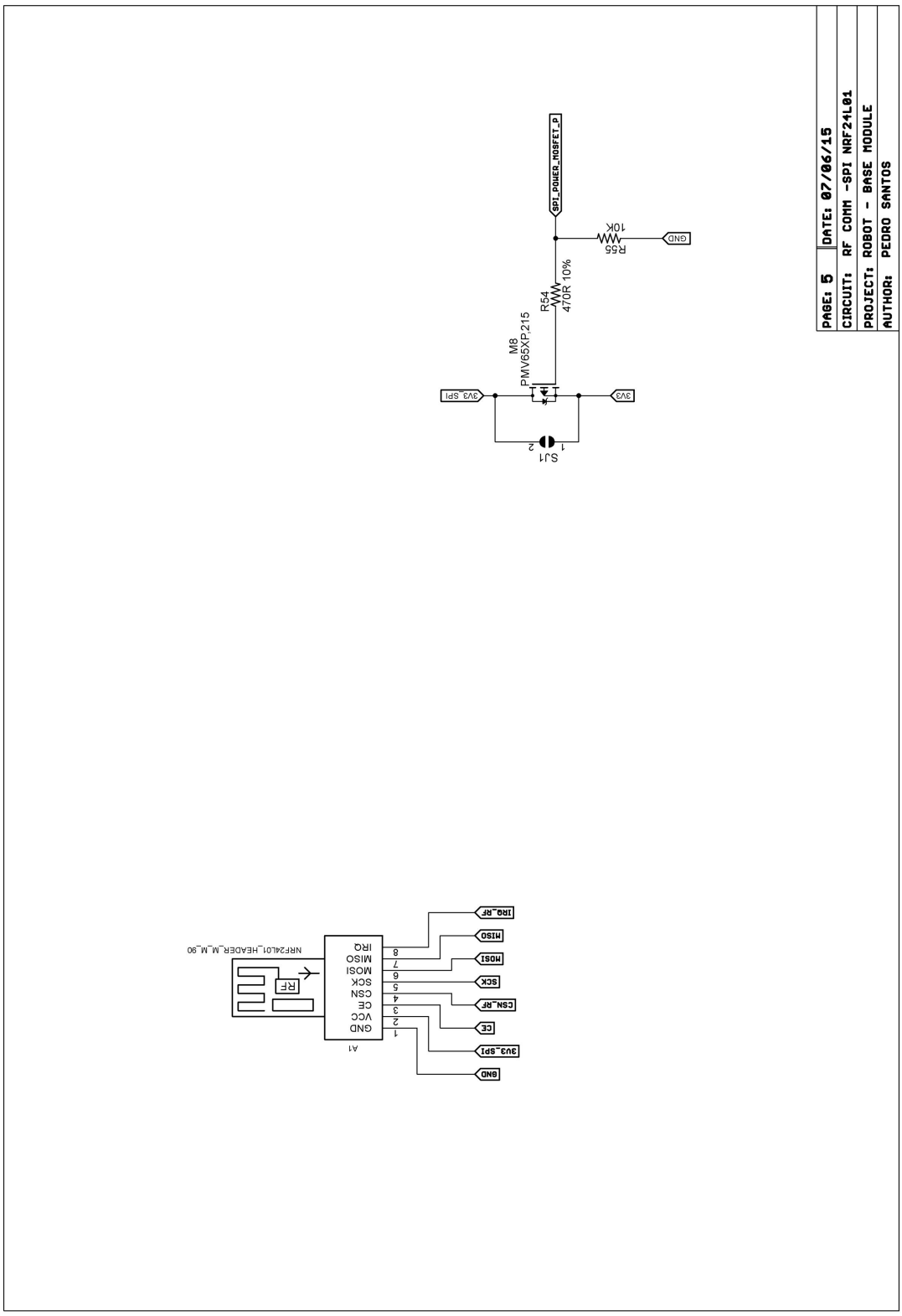
PAGE: 5
DATE: 07/06/15
CIRCUIT: RF COMM -SPI NRF24L01
PROJECT: ROBOT - BASE MODULE
AUTHOR: PEDRO SANTOS
SPI_POWER_MOSFET_P
R55
10K
GND
R54
470R 10%
M8
PMV65XP,215
3V3_SPI
3V3
S1
NRF24L01_HEADER_M_M_90
RF
A1
GND
VCC
CE
CSN
SCK
MOSI
MISO
IRQ
IRQ_RF
MISO
MOSI
SCK
CSN_RF
CE
3V3_SPI
GND

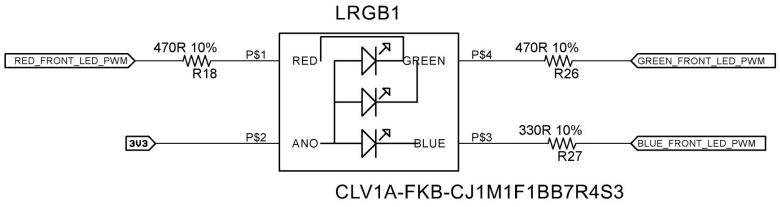

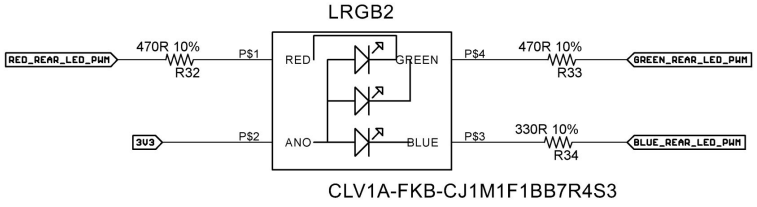

PAGE: 6	DATE: 07/06/15
CIRCUIT: RGB LEDS	
PROJECT: ROBOT - BASE MODULE	
AUTHOR: PEDRO SANTOS	

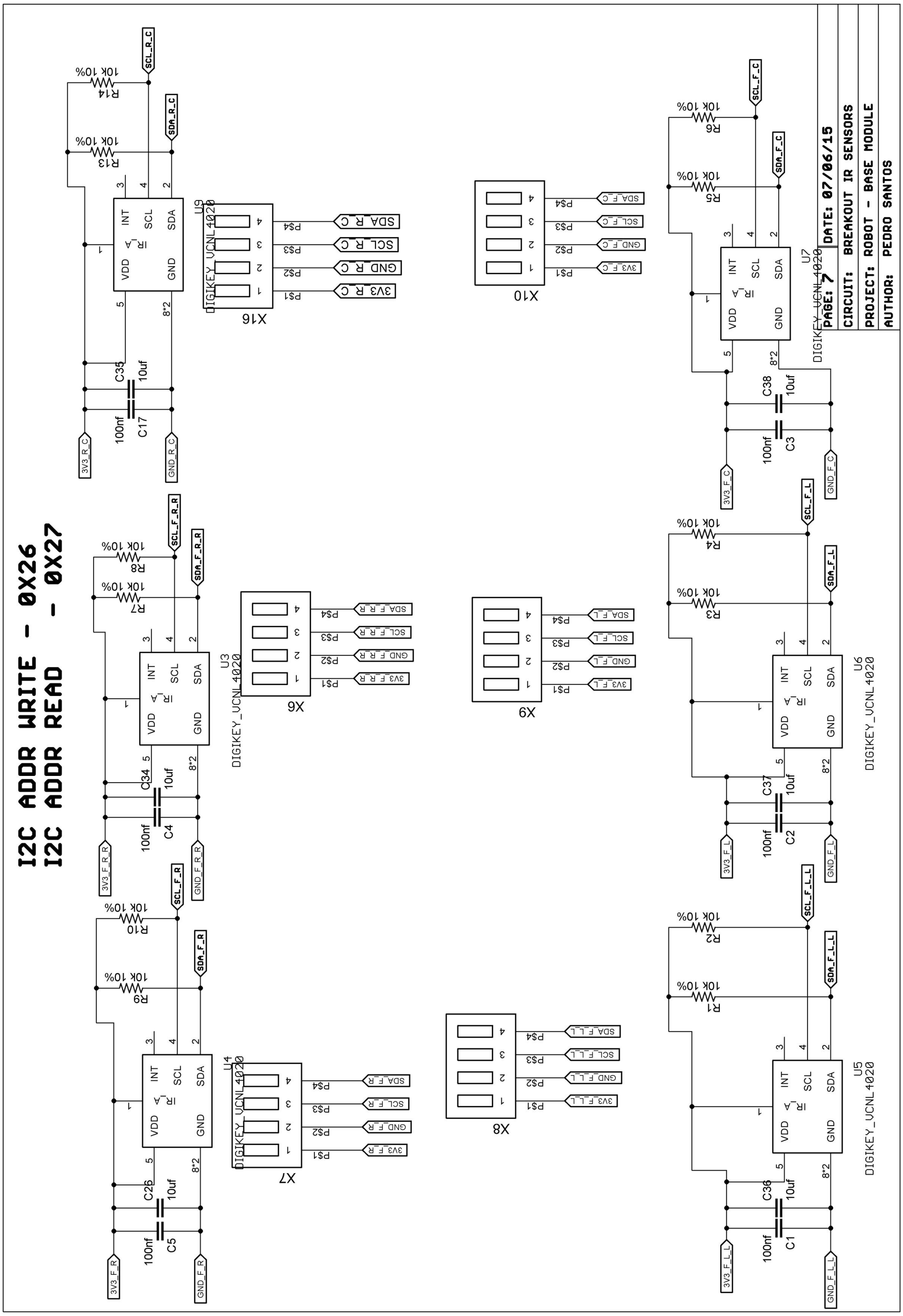
I2C ADDR WRITE - 0X26
I2C ADDR READ - 0X27
PAGE: 7
DATE: 07/06/15
CIRCUIT: BREAKOUT IR SENSORS
PROJECT: ROBOT - BASE MODULE
AUTHOR: PEDRO SANTOS
DIGIKEY_UCNL4020
SDA_R_C
SCL_R_C
GND_R_C
3V3_R_C
X16
X10
X6
X9
X7
X8
U3
U4
U5
U6
U7
U9
10K 10%
100nf
10uf

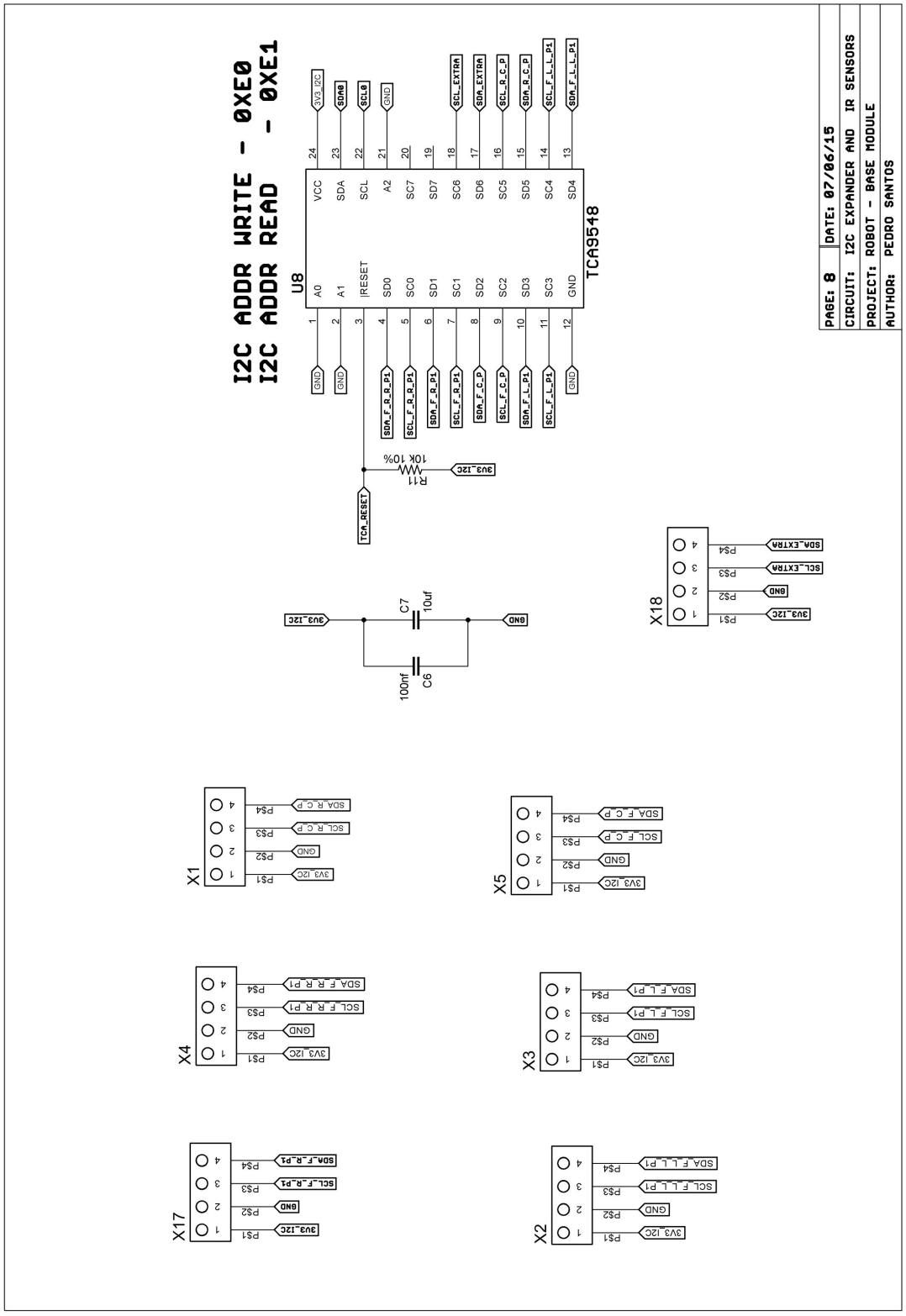
I2C ADDR WRITE - 0XE0
I2C ADDR READ - 0XE1
U8
TCA9548
PAGE: 8
DATE: 07/06/15
CIRCUIT: I2C EXPANDER AND IR SENSORS
PROJECT: ROBOT - BASE MODULE
AUTHOR: PEDRO SANTOS
X1
X2
X3
X4
X5
X17
X18
C6
C7
100nf
10uf
R11
10k 10%

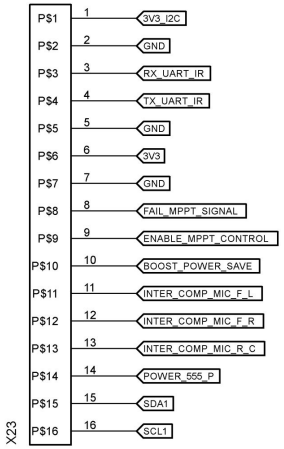

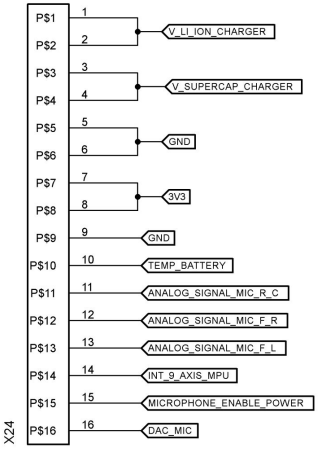

PAGE: 9	DATE: 07/06/15
CIRCUIT: ROBOT BUS - OTHER BOARDS	
PROJECT: ROBOT - BASE MODULE	
AUTHOR: PEDRO SANTOS	

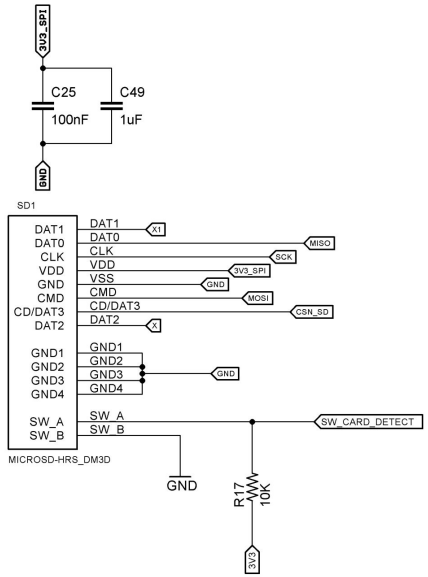

PAGE: 10	DATE: 07/06/15
CIRCUIT: MICRO SD CARD	
PROJECT: ROBOT - BASE MODULE	
AUTHOR: PEDRO SANTOS	

PAGE: 11
DATE: 07/06/15
CIRCUIT: BUZZER
PROJECT: ROBOT - BASE MODULE
AUTHOR: PEDRO SANTOS
BZ1
3V3
D3
CGRM4001-G
R15
100R
M1
NDS331N
GND
R16
470R
BUZ_PWM
C18
10uf
C24
100nf

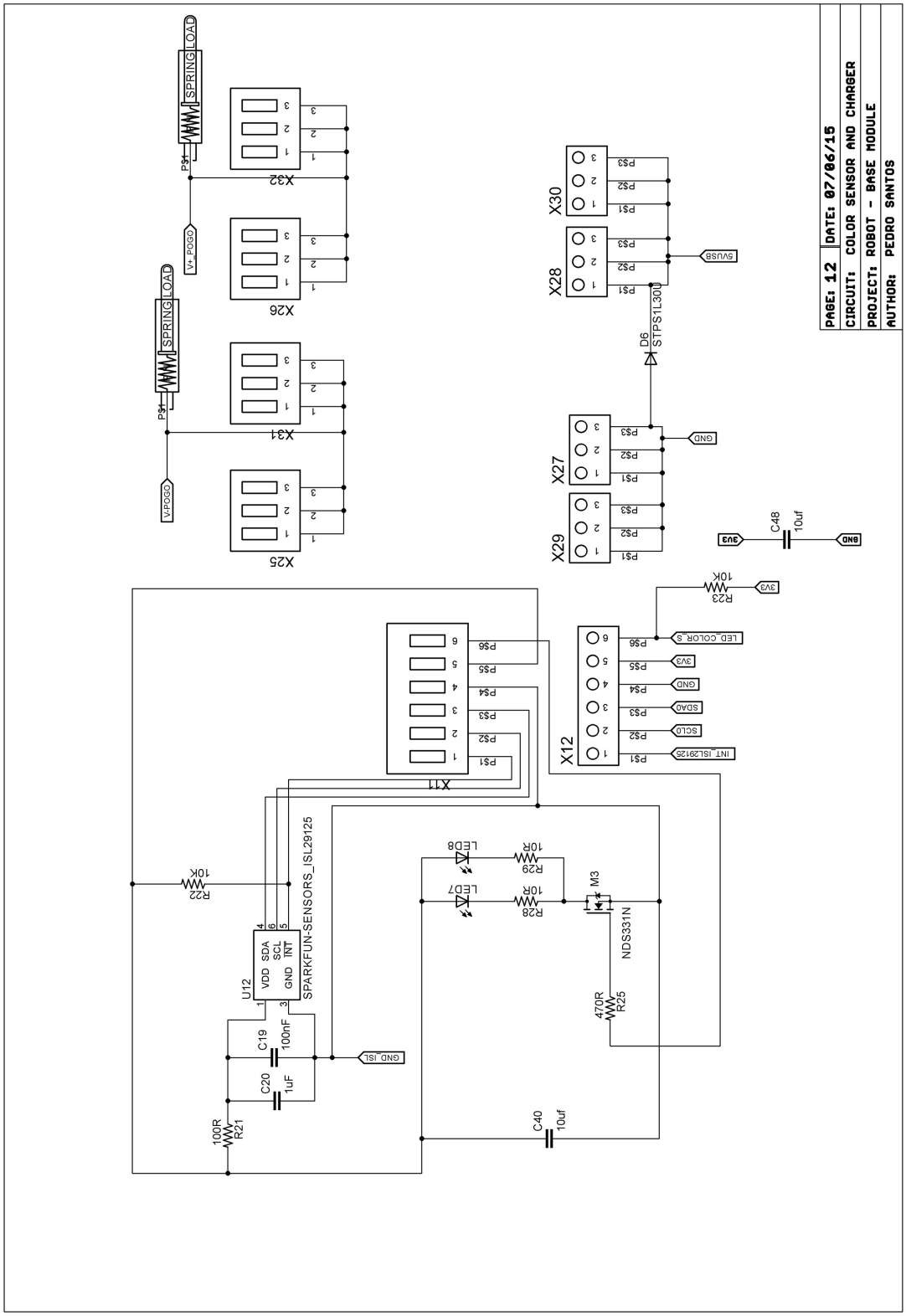
PAGE: 12
DATE: 07/06/15
CIRCUIT: COLOR SENSOR AND CHARGER
PROJECT: ROBOT - BASE MODULE
AUTHOR: PEDRO SANTOS
SPRINGLOAD
V+POGO
X25
X26
X31
X32
X27
X28
X29
X30
D6
STPS1L30U
5VUSB
GND
C48
10uf
3V3
R23
10K
X11
X12
LED_COLOR_S
INT_ISL29125
SCLO
SDAO
U12
SPARKFUN-SENSORS_ISL29125
VDD
SDA
SCL
INT
GND
R22
C19
100nF
C20
1uF
GND_ISL
100R
R21
LED8
LED7
R29
R28
M3
NDS331N
470R
R25
C40
10uf

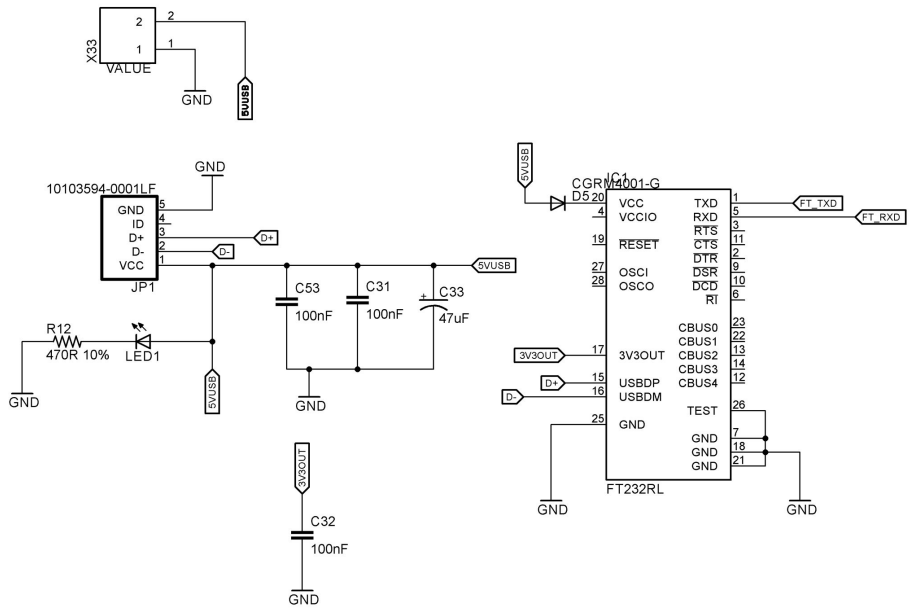

PAGE: 13	DATE: 07/06/15
CIRCUIT: UART COMM AND CHARGER	
PROJECT: ROBOT - BASE MODULE	
AUTHOR: PEDRO SANTOS	

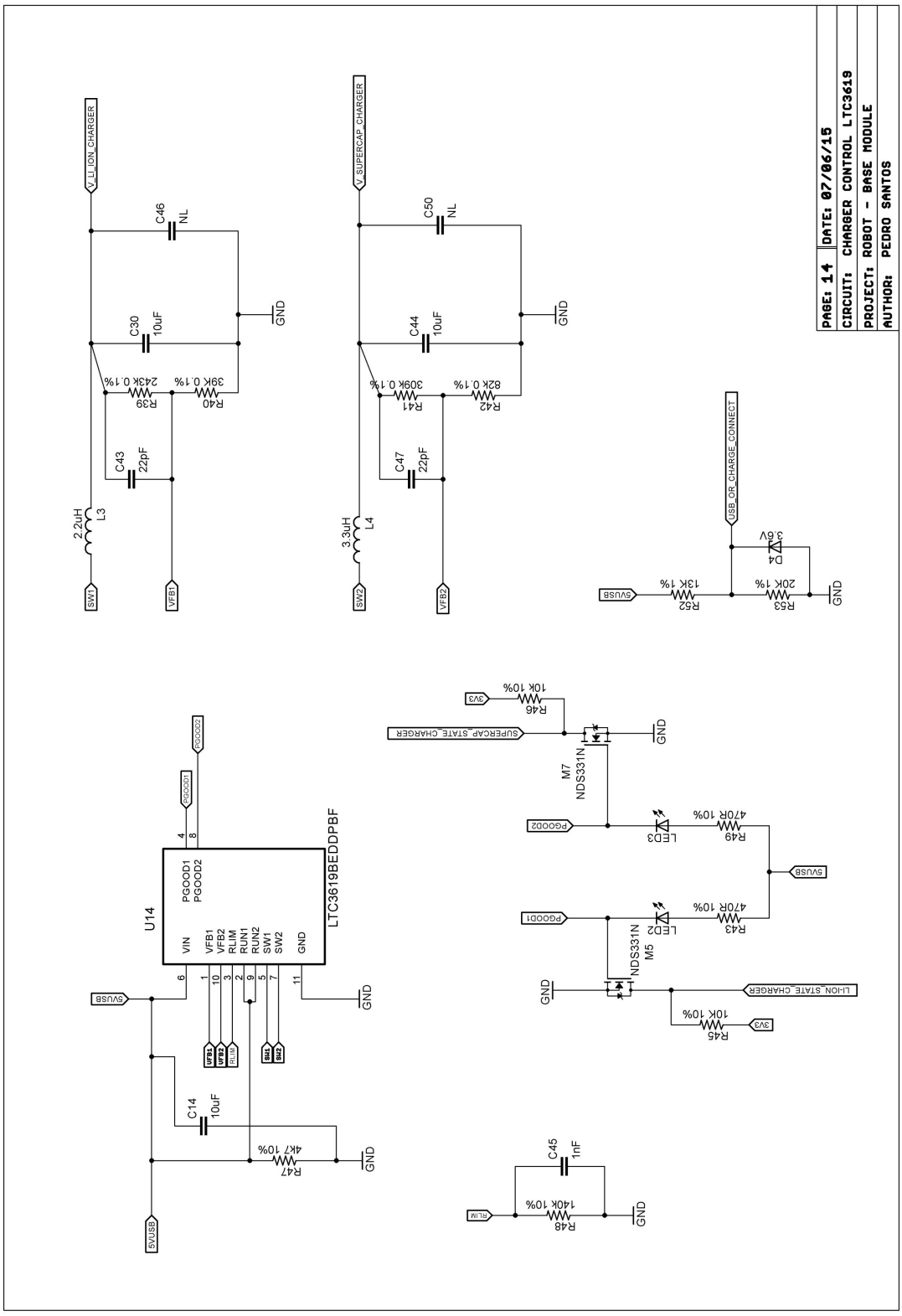
PAGE: 14
DATE: 07/06/15
CIRCUIT: CHARGER CONTROL LTC3619
PROJECT: ROBOT - BASE MODULE
AUTHOR: PEDRO SANTOS
V_LI_ION_CHARGER
C46
NL
C30
10uF
GND
39K 0.1%
R40
243K 0.1%
R39
C43
22pF
2.2uH
L3
SW1
VFB1
V_SUPERCAP_CHARGER
C50
NL
C44
10uF
GND
82K 0.1%
R42
309K 0.1%
R41
C47
22pF
3.3uH
L4
SW2
VFB2
USB_OR_CHARGE_CONNECT
3.6V
D4
5VUSB
13K 1%
R52
20K 1%
R53
GND
U14
LTC3619BEDDPBF
PGOOD1
PGOOD2
VIN
VFB1
VFB2
RLIM
RUN1
RUN2
SW1
SW2
GND
PGOOD1
PGOOD2
5VUSB
GND
C14
10uF
4K7 10%
R47
GND
5VUSB
SUPERCAP_STATE_CHARGER
3V3
10K 10%
R46
M7
NDS331N
PGOOD2
LED3
470R 10%
R49
5VUSB
PGOOD1
LED2
470R 10%
R43
NDS331N
M5
GND
LI-ION_STATE_CHARGER
3V3
10K 10%
R45
C45
1nF
RLIM
140K 10%
R48
GND

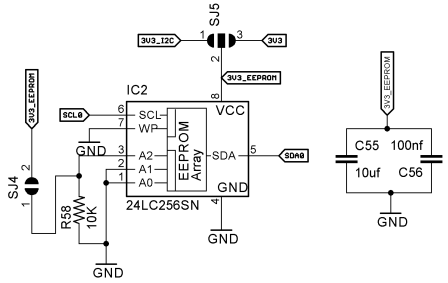

PAGE: 15	DATE: 15/03/16
CIRCUIT: EEPROM 24LC256	
PROJECT: ROBOT - BASE MODULE	
AUTHOR: PEDRO SANTOS	

B.1.2 Sensor module scheme

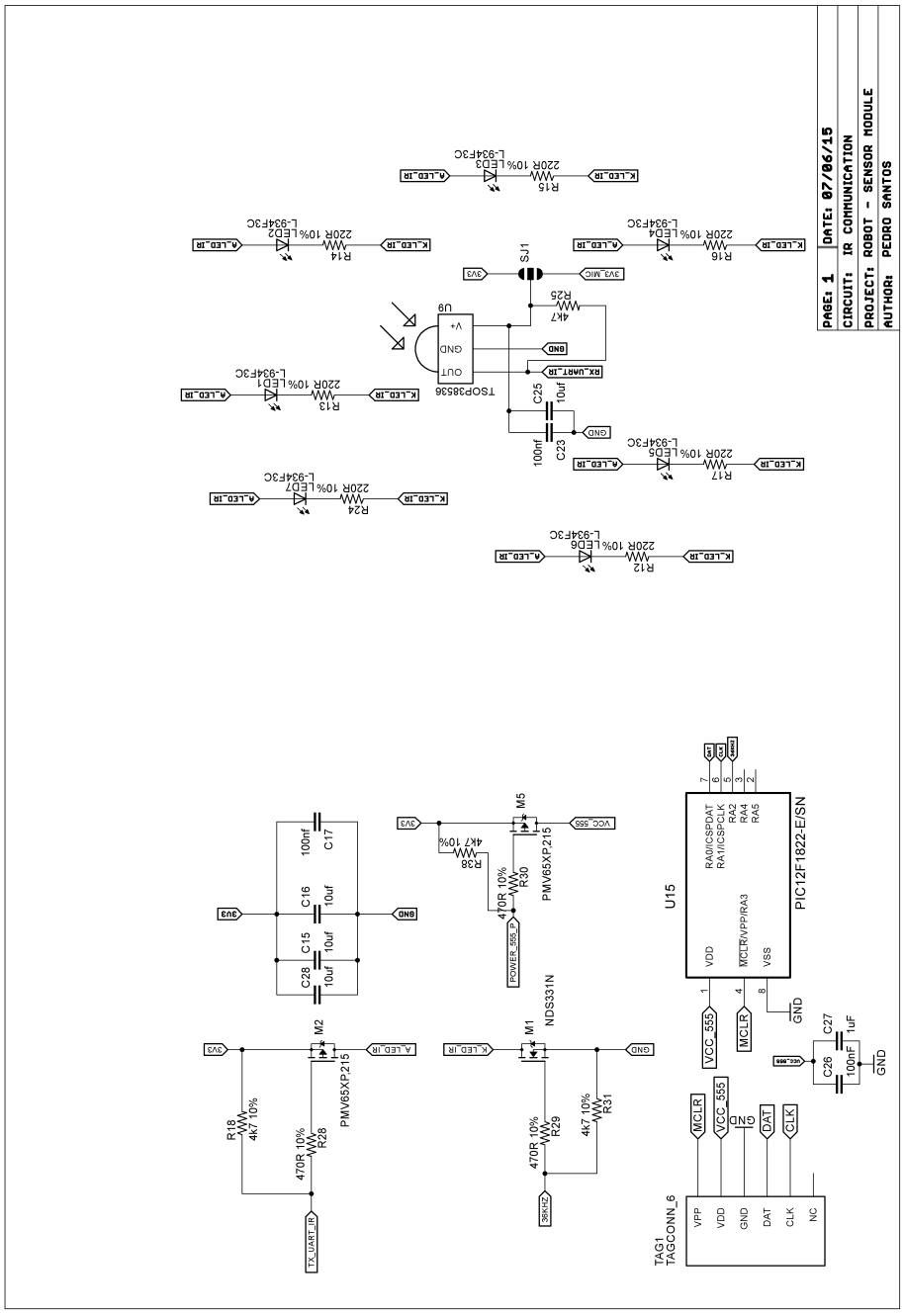

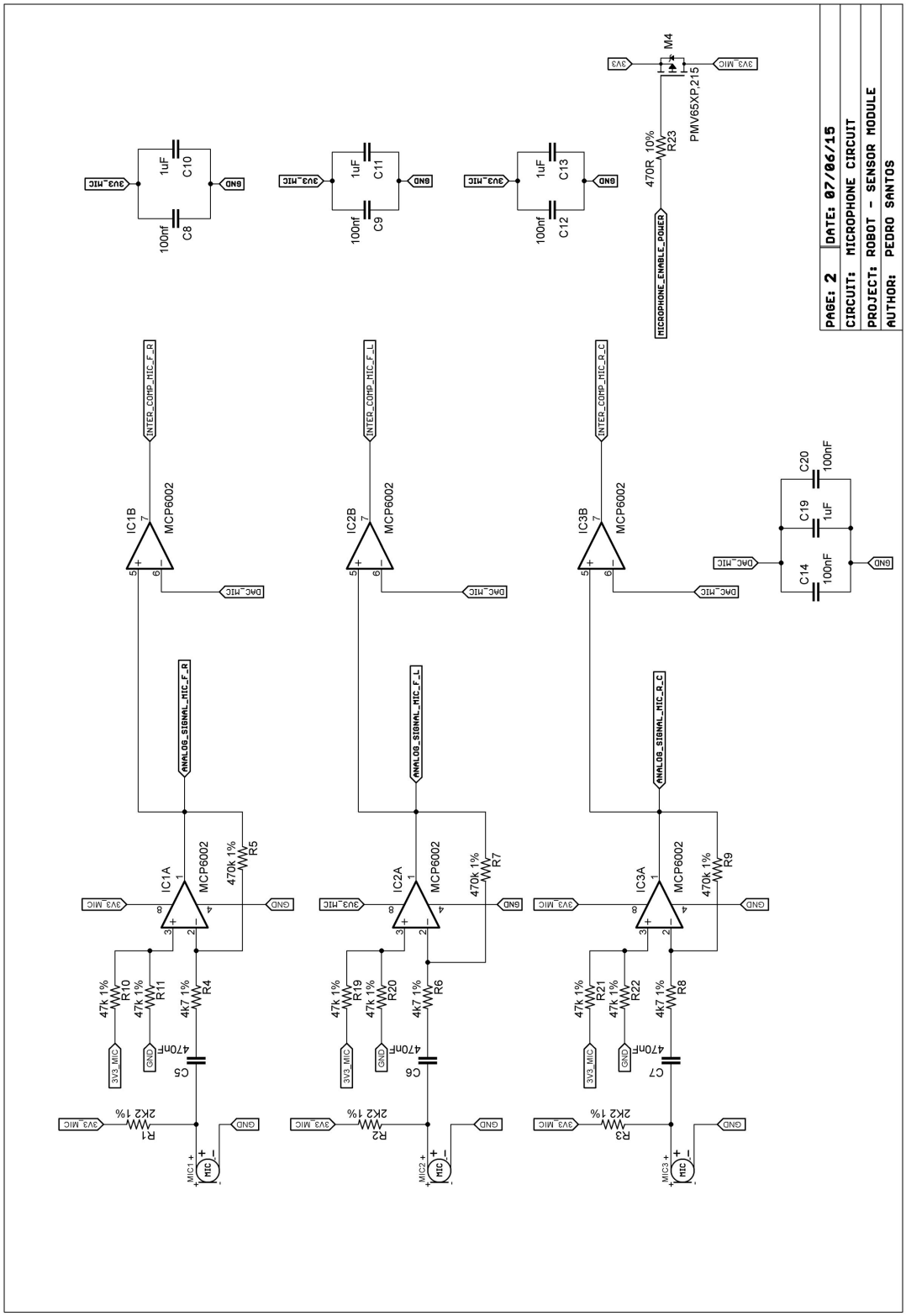
PAGE: 2
DATE: 07/06/15
CIRCUIT: MICROPHONE CIRCUIT
PROJECT: ROBOT - SENSOR MODULE
AUTHOR: PEDRO SANTOS
M4
PMV65XP,215
470R 10%
R23
MICROPHONE_ENABLE_POWER
3V3
3V3_MIC
GND
C10
1uF
C8
100nf
C11
C9
C13
C12
C20
100nF
C19
C14
DAC_MIC
IC1B
IC2B
IC3B
MCP6002
INTER_COMP_MIC_F_R
INTER_COMP_MIC_F_L
INTER_COMP_MIC_R_C
IC1A
IC2A
IC3A
ANALOG_SIGNAL_MIC_F_R
ANALOG_SIGNAL_MIC_F_L
ANALOG_SIGNAL_MIC_R_C
470k 1%
R5
R7
R9
47k 1%
R10
R11
R19
R20
R21
R22
4k7 1%
R4
R6
R8
3V3_MIC
GND
470nF
C5
C6
C7
2K2 1%
R1
R2
R3
MIC1
MIC2
MIC3

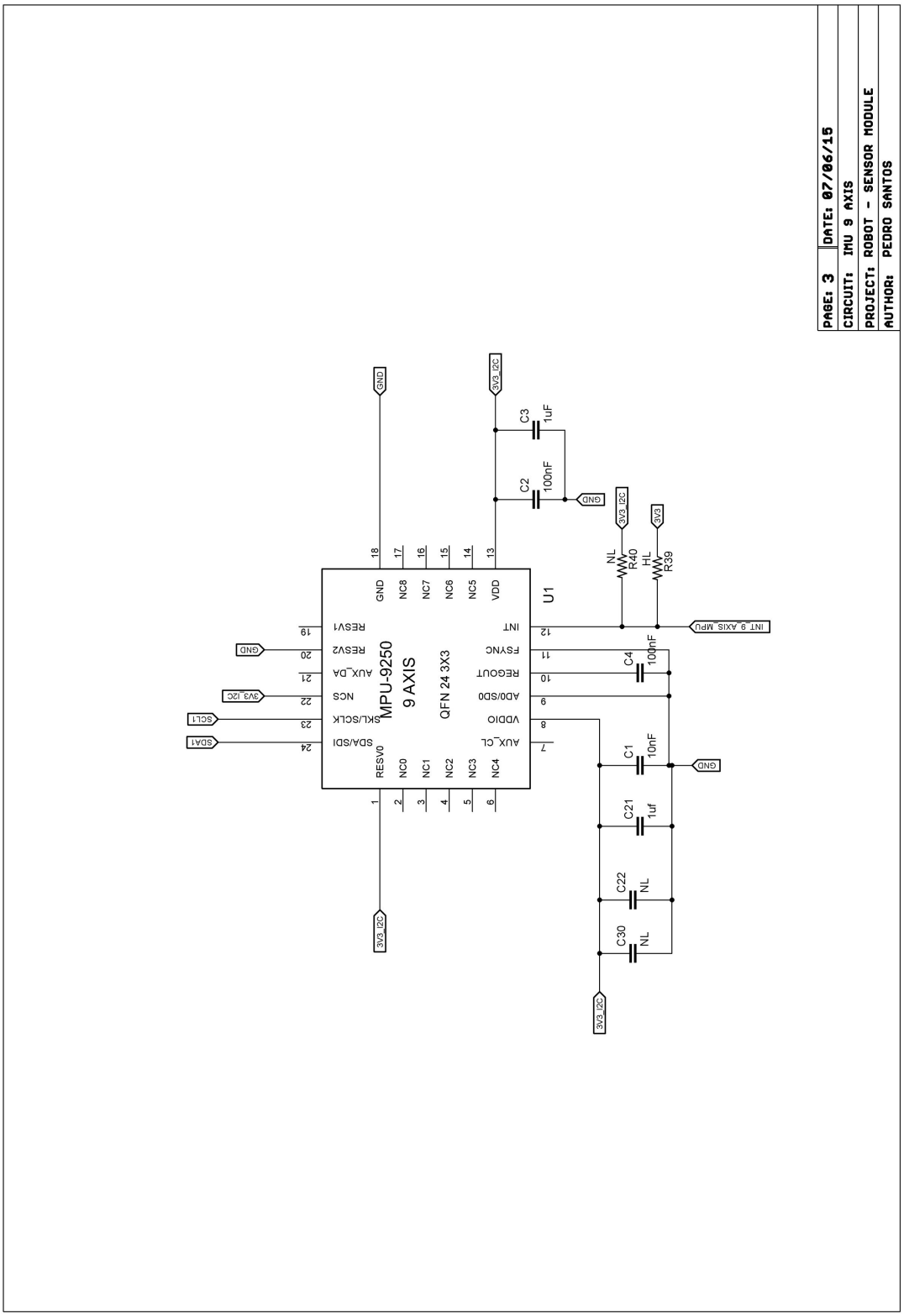
PAGE: 3
DATE: 07/06/15
CIRCUIT: IMU 9 AXIS
PROJECT: ROBOT - SENSOR MODULE
AUTHOR: PEDRO SANTOS
U1
MPU-9250
9 AXIS
QFN 24 3X3
GND
NC8
NC7
NC6
NC5
VDD
INT
FSYNC
REGOUT
AD0/SD0
VDDIO
AUX_CL
SDA/SDI
SCL/SCLK
NCS
AUX_DA
RESV2
RESV1
RESV0
NC0
NC1
NC2
NC3
NC4
C1 10nF
C2 100nF
C3 1uF
C4 100nF
C21 1uf
C22 NL
C30 NL
R39 HL
R40 NL
GND
3V3_I2C
3V3
INT_9_AXIS_MPU
SCLI
SDAI

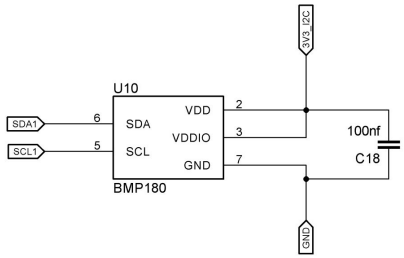

PAGE: 4	DATE: 07/06/15
CIRCUIT: BAROMETER	
PROJECT: ROBOT - SENSOR MODULE	
AUTHOR: PEDRO SANTOS	

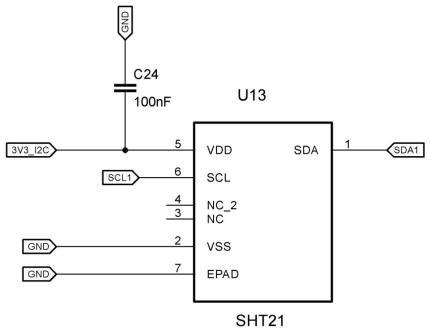

PAGE: 5	DATE: 07/06/15
CIRCUIT:	HUMIDITY SENSOR
PROJECT:	ROBOT - SENSOR MODULE
AUTHOR:	PEDRO SANTOS

ISR_COIMBRA

ISR_COIMBRA

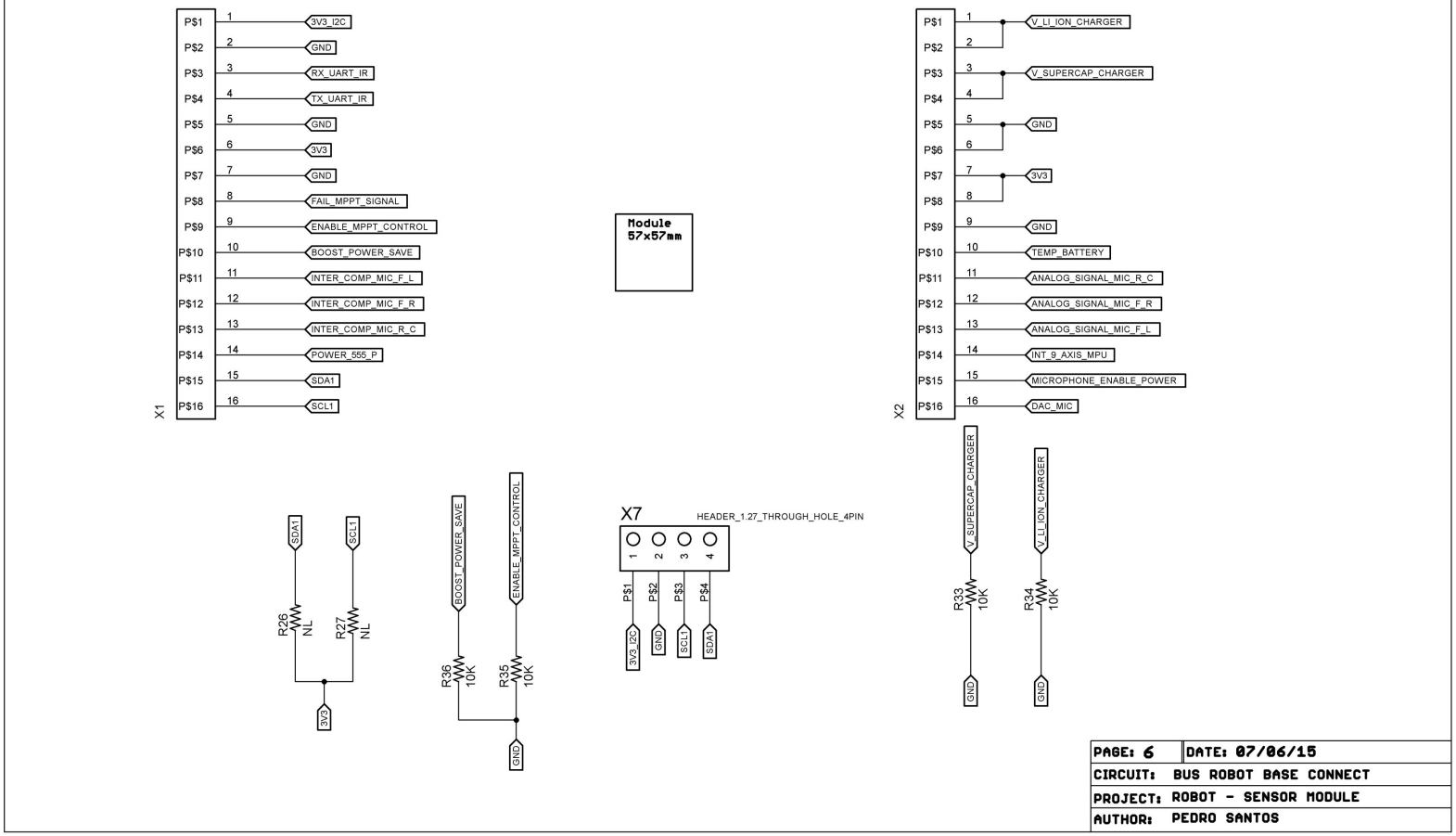

PAGE: 6	DATE: 07/06/15
CIRCUIT:	BUS ROBOT BASE CONNECT
PROJECT:	ROBOT - SENSOR MODULE
AUTHOR:	PEDRO SANTOS

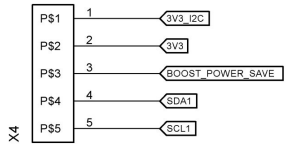

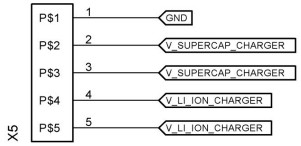

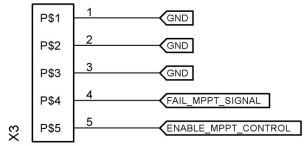

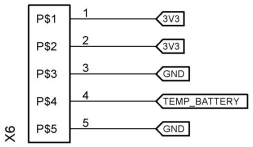

PAGE: 7	DATE: 07/06/15
CIRCUIT:	BUS ROBOT STORAGE CONNECT
PROJECT:	ROBOT - SENSOR MODULE
AUTHOR:	PEDRO SANTOS

B.1.3 Harvester module scheme

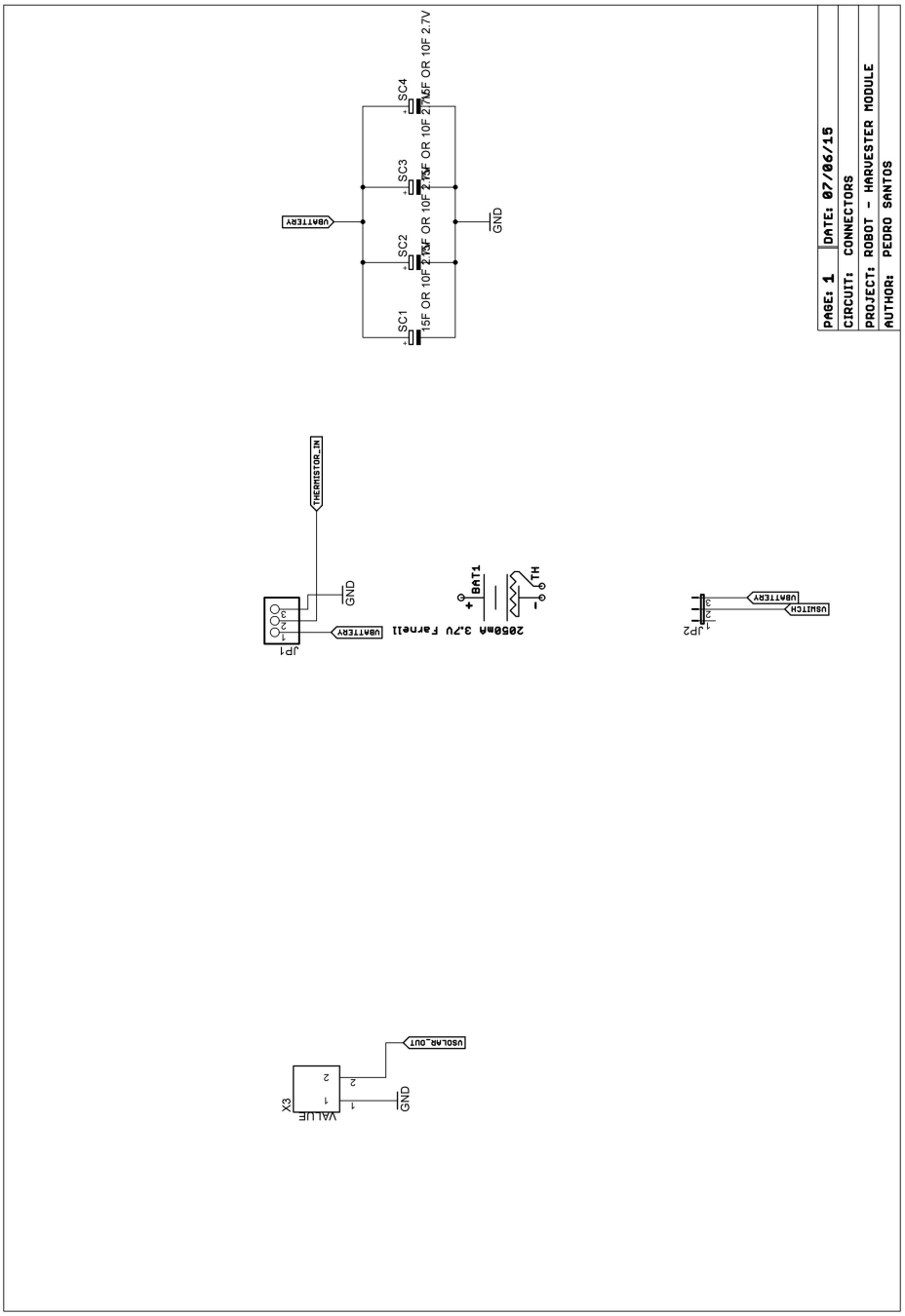

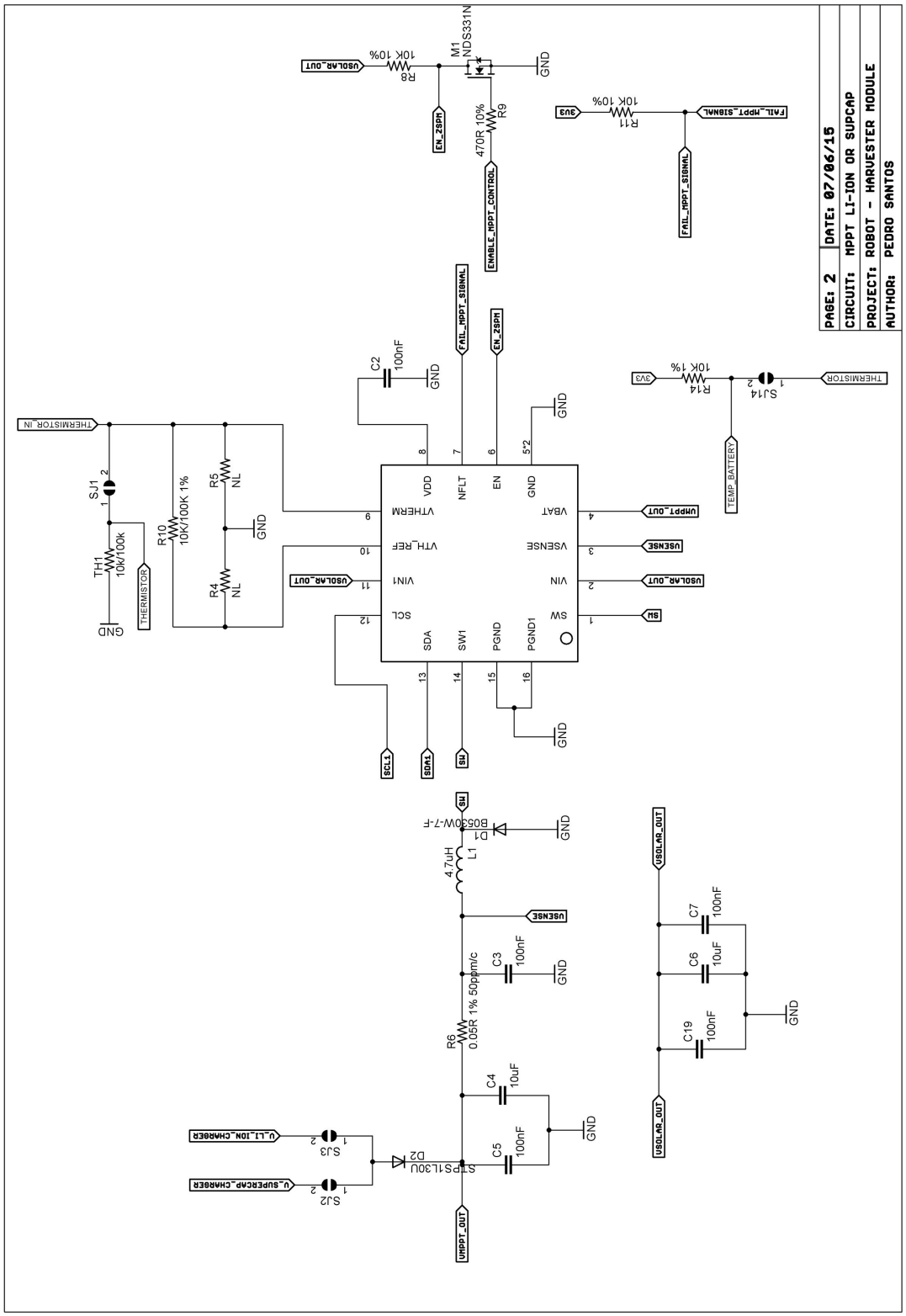
PAGE: 2
DATE: 07/06/15
CIRCUIT: MPPT LI-ION OR SUPCAP
PROJECT: ROBOT - HARVESTER MODULE
AUTHOR: PEDRO SANTOS
M1
NDS331N
R8
10K 10%
R9
470R 10%
R11
10K 10%
R14
10K 1%
SJ14
THERMISTOR
TEMP_BATTERY
C2
100nF
R5
NL
R10
10K/100K 1%
R4
NL
SJ1
TH1
10k/100k
THERMISTOR_IN
VDD
NFLT
EN
GND
VTHERM
VTH_REF
VBAT
VSENSE
VIN1
VIN
SCL
SDA
SW1
PGND
PGND1
SW
D1
B0530W-7-F
L1
4.7uH
R6
0.05R 1% 50ppm/c
C3
100nF
C4
10uF
C5
100nF
D2
STPS1L30U
SJ2
SJ3
C7
100nF
C6
10uF
C19
100nF
EN_2SPM
FAIL_MPPT_SIGNAL
ENABLE_MPPT_CONTROL
VSOLAR_OUT
VMPPT_OUT
U_SUPERCAP_CHARGER
U_LI-ION_CHARGER
SCL1
SDA1
RS
SW

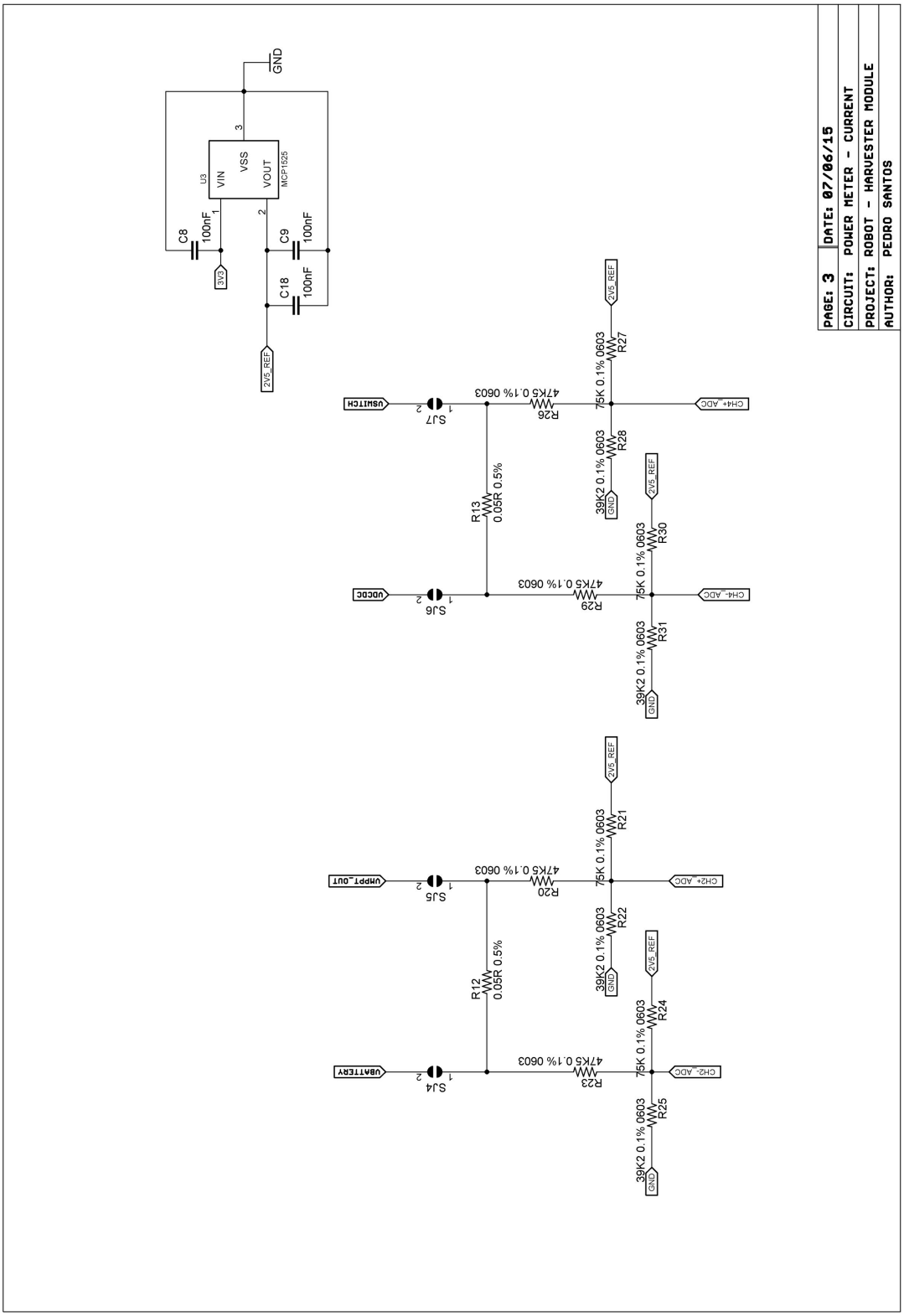
GND
U3
VIN
VSS
VOUT
MCP1525
3
1
2
C8
100nF
C9
100nF
C18
100nF
3V3
2V5_REF
USWITCH
UBATTERY
UMPPT_OUT
UDCDC
S17
S16
S15
S14
R26
47K5 0.1% 0603
R27
75K 0.1% 0603
R28
39K2 0.1% 0603
R13
0.05R 0.5%
R29
R30
R31
R20
R21
R22
R12
R23
R24
R25
CH4+_ADC
CH4-_ADC
CH2+_ADC
CH2-_ADC
PAGE: 3
DATE: 07/06/15
CIRCUIT: POWER METER - CURRENT
PROJECT: ROBOT - HARVESTER MODULE
AUTHOR: PEDRO SANTOS

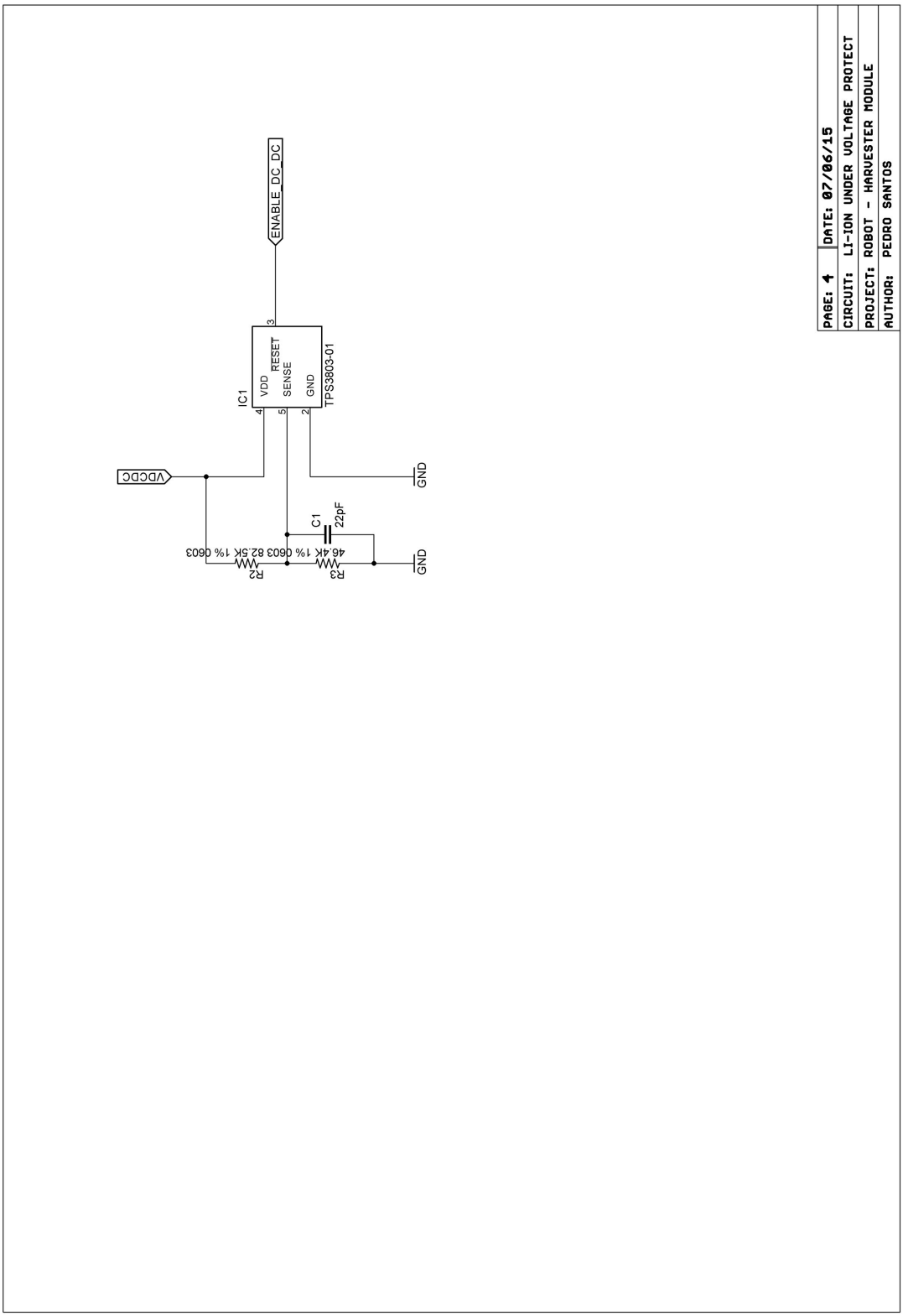
ENABLE_DC_DC
IC1
VDD
RESET
SENSE
GND
TPS3803-01
VDCDC
GND
C1
22pF
R2
82.5K 1% 0603
R3
46.4K 1% 0603
GND
PAGE: 4
DATE: 07/06/15
CIRCUIT: LI-ION UNDER VOLTAGE PROTECT
PROJECT: ROBOT - HARVESTER MODULE
AUTHOR: PEDRO SANTOS

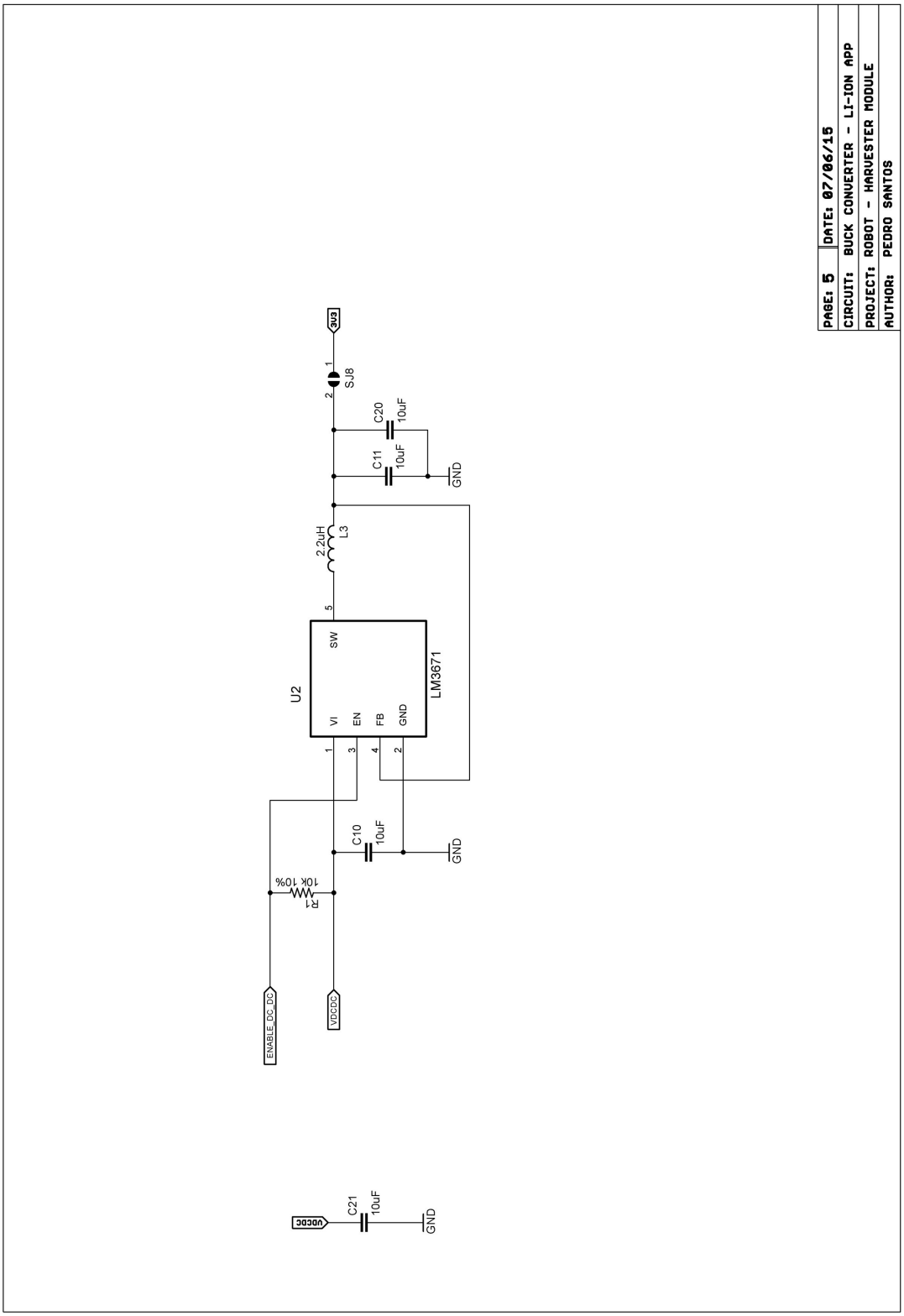
PAGE: 5
DATE: 07/06/15
CIRCUIT: BUCK CONVERTER - LI-ION APP
PROJECT: ROBOT - HARVESTER MODULE
AUTHOR: PEDRO SANTOS
3V3
SJ8
C20
10uF
C11
10uF
GND
2.2uH
L3
U2
SW
LM3671
VI
EN
FB
GND
C10
10uF
GND
10K 10%
R1
ENABLE_DC_DC
VDCDC
VDCDC
C21
10uF
GND

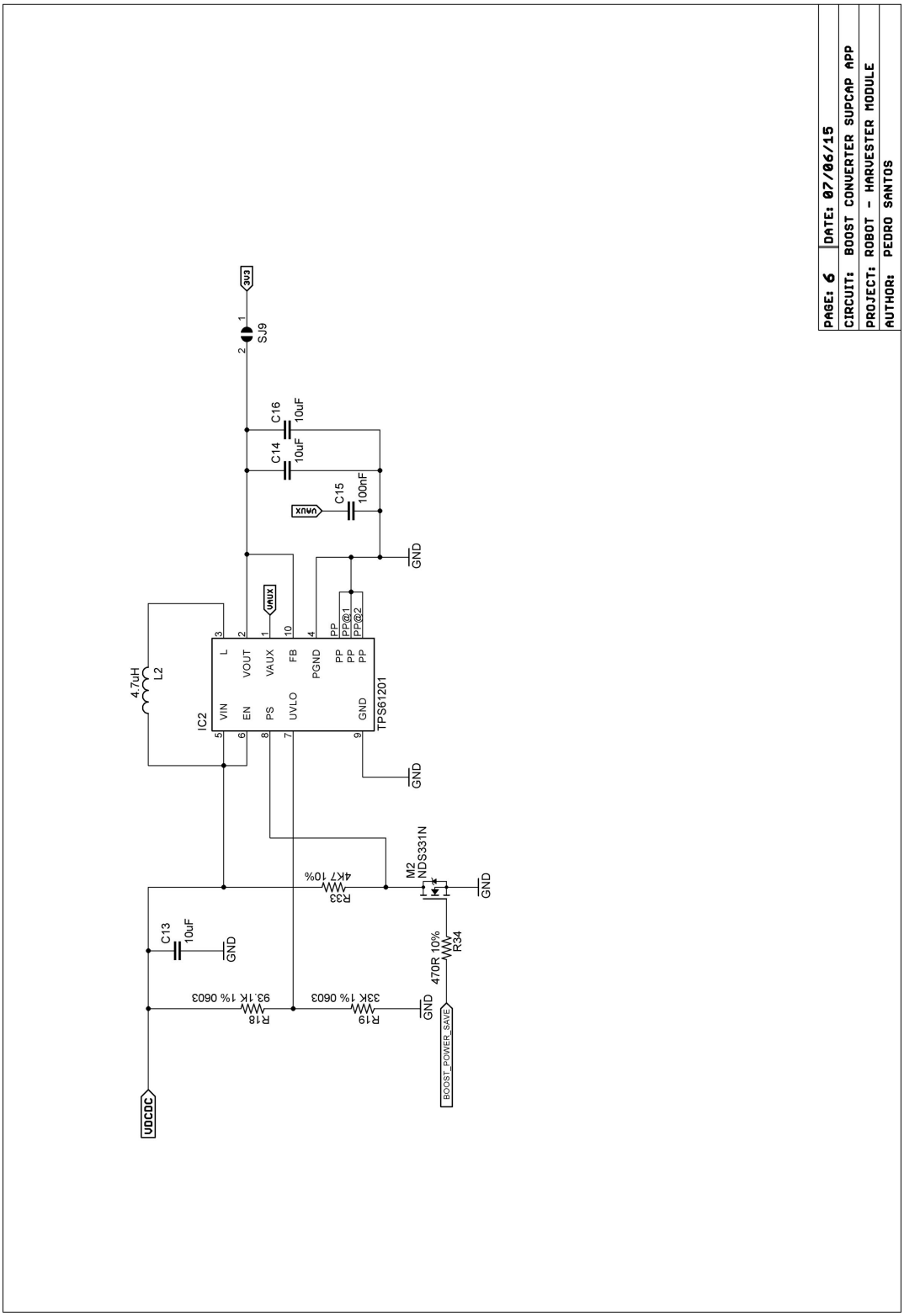
PAGE: 6
DATE: 07/06/15
CIRCUIT: BOOST CONVERTER SUPCAP APP
PROJECT: ROBOT - HARVESTER MODULE
AUTHOR: PEDRO SANTOS
aux
SJ9
C16
10uF
C14
10uF
C15
100nF
vaux
GND
IC2
TPS61201
VIN
EN
PS
UVLO
L
VOUT
VAUX
FB
PGND
PP
PP
PP
PP@1
PP@2
GND
4.7uH
L2
C13
10uF
R33
4K7 10%
M2
NDS331N
470R 10%
R34
R18
93.1K 1% 0603
R19
33K 1% 0603
BOOST_POWER_SAVE
VDCDC

ISR_COIMBRA

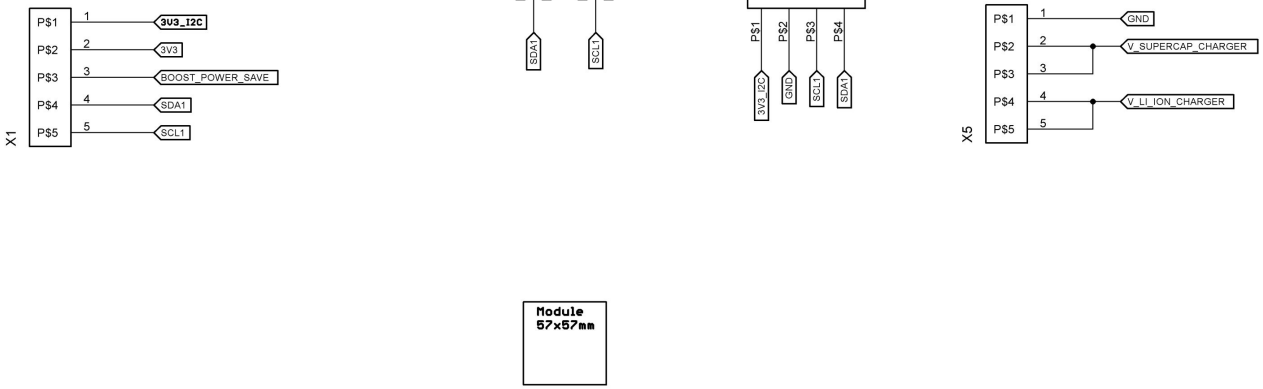

PAGE: 7	DATE: 07/06/15
CIRCUIT:	BUS ROBOT CONNECT SENSOR MODULE
PROJECT:	ROBOT - HARVESTER MODULE
AUTHOR:	PEDRO SANTOS

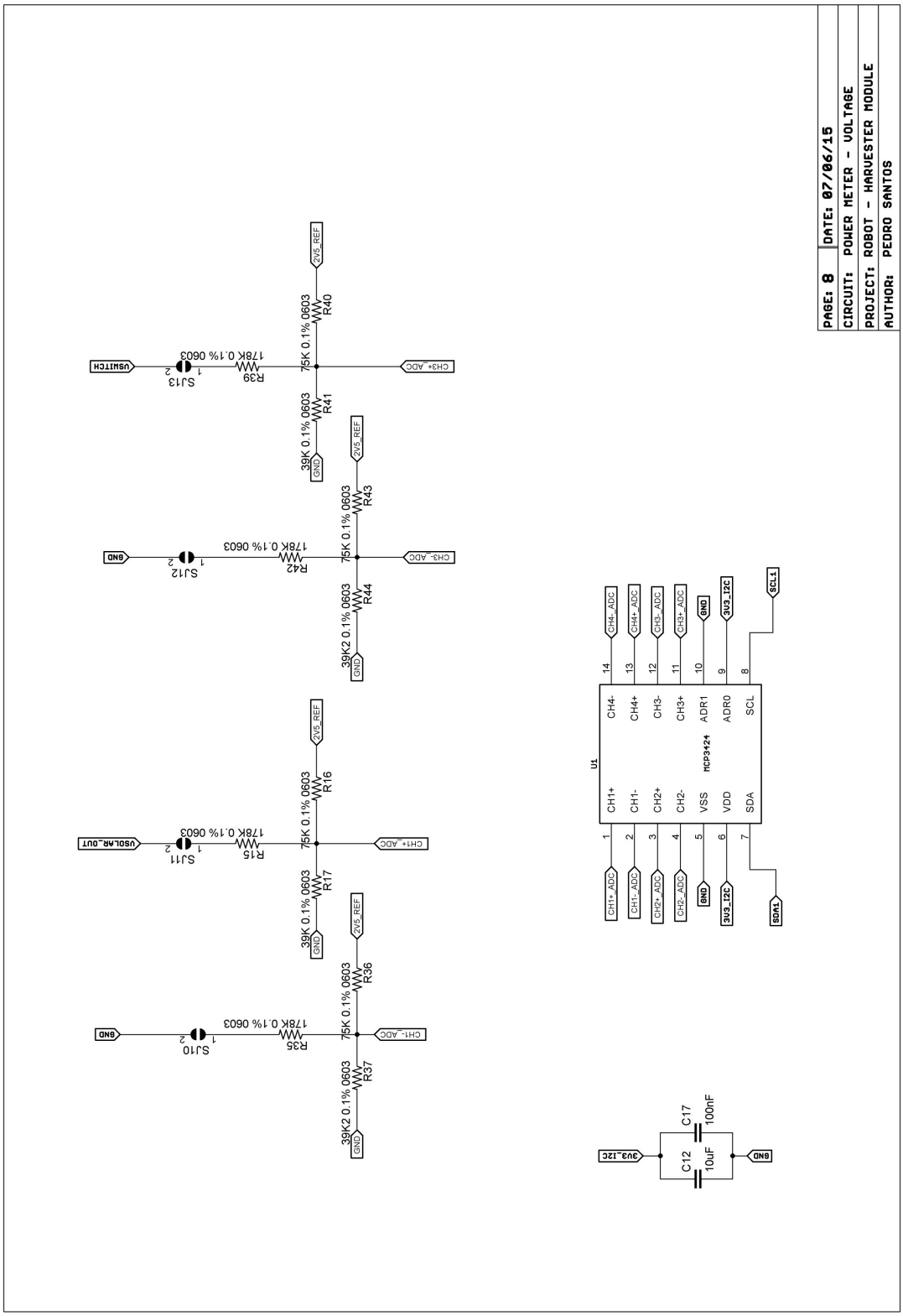
PAGE: 8
DATE: 07/06/15
CIRCUIT: POWER METER - VOLTAGE
PROJECT: ROBOT - HARVESTER MODULE
AUTHOR: PEDRO SANTOS
U1
MCP3424
CH1+
CH1-
CH2+
CH2-
VSS
VDD
SDA
CH4-
CH4+
CH3-
CH3+
ADR1
ADR0
SCL
CH1+_ADC
CH1-_ADC
CH2+_ADC
CH2-_ADC
GND
3V3_I2C
SDA1
SCL1
CH4-_ADC
CH4+_ADC
CH3-_ADC
CH3+_ADC
C12
10uF
C17
100nF
CH1+_ADC
R35
178K 0.1% 0603
75K 0.1% 0603
R36
39K 0.1% 0603
R37
39K2 0.1% 0603
GND
2V5_REF
VSOLAR_OUT
S_J10
S_J11
R15
R16
R17
CH2+_ADC
R42
R43
R44
S_J12
CH3-_ADC
VSWITCH
R39
R40
R41
S_J13
CH3+_ADC

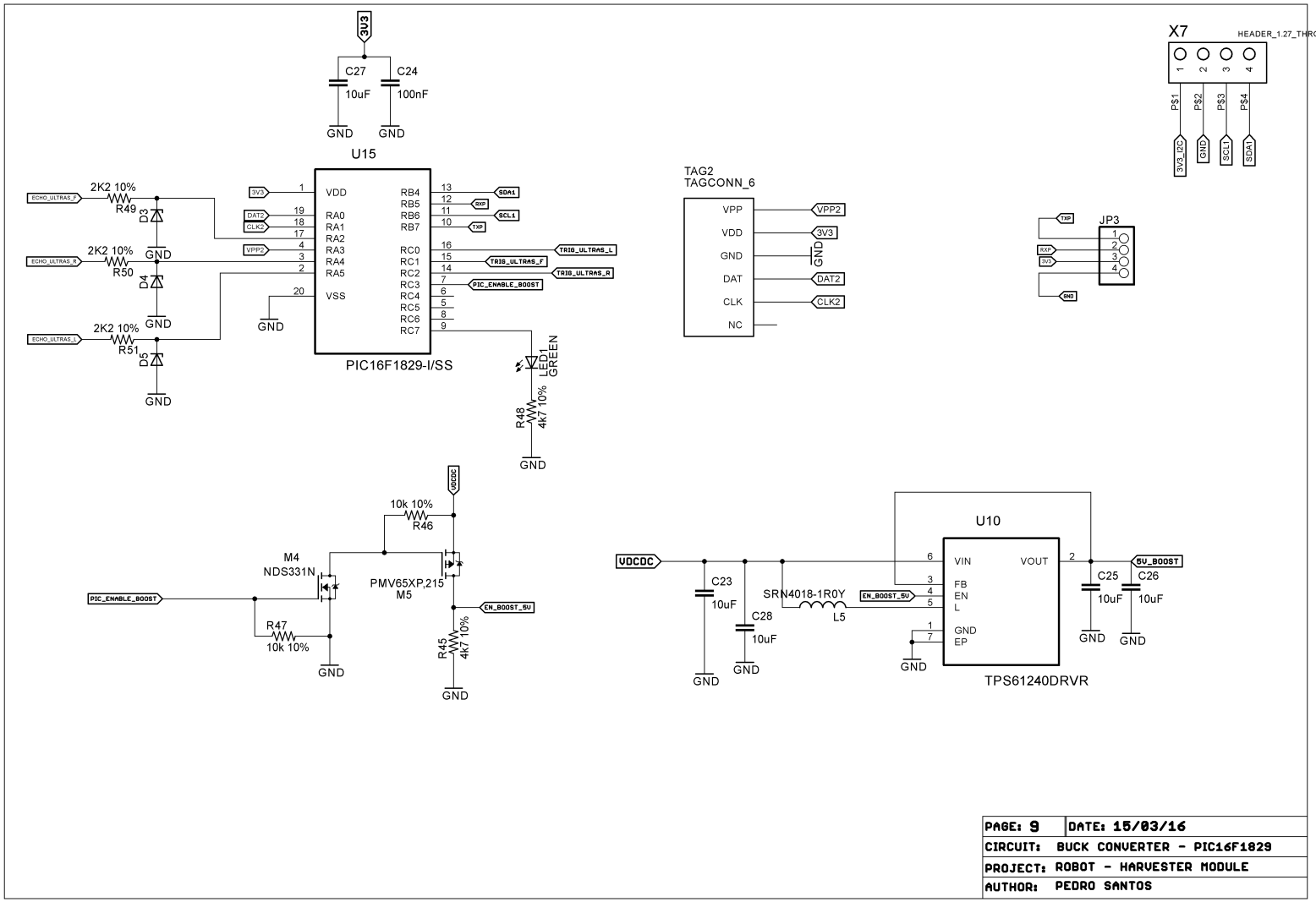
3V3
C27
10uF
C24
100nF
GND
GND
U15
PIC16F1829-I/SS
2K2 10%
R49
R50
R51
D3
D4
D5
ECHO_ULTRAS_F
ECHO_ULTRAS_R
ECHO_ULTRAS_L
VDD
VSS
RA0
RA1
RA2
RA3
RA4
RA5
RB4
RB5
RB6
RB7
RC0
RC1
RC2
RC3
RC4
RC5
RC6
RC7
SDA1
SCL1
TRIG_ULTRAS_L
TRIG_ULTRAS_F
TRIG_ULTRAS_R
PIC_ENABLE_BOOST
LED1
GREEN
R48
4K7 10%
TAG2
TAGCONN_6
VPP
VDD
GND
DAT
CLK
NC
VPP2
DAT2
CLK2
X7
HEADER_1.27_THRC
PS1
PS2
PS3
PS4
3V3_I2C
SCL1
SDA1
JP3
TXP
RXP
M4
NDS331N
PMV65XP,215
M5
10k 10%
R46
R47
10k 10%
R45
4k7 10%
EN_BOOST_5V
VDCDC
U10
TPS61240DRVR
VIN
VOUT
FB
EN
L
GND
EP
C23
10uF
C28
10uF
SRN4018-1R0Y
L5
C25
10uF
C26
10uF
5V_BOOST
PAGE: 9
DATE: 15/03/16
CIRCUIT: BUCK CONVERTER - PIC16F1829
PROJECT: ROBOT - HARVESTER MODULE
AUTHOR: PEDRO SANTOS

PAGE: 10
DATE: 15/03/16
CIRCUIT: ULTRASONIC MODULES
PROJECT: ROBOT - HARVESTER MODULE
AUTHOR: PEDRO SANTOS
5V_BOOST
C29
10uF
C30
10uF
C31
10uF
GND
HC-SR04
TX
RX
GND
ECHO
TRIG
VCC
GND
ECHO_ULTRAS_R
TRIG_ULTRAS_R
5V_BOOST
ECHO_ULTRAS_F
TRIG_ULTRAS_F
ECHO_ULTRAS_L
TRIG_ULTRAS_L
E_4PIN

B.2 PCB

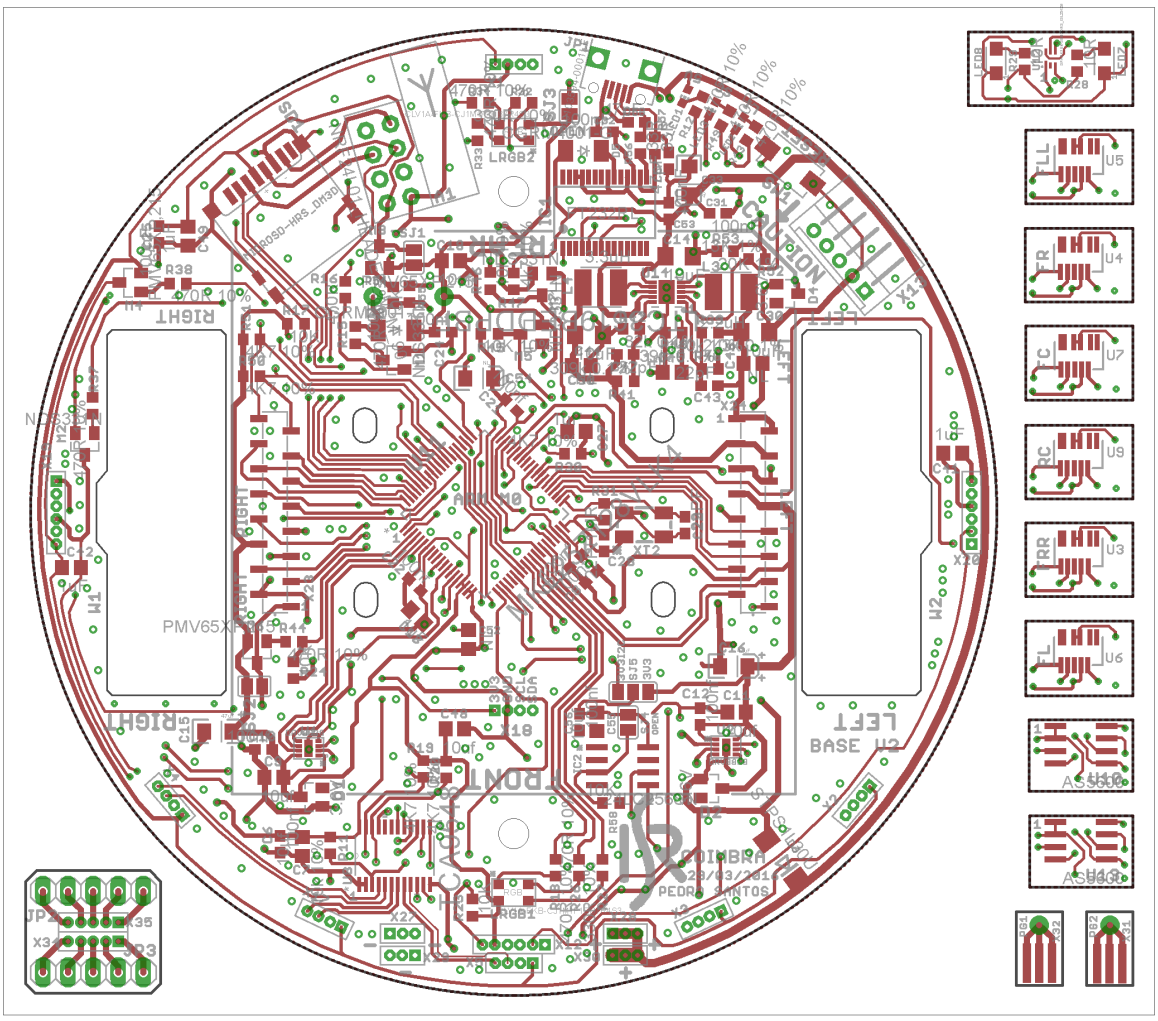

Figure B.1: *Layer top*, *base* module;

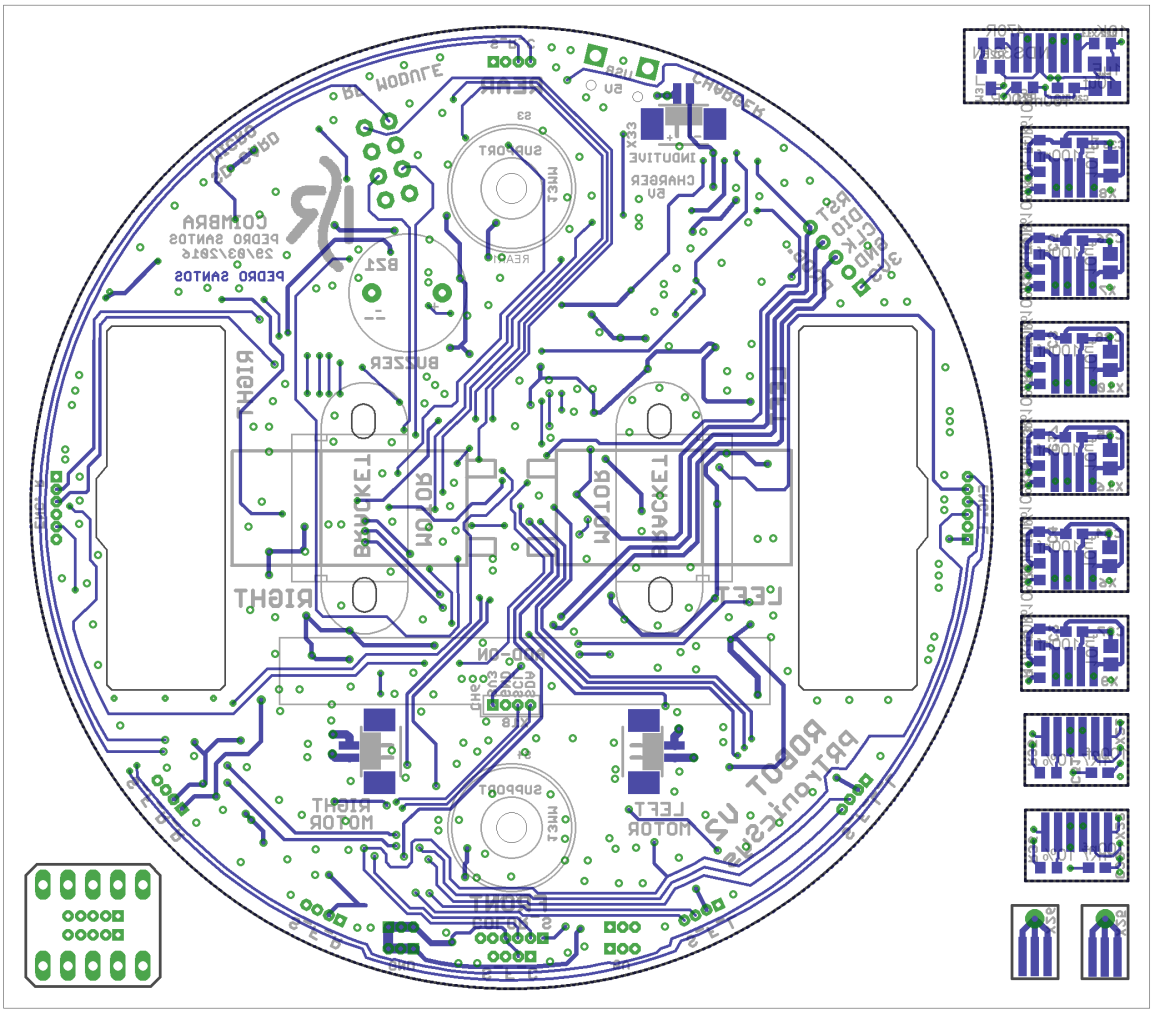

Figure B.2: *Layer bottom*, *base* module;

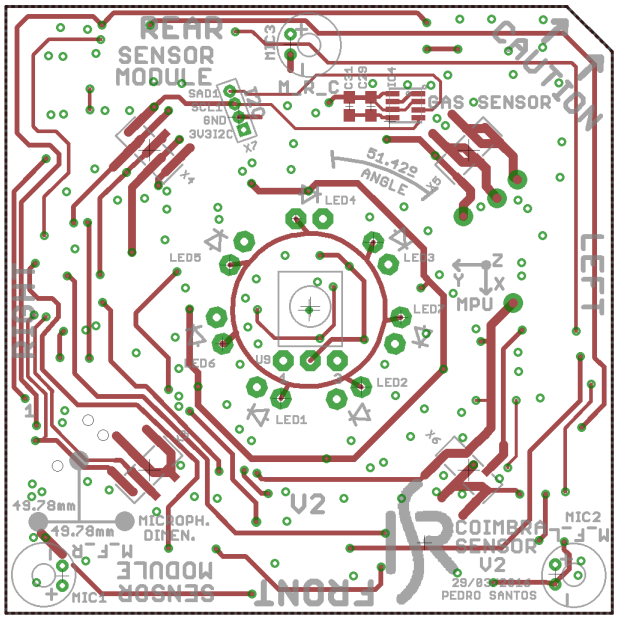

Figure B.3: *Layer top*, *sensor* module;

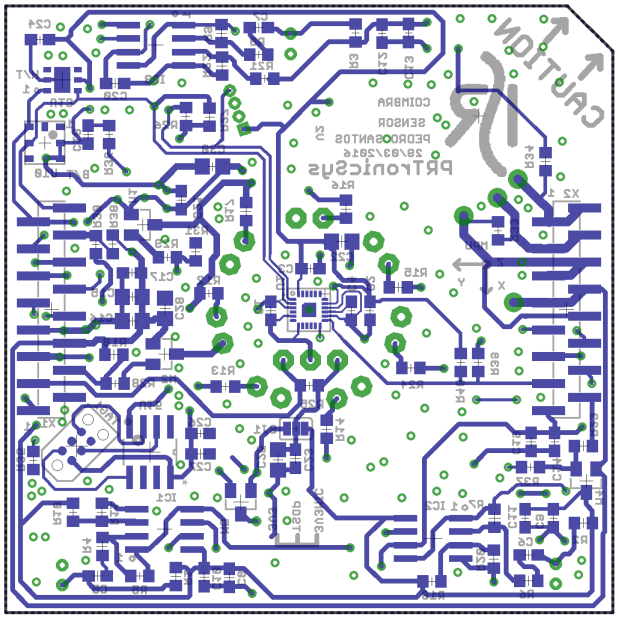

Figure B.4: *Layer bottom*, *sensor* module;

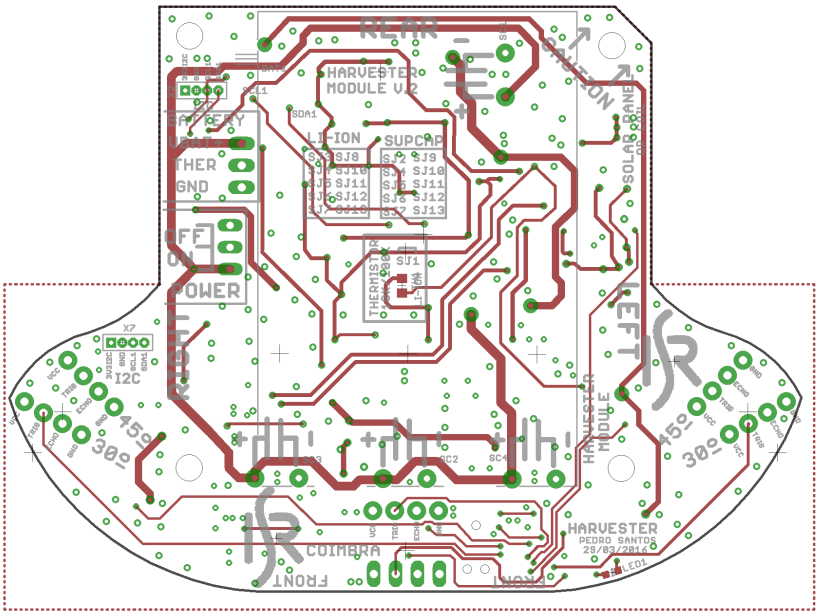

Figure B.5: *Layer top*, *harvester* module;

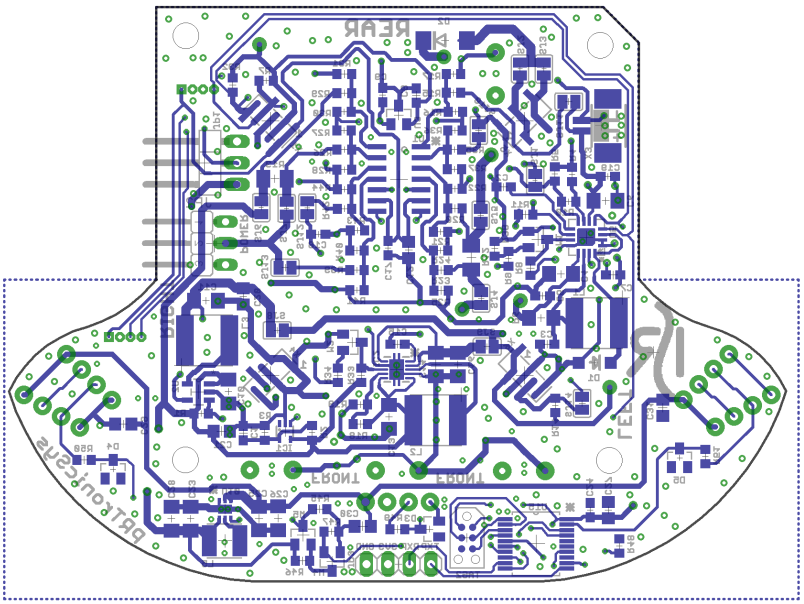

Figure B.6: *Layer bottom*, *harvester* module;

B.3 Bill of material

Table B.1: Bill of material of the base module;

Design P/N	Value	Voltage	Power	Tolerance	Package	Man. Reference	Quanty
U10,U13	AS5600	Undef.	Undef.	Undef.	SOIC-8	AS5600-ASOM	2
C42,C41,C27,C13,C49,C20	1uF	>=6,3	Undef.	Undef.	0805	MC0805B105K100CT	6
C45	1nF	>=6,3	Undef.	Undef.	0805	C0805C102K1RACTU	1
C51, C39, C12, C10, C22, C8, C21, C23, C5, C4, C17, C1, C2, C3, C6, C25, C24, C19, C31, C32, C53, C56	100nF	>=6,3	Undef.	Undef.	0603	MC0603B104K160CT	22
C11, C9, C26, C34, C35, C36, C37, C38, C7, C18, C48, C40, C55	10uF	>=6,3	Undef.	Undef.	0805	MC0805B106K6R3CT	13
C14,C30,C44	10uF	>=6,3	Undef.	Undef.	1206	JMK316B7106KL-T	3
C29,C28,C43,C47	22pF	>=6,3	Undef.	Undef.	0603	MC0603N220K500CT	4
C58, C57	47pF	>=6,4	Undef.	Undef.	603		2
C16,C15,C33	47uF	>=6,3	Undef.	Undef.	1206	293D476X96R3A2TE3	3
C54	NL						
R35,R36,R19,R20,R50,R51,R30,R47	4K7	Undef.	Undef.	Undef.	0603	RC0603FR-074K7L	8
R37, R38, R44, R54, R18, R26, R32, R33, R16, R25, R12, R43, R49	470R	Undef.	>=63mW	Undef.	0603	RC0603FR-07470RL	13
R31	1M	Undef.	Undef.	Undef.	0603	NL	0
R27,R34	330R	Undef.	>=63mW	Undef.	0603	RC0603FR-07330RL	2
R9,R10,R7,R8,R13,R14,R1, R2, R3, R4, R5,R6, R11, R17, R22, R45, R46, R23, R24, R55	10K	Undef.	>=63mW	0,05	0603	CRGH0603J10K	20
R15,R21	100R	Undef.	>=100mW	Undef.	0603	CR0603-JW-101ELF	2
R56, R57	33R	Undef.	>=100mW	Undef.	0604		2
R28,R29	10R	Undef.	>=100mW	Undef.	0603	RC0603FR-0710RL	2
R39	249K	Undef.	>=63mW	0,001	0603	CPF0603B249KE1	1
R40	39K	Undef.	>=63mW	0,001	0603	CPF0603B39KE1	1
R41	316K	Undef.	>=63mW	0,001	0603	RN731JTTD3163B25	1
R42	82K	Undef.	>=63mW	0,001	0603	CPF0603B82KE1	1
R52	13K	Undef.	>=63mW	0,01	0603	CPF0603F13KC1	1
R53	20K	Undef.	>=63mW	0,01	0603	CPF0603F20KC1	1
R48	140K	Undef.	>=63mW	0,01	0603	MCTC0525B1403T5E	1
A1	NRF24l01	Undef.	Undef.	Undef.	Undef.	nRF24L01	1
BZ1	ABT-410-RC	Undef.	Undef.	Undef.	TH	ABT-410-RC	1
D1,D2	3,6V	Undef.	Undef.	Undef.	SOT-23	BZX84C3V6LT1G	2
D4	NL						
D6	STPS1L30U	0,26	Undef.	Undef.	DO-214AA	STPS1L30U	1
D3,D5	Undef.	Undef.	Undef.	Undef.	SOD-123	MBR0520LT1G	2
IC1	FT232L	Undef.	Undef.	Undef.	SSOP	FT232RL	1
L3	2,2uH	Undef.	Undef.	Undef.	4x4x2,5	SRN4026-2R2Y	1
L4	3,3uH	Undef.	Undef.	Undef.	4x4x2,5	SRN4026-3R3M	1
LED1	Green	Undef.	Undef.	Undef.	0603	KPHM-1608CGCK	1
LED2,LED3	Red	Undef.	Undef.	Undef.	0603	KP-1608SURCK	2
LED7, LED8	White	Undef.	Undef.	Undef.	2,7x2,0	CLM3C-WKW-CWBYA453	2
LRGB1,LRGB2	Rgb	Undef.	Undef.	Undef.	SMD	CLV1A-FKB-CJ1M1F1BB7R4S3	2
M1,M2,M3,M5,M7	NFET	Undef.	Undef.	Undef.	SOT-23	NDS331N	5
M4,M6,M8	PFET	Undef.	Undef.	Undef.	SOT-23	PMV65XP,215	3
MAG1,MAG2	MD6SH-1	Undef.	Undef.	Undef.	6X2mm	AS5000-MD6SH-1	2
Parafuso M2+porca M2							
MB1,MB2	N20 Motor	Undef.	Undef.	Undef.	15x11,5x25	10PCS N20 Motor	2
MT1,MT2	298:1 100RPM	Undef.	Undef.	Undef.	Undef.	RB-Esm-07	2
PG1,PG2	Spring Probe	Undef.	Undef.	Undef.	10,59mm	0914-0-15-20-77-14-11-0	2
S3,S4	Nylon Support	Undef.	Undef.	Undef.	13lx15d(mm)		2
SD1	DM3D-SF	Undef.	Undef.	Undef.	Socket	DM3D-SF	1
SD CARD 2Gb							1
SW1	EVQPE104K	Undef.	Undef.	Undef.	6x3,5mm	EVQPE104K	1
U1,U2	DRV8838	Undef.	Undef.	Undef.	QFN8	DRV8838DSGT	2
U3,U4,U5,U6,U7,U9	VCNL4020	Undef.	Undef.	Undef.	QFN11	VCNL4020-GS08	6
U8	TCA9548	Undef.	Undef.	Undef.	SOIC24	TCA9548APWR	1
U11	MKL25Z128VLK4	Undef.	Undef.	Undef.	LQFP-80	MKL25Z128VLK4	1
U12	ISL29125	Undef.	Undef.	Undef.	ODFN-6	ISL29125IROZ-T7A	1
U14	LTC3619BEDD#PBF	Undef.	Undef.	Undef.	DFN-10	LTC3619BEDD#PBF	1
W1,W2	INM-0125	Undef.	Undef.	Undef.	7x32mm	INM-0125	1
X1,X2,X3,X4,X5, X6, X7, X8, X9, X10, X16, X17, X11, X12, X18 ,X19, X20, X21, X22, X25, X31, X26, X32, X29, X27, X28, X30	20pin head.	Undef.	Undef.	Undef.	1,27mm pitch	M52-040023V2045	4
X13 - HEADER 90º	5pins	Undef.	Undef.	Undef.	2mm pitch	S5B-PH-K-S (LF)(SN)	1
X13 - RECEPTABLE	5pins	Undef.	Undef.	Undef.	2mm pitch	PHR-5	1
X13- CONTACT	5pins	Undef.	Undef.	Undef.	2mm pitch	SPH-004T-P0.5S	5
X14,X15,X33 ,- HEADER	2pins	Undef.	Undef.	Undef.	1,25mm pitch	10114830-10102LF	3
X14,X15,X33- RECEPTABLE	2pins	Undef.	Undef.	Undef.	1,25mm pitch	10114826-00002LF	3
X14,X15,X33- CONTACT	2pins	Undef.	Undef.	Undef.	1,25mm pitch	10114827-001LF	8
X23,X24	16pins	Undef.	Undef.	Undef.	1,27mm pitch	M52-5052545	2
JP1	5 pins	Undef.	Undef.	Undef.	Type b	10103594-0001LF	1
XT2	8Mhz	Undef.	Undef.	Undef.	5x3,2mm	ABM3B-8.000MHZ-B2-T	1
IC2	24LC256SN	Undef.	Undef.	Undef.	Soic8	24LC256SN	1
Indutive ChargerKIT	5V Samsung S3	Undef.	Undef.	Undef.	Undef.	Undef.	1
Indutive charger plastic suport	Plastic Suport	Undef.	Undef.	Undef.	Undef.	Undef.	1
Programmer Board	Board	Undef.	Undef.	Undef.	Undef.	FRDM-KL25Z	1

Table B.2: Bill of material of the sensor module;

Design P/N	Value	Voltage	Power	Tolerance	Package	Man. Reference	Quanty
C2,C4, C14, C20, C24, C8, C9, C12,C17, C18, C23, C26, C29	100nF	>=6,3	Undef.	Undef.	0603	MC0603B104K160CT	14
C1	10nF	>=6,3	Undef.	Undef.	0603	MC0603B103K250CT	1
C15,C16,C25, C28, C22	10uF	>=6,3	Undef.	Undef.	0805	MC0805B106K6R3CT	5
C25	NL						
C3,C10,C11,C13,C19,C21, C27, C31	1uF	>=6,3	Undef.	Undef.	0603	MC0603B105K160CT	8
C5,C6,C7	470nF	>=6,4	Undef.	Undef.	0603	GRM188R71E474KA12D	3
R12, R13, R14, R15, R16, R17, R24	220R	Undef.	>=63mW	Undef.	0603	ERJ3EKF2200V	7
R1, R2, R3	2K2	Undef.	>=63mW	0,01	0603	RC0603FR-072K2L	3
R23,R28,R29,R30	470R	Undef.	>=63mW	Undef.	0603	RC0603FR-07470RL	4
R5, R7, R9	470K	Undef.	>=63mW	0,01	0603	RC0603FR-07470KL	3
R10, R11, R19, R20, R21, R22	47K	Undef.	>=63mW	0,01	0603	RC0603FR-0747KL	6
R25,R4,R6,R8,R18,R38,R31	4K7	Undef.	>=63mW	0,01	0603	CRGH0603F4K7	7
R36,R35,R33,R34,R37	10K	Undef.	>=63mW	5%	0603	CRGH0603J10K	5
C27	1nF	>=6,3	Undef.	0,1	0603	GRM1885C1H102FA01D	1
U10	BMP180	Undef.	Undef.	Undef.	QFN-7	BMP180	1
U15	PIC12F1822	Undef.	Undef.	Undef.	Soic 8	PIC12F1822-E/SN	1
U13	SHT21	Undef.	Undef.	Undef.	QFN-6	SHT21	1
LED1, LED2, LED3, LED4, LED5, LED6, LED7	L-934F3C	Undef.	Undef.	Undef.	TH	L-934F3C	7
IC1,IC2,IC3	MCP6002	Undef.	Undef.	Undef.	SOIC-8	MCP6002-E/SN	3
U9	TSOP38536	Undef.	Undef.	Undef.	TH	TSOP38536	1
U1	MPU9250	Undef.	Undef.	Undef.	QFN	MPU-9250	1
MIC1,MIC2,MIC3	MIC_pul	Undef.	Undef.	Undef.	TH	POM-1644P-NF-R	3
M1	NDS331N	Undef.	Undef.	Undef.	SOT-23	NDS331N	1
M2,M4,M5	PMV65XP,215	Undef.	Undef.	Undef.	SOT-23	PMV65XP,215	3
X1,X2	16pins	Undef.	Undef.	Undef.	1,27 pitch	M52-040000P2545	2
X3, X4, X5, X6	5pins	Undef.	Undef.	Undef.	1,27 pitch	M52-5050545	4
IC4	BME680	Undef.	Undef.	Undef.	3X3mm	BME680	1
IC5	CCS811	Undef.	Undef.	Undef.	2,7x4mm	CCS811	1

Table B.3: Bill of material of the harvester module - supercapacitors;

Design P/N	Value	Voltage	Power	Tolerance	Package	Man. Reference	Quanty
C2, C3, C5, C7, C8, C9, C15, C17, C18, C19	100nF	>=6,3	Undef.	Undef.	0603	MC0603B104K160CT	10
C4,C6,C13,C14,C16, C23, C28, C25, C26	10uF	>=6,3	Undef.	Undef.	1206	JMK316B7106KL-T	9
C12	10uF	>=6,3	Undef.	Undef.	0805	MC0805B106K6R3CT	1
R12, R13	0,05R	Undef.	0,5W	0,50%	1206	LVK12R050DER	2
R6	0,05R	Undef.	0,5W	1%	1207	LVK12R050FER	1
R17,R22,R25,R28,R31,R37,R41,R44	39K2	Undef.	>=63mW	0,10%	0603	RP73PF1J39K2BTDF	8
R16, R21, R24, R27, R30, R36, R40, R43	75K	Undef.	>=63mW	0,10%	0603	RP73PF1J75KBTDF	8
R20,R23,R26,R29	47K5	Undef.	>=63mW	0,10%	0603	RP73PF1J47K5BTDF	4
R33, R45	4K7	Undef.	>=63mW	Undef.	0603	RC0603FR-074K7L	2
R9, R34	470R	Undef.	>=63mW	Undef.	0603	RC0603FR-07470RL	2
R15, R35, R39, R42	178K	Undef.	>=63mW	0,10%	0603	MCTC0525B1783T5E	4
R49, R50, R51	2K2	Undef.	Undef.	Undef.	0603	RC0603JR-072K2L	3
R8,R11, R46, R47	10K	Undef.	>=63mW	5%	0603	CRGH0603J10K	4
R14	10K	Undef.	>=63mW	1%	0603	CRCW060310K0FKTA	1
R19	33K	Undef.	>=63mW	1%	0603	RC0603FR-0733KL	1
R18	93K1	Undef.	>=63mW	1%	0603	CRCW060393K1FKEA	1
L1,L2	4,7uH	Undef.	Undef.	Undef.	6x6x2,8	SRN6028-4R7M	2
D1	B0530W-7-F	<=0,7	Undef.	Undef.	SOD-123	B0530W-7-F	1
D2	STPS1L30U	0,26	Undef.	Undef.	DO-214AA	STPS1L30U	1
D3, D4, D5	DZ23C3V3-E3-08	3v3	Undef.	Undef.	SOT-23	DZ23C3V3-E3-08	3
M1,M2, M4	NDS331N	Undef.	Undef.	Undef.	SOT-23	NDS331N	3
SC1,SC2,SC3,SC4	15F or 10F	2,7	Undef.	Undef.	TH	HV1030-2R7106-R	4
U1	MCP3424	Undef.	Undef.	Undef.	SOIC-14	MCP3424-E/SL	1
U3	MCP1525T	2,5	Undef.	Undef.	SOT-23	MCP1525T-I/TT	1
IC2	TPS61201	3,3	Undef.	Undef.	QFN	TPS61201DRCT	1
U5	ZSPM4523	2,65	Undef.	Undef.	QFN16	ZSPM4523AA1W	1
X3 - Header	2pins	Undef.	Undef.	Undef.	1,25mm pitch	10114830-10102LF	1
X3 - Receptable	2pins	Undef.	Undef.	Undef.	1,25mm pitch	10114826-00002LF	1
X3 - Contact	2pins	Undef.	Undef.	Undef.	1,25mm pitch	10114827-001LF	3
X1, X4, X5, X6	5pins	Undef.	Undef.	Undef.	1,27 pitch	M52-5050545	4
X1, X4, X5, X6	25 pins	Undef.	Undef.	Undef.	1,27 pitch	HTMS-125-01-G-S	1
JP2W	3Pins	Undef.	Undef.	Undef.	2,54 pitch	61300311021	1
Jumper ON/OFF	2pins	Undef.	Undef.	Undef.	2,54 pitch	881545-2	1
SOLAR PANEL	66mA	5,5V	0,33W	Undef.	60x60		1
Ultrasoni Module Sensor	HC-SR05	Undef.	Undef.	Undef.			3
L5	1uH	Undef.	Undef.	Undef.	4x4x2,8mm	SRN4018-1R0Y	1
U15	PIC16F1829-I/SS	Undef.	Undef.	Undef.	Soic 20	PIC16F1829-I/SS	1
M5	PFET	Undef.	Undef.	Undef.	SOT-23	PMV65XP,215	1
R45	4K7	Undef.	Undef.	Undef.	0603	RC0603FR-074K7L	1
U10	TPS61240DRVR	Undef.	Undef.	Undef.			1
LED1		Undef.	Undef.	Undef.	0603		1

Table B.4: Bill of material of the harvester module - lithium;

Design P/N	Value	Voltage	Power	Tolerance	Package	Man. Reference	Quanty
C2,C3,C5,C7,C8,C9,C17,C18,C19, C24	100nF	>=6,3	Undef.	Undef.	0603	MC0603B104K160CT	11
C4,C6,C10,C11, C23, C28, C25, C26	10uF	>=6,3	Undef.	Undef.	1206	JMK316B7106KL-T	8
C12,C20,C21, C27, C29, C30, C31	10uF	>=6,3	Undef.	Undef.	0805	MC0805B106K6R3CT	7
C1	22pF	>=6,3	Undef.	Undef.	0603	MC0603N220K500CT	1
R12, R13	0,05R	Undef.	0,5W	0,50%	1206	LVK12R050DER	2
R6	0,05R	Undef.	0,5W	1%	1206	LVK12R050FER	1
R17,R22,R25,R28,R31,R37,R41,R44	39K2	Undef.	>=63mW	0,10%	0603	RP73PF1J39K2BTDF	8
R16, R21, R24, R27, R30, R36, R40, R43	75K	Undef.	>=63mW	0,10%	0603	RP73PF1J75KBTDF	8
R20,R23,R26,R29	47K5	Undef.	>=63mW	0,10%	0603	RP73PF1J47K5BTDF	4
R48	330R						
R9	470R	Undef.	>=63mW	Undef.	0603	RC0603FR-07470RL	1
R15, R35, R39, R42	178K	Undef.	>=63mW	0,10%	0603	MCTC0525B1783T5E	4
R1,R8,R11, R47, R45,R46,R38	10K	Undef.	>=63mW	5%	0603	CRGH0603J10K	5
R10,R14	10K	Undef.	>=63mW	1%	0603	CRCW060310K0FKTA	2
R49, R50, R51	2K2	Undef.	Undef.	Undef.	0603	RC0603JR-072K2L	3
R45, R48	4K7	Undef.	Undef.	Undef.	0603		2
R3	46K4	Undef.	>=63mW	1%	0603	CRCW060346K4FKEA	1
R2	82K5	Undef.	>=63mW	1%	0603	CRCW060382K5FKEA	1
TH1	10K	Undef.	Undef.	5%	0603	ERTJ1VG103FA	1
L3	2,2uH	Undef.	Undef.	Undef.	6x6x2,8	SRN6028-2R2Y	1
L1	4,7uH	Undef.	Undef.	Undef.	6x6x2,8	SRN6028-4R7M	1
D1	B0530W-7-F	<=0,7	Undef.	Undef.	SOD-123	B0530W-7-F	1
D2	STPS1L30U	0,26	Undef.	Undef.	DO-214AA	STPS1L30U	1
D3, D4, D5	DZ23C3V3-E3-08	3v3	Undef.	Undef.	SOT-23	DZ23C3V3-E3-08	3
M1, M4	NDS331N	Undef.	Undef.	Undef.	SOT-23	NDS331N	2
BAT1	2050mA	3,7	Undef.	Undef.	TH	103456A-1S-3M	1
U1	MCP3424	Undef.	Undef.	Undef.	SOIC-14	MCP3424-E/SL	1
U3	MCP1525T	2,5	Undef.	Undef.	SOT-23	MCP1525T-I/TT	1
IC1	TPS3803	Ajust	Undef.	Undef.	SC-70	TPS3803-01DCKRG4	1
U2	LM3671	3,3	Undef.	Undef.	SOT-23	LM3671MF-3.3/NOPB	1
U5	ZSPM4521	4,175	Undef.	Undef.	QFN16	ZSPM4521AA1W	1
X3 - Header	2pins	Undef.	Undef.	Undef.	1,25mm pitch	10114830-10102LF	1
X3 - Receptable	2pins	Undef.	Undef.	Undef.	1,25mm pitch	10114826-00002LF	1
X3 - Contact	2pins	Undef.	Undef.	Undef.	1,25mm pitch	10114827-001LF	3
X1, X4, X5, X6	5pins	Undef.	Undef.	Undef.	1,27 pitch	M52-5050545	4
X1, X4, X5, X6	25 pins	Undef.	Undef.	Undef.	1,27 pitch	HTMS-125-01-G-S	1
JP1	3 Pins	Undef.	Undef.	Undef.	2,54 pitch	640457-3	1
JP2W	3Pins	Undef.	Undef.	Undef.	2,54 pitch	61300311021	1
Jumper ON/OFF	2pins	Undef.	Undef.	Undef.	2,54 pitch	881545-2	1
SOLAR PANEL	66mA	5,5V	0,33W	Undef.	60x60		1
Ultrasoni Module Sensor	HC-SR05	Undef.	Undef.	Undef.			3
L5	1uH	Undef.	Undef.	Undef.	4x4x2,8mm	SRN4018-1R0Y	1
U15	PIC16F1829-I/SS	Undef.	Undef.	Undef.	Soic 20	PIC16F1829-I/SS	1
M5	PFET	Undef.	Undef.	Undef.	SOT-23	PMV65XP,215	1
R45	4K7	Undef.	Undef.	Undef.	0603	RC0603FR-074K7L	1
U10	TPS61240DRVR	Undef.	Undef.	Undef.			1
LED1		Undef.	Undef.	Undef.	0603		1